Machine Learning in Optical Fibre Networking Under Uncertainty

By

FANCHAO MENG

Department of Electrical and Electronic Engineering
UNIVERSITY OF BRISTOL

A dissertation submitted to the University of Bristol
in accordance with the requirements of the degree of
DOCTOR OF PHILOSOPHY in the Faculty of Engineering.

NOVEMBER 2018

Word count:40,000

Abstract

During the past three decades, there have been major achievements on accurate modelling of behaviour and operation of telecommunication networks utilising classical methods with analytical or heuristic models. Currently, there is a big hype on the application of Artificial Intelligence (AI) and Machine Learning (ML) in the telecommunication space. However, there is a gap on scientific scrutiny of advantages of AI and ML compared to existing methods. Analogue telecommunication networks, i.e., optical and wireless networks seem to be the most suitable problem space for AI and ML. They are complicated network systems in nature that are highly dependent on ubiquitous physical layer uncertainties induced by subsystems and transmission mediums such as amplifiers, fibres, switches and transceivers. The problem space becomes even more complicated with recent advances in optical and wireless technologies that allow the development and operation of a fully programmable and dynamic network. This work focuses on benefits and applications of learning agents built on top of cognitive optical networks. It discusses the appropriateness of employing AI methods for specific problems in optical networks and address the importance of online learning with restricted monitoring data. It proposes and experimentally demonstrates a brand new way of carrying out optical network analytics utilising hybrid probabilistic and generative learning model which differs from traditional deterministic models. The result of this investigation, for the first time, can shed light into future AI and ML research in the optical network planning under uncertainty.

Dedication and acknowledgements

Firstly I would like to thank my supervisor Dimitra Simeonidou. She offers me the chance to pursue my PhD degree direct after my undergraduate. I genuinely appreciate her trust and effort all the way for me. I would also like to thank Reza Nejabati for his patient guidance on my research. Although officially Prof. Nejabati is not my supervisor, he has a great impact on me for his strong knowledge of optical networking and scientific research methodology. I am very grateful to the EPSRC TOUCAN and INSIGHT projects for funding my PhD.

The members of High Performance Networks (HPN) group also support me throughout my PhD. I would give my best appreciation to all the colleagues that helped me. To Shuangyi Yan, Emilio Hugues-Salas, Yanni Ou, Rui Wang, Yu Bi for supporting me on carrying out optical network experiments. To Shuping Peng for her encouragement and supervision during my first year when I almost knew nothing about the field. Except for the HPN colleagues, I would also like to express my gratitude to Tianhua Xu from Warwick University (previously from UCL) for his patient teaching on the theoretical models of optical communications.

In addition, I would like to give my best gratitude to several people who I have never met but have tremendous influence on my research. To Jun Wu for his Chinese books 'The Beauty of Maths', 'The Age of Intelligence', etc. that arouse my great interest in AI. To Andrew Yan-Tak Ng and Nando de Freitas for their illuminating online courses that develop my deep understanding and skills in ML.

Besides the academic aspect, my heartfelt thanks go to my family for their all-out support and trust in my education throughout my life. Their support will always be the root cause of all my successes. I would also like to thank my girlfriend Yudie Xi for her continuing confidence in me, my best friends Hui Yuan, Xingyu Li, Chaoyi Li, Yanjun He, Ka Ho Chiu, Keyang Yuan, Tianyuan Huan, etc. for their help and supports in my daily life. I am also very grateful to Siyuan Yu, my undergraduate tutor, who tried his best to give advice and recommendation for my future plan. I am indebted to his patience, commitment, encouragement and guidance for me.

Finally, I would give my best gratitude to the University of Bristol who fosters me for more than seven years from undergraduate to PhD. This seven-year educational experience is golden for all my life. Bristol witnesses my youth.

Author's declaration

I declare that the work in this dissertation was carried out in accordance with the requirements of the University's Regulations and Code of Practice for Research Degree Programmes and that it has not been submitted for any other academic award. Except where indicated by specific reference in the text, the work is the candidate's own work. Work done in collaboration with, or with the assistance of, others, is indicated as such. Any views expressed in the dissertation are those of the author.

SIGNED: ..... DATE: .....

TABLE OF CONTENTS

List of Tables

Table **Page**

List of Figures

Figure **Page**

Acronyms

ABNO Application-Based Network Operations. 45

ADC Analogue-to-Digital Converters. 22

AI Artificial Intelligence. 8

AL Application Layer. 14

ANN Artificial Neural Network. 26, 32

API Application Program Interface. 19

ARIMA Auto-Regressive Integrated Moving Average. 44

ASE Amplified Spontaneous Emission. 2

BER Bit Error Rate. 17

BO Bayesian Optimisation. 124

BoL Beginning of Life. 20

BVT Bandwidth Variable Transmitter. 111

CBR Case-Based Reasoning. 34

CD Chromatic Dispersion. 3

CHRON Cognitive Heterogeneous Reconfigurable Optical Network. 16

CNN Convolutional Neural Network. 33

CO-OFDM Coherent Optical Orthogonal Frequency Division Multiplexing. 42

CP Control Plane. 14

CV Computer Vision. 5

CWMH Component-Wise Metropolis-Hasting. 87

DAC Digital-to-Analogue Converters. 22

DAG Directed Acyclic Graphs. 48

DC Data Centre. 50

DL Deep learning. 5

DLI Delay-Line Interferometer. 123

DNN Deep Neural Network. 33

DSP Digital Signal Processing. 3

DWDM Dense Wavelength Division Multiplexing. 39

ECI Estimation Confidence Interval. 61

ECL External Cavity Laser. 112

EDFA Erbium-doped Fibre Amplifier. 21

ELM Extreme Learning Machine. 42

EM Expectation Maximisation. 41

EoL End of Life. 20

EPON Ethernet Passive Optical Network. 53

EVM Error Vector Magnitude. 63, 104

FTTB Fibre-To-The-Building. 51

FTTC Fibre-To-The-Curb. 51

FTTH Fibre-To-The-Home. 51

FWM Four-Wave Mixing. 22

GA Genetic Algorithm. 45

GD Gradient Descent. 97

GEP Genetic Expression Programming. 53

GMRF Gaussian Model Reference Formular. 24

GP Gaussian Process. 36

GPON-FTTH Gigabit Passive Optical Network-Fibre To The Home. 47

HDFEC Hard-Decision Forward Error Correction. 36

IID Independent and Identically Distributed. 36

ILP Integer Linear Programming. 4

IM/DD Intensity Modulation/Direct Detection. 35

KBR Kernel-Based nonlinear Regression. 38

KNN K-Nearest Neighbour. 41

KP Knowledge Plane. 19

KPI Key Performance Indicator. 3

LPRR LightPath Re-Routing. 111

LSLR Least-Square Linear Regression. 67

LSTM Long Short-Term Memory. 46

LTE Long-Term Evolution. 52

MAC Medium Access Control. 14

MAP Maximum A Posteriori. 30

MCMC Markov Chain Monte Carlo. 76

MF Modulation Format. 105

MFS Modulation Format Switching. 111

ML Machine Learning. 4

MLE Maximum Likelihood Estimation. 30

MLNN Multi-Layer Neural Network. 35

MLP Multilayer Perceptrons. 45

MoD Monitoring on-Demand. 121

NA Neighbour Average. 67

NCMDB Network-scale Configuration and performance Monitoring DataBase. 35

NDFIS National Dark Fibre Infrastructure Service. 62

NF Noise Figure. 23

NK Network Kriging. 37

NLI NonLinear Interference. 23

NLP Natural Language Processing. 5

NLPN NonLinear Phase Noise. 41

NN Neural Network. 35

NPDM Network Planner and Decision Maker. 44

OCM Optical Channel Monitor. 79, 84

OLT Optical Line Terminals. 47

OMA Optical Modulation Analyser. 63

ONT Optical Network Terminals. 47

ONU Optical Network Units. 51

OOK On-Off Keying. 32

OPM Optical Performance Monitoring. 32

OSA Optical Spectrum Analyser. 49

OSNR Optical Signal-to-Noise Ratio. 3

OTC Optical Testing Channel. 48, 49

PBC Polarisation Beam Combiner. 62

PBS Polarisation Beam Splitter. 62

PCA Principal Component Analysis. 34

PDF Probability Density Function. 89

PDL Polarisation Dependent Loss. 20

PDM Polarisation Division Multiplexing. 62

PID Proportional-Integral-Derivative. 53

PLIs Physical Layer Impairments. 2

PON Passive Optical Networks. 51

PRBS Pseudo-Random Bit Sequences. 62, 81

QAM Quadrature Amplitude Modulation. 27

QoS Quality of Service. 1

QoT Quality of Transmission. 3, 5

QPSK Quadrature Phase Shift Keying. 27

RBF Radial Basis Function. 59

RF Random Forest. 37

RM Random Monitoring. 132

RMSD Root Mean Squared Deviation. 68

RNNs Recurrent Neural Networks. 44

ROADM Reconfigurable Optical Add-Drop Multiplexer. 76

ROADMs Reconfigurable Optical Add-Drop Multiplexers. 2

RWA Routing and Wavelength Assignment. 1

SBS Stimulated Brillouin Scattering. 22

SDN Software-Defined Networking. 19

SL Sustained Learning. 6

SM Sequential Monitoring. 132

SNR Signal-to-Noise Ratio. 3

SP Shortest Path. 4

SPM Self-Phase Modulation. 22

SRS Stimulated Raman Scattering. 22

SVM Support Vector Machine. 26

TCP Transmission Control Protocol. 50

VNT Virtual Network Topology. 44

WA WaveAnalyser. 108

WDM Wavelength Division Multiplexing. 2

WSS Wavelength Selective Switch. 63

XPM Cross-Phase Modulation. 22

CHAPTER 1

INTRODUCTION

Optical networks form the backbone of modern communication networks and the Internet. It is seen as the foundation in supporting the ever-increasing Internet traffic due to the high bandwidth capacity and relatively low costs. Therefore, fibre optic networks are deployed widely around the world. Such large-scale and complex network systems need a robust control mechanism. The optical network control plane is mainly responsible for resource management tasks such as flex-grid, Routing and Wavelength Assignment (RWA) [1] etc. A high-performance control plane can benefit many aspects of the optical network. For example, an accurate RWA can enable a low-margin, proactive optical network that runs close to its performance limits and saves significant bandwidth resources [2]. Also, the control plane provides network analytics and performance predictions which enable network reliability [3]. Network reliability is critical in delivering application services to end users, i.e., guaranteeing the Quality of Service (QoS) [4]. Network telemetry and machine learning (especially sustained learning) capabilities are required to support such high-performance control plane.

1.1 Motivation for network telemetry

TraditionalWavelength Division Multiplexing (WDM) optical networks establish rigid connections (lightpaths) with fixed bit rates and modulation formats. Such static networks can not efficiently support the increasingly dynamic traffic demands [5]. Recent advances in optical networks, such as bandwidth adaptive transceivers, Reconfigurable Optical Add-Drop Multiplexers (ROADMs), elastic frequency grid, etc. [5] have transformed the static optical networks into more flexible and dynamic infrastructures. Such flexible optical networks aim to support traffic that is heterogeneous. However, as the traffic patterns become more and more dynamic, the Physical Layer Impairments (PLIs) also become path, load and configuration dependent, hence making them difficult to predict [6]. These PLIs can significantly degrade the transmission performance, hence restrict the QoS. Common PLIs in optical networks are Amplified Spontaneous Emission (ASE) noise, Polarisation Mode Dispersion (PMD), crosstalk, etc. [7]

Much research work has been focused on building sophisticated physical layer models to capture the PLI effects that can accumulate along the transmission path [8, 9]. Although these classical models are effective during the network planning phase, for in-service (running) optical networks, these high-complexity models need time-consuming procedures to be updated in real-time [7]. Data-driven, cognitive optical network architectures are proposed [7, 10, 11] to mitigate these complexity problems. On the other hand, lots of research has been focused on the PLI-aware RWA algorithms [12–14]. The common assumption is that all the PLIs calculated or predicted from the theoretical models are accurate. However, this assumption does not hold under network knowledge uncertainty. The network knowledge uncertainty is defined as the incomplete or non-deterministic knowledge of a system or a model. Previous research has shown that network knowledge uncertainty exists which can lead to the inaccuracy of the design tools [2]. The network performance may differ from what is expected from the model predictions. As such,

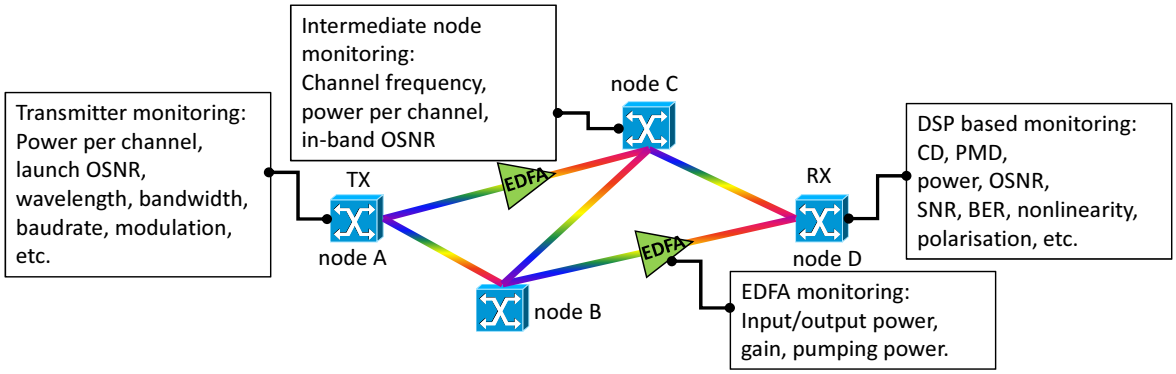

FIGURE 1.1. Optical network monitoring overview. Signals are transmitted at node A and coherently received at node D. Node B and C serve as intermediate nodes or re-configurable optical add-drop multiplexers (ROADMs) where signals can add/drop/by-pass. Besides the receiver DSP side, monitoring information can also be obtained in the transmitter, intermediate nodes and amplifiers.

network telemetry, or network performance monitoring, is employed as the key enabler bridging the control plane and the underlying data plane. Such data-driven network is expected to perceive, learn, adapt and take actions if necessary [10].

In optical networks, the monitoring information mainly arises from two sources: transceivers and intermediate nodes. Metrics such as power, Chromatic Dispersion (CD), PMD, Optical Signal-to-Noise Ratio (OSNR), etc. can be directly monitored in the transceiver. In particular, thanks to the development of Digital Signal Processing (DSP) based coherent technology, most of the linear impairments can be fully compensated at reception in the electrical domain. OSNR is the Key Performance Indicator (KPI) for the Quality of Transmission (QoT) of a lightpath [15]. From the power measurement perspective, OSNR is defined as the ratio of the total optical signal over the noise power measured within 0.1nm bandwidth, while the Signal-to-Noise Ratio (SNR) is the optical signal to noise power ratio both measured within the whole spectrum bandwidth. Apart from the transceivers, intermediate nodes also support monitoring functions for optical power, fre-

quency drift and in-band OSNR [6, 16, 17]. Fig. 1.1 shows the majority of the information that can be monitored in optical networks.

1.2 Motivation for machine learning

The optical network control plane has long been studied using optimisation techniques such as the Shortest Path (SP), Integer Linear Programming (ILP), searching algorithms, etc. [18] They all belong to planning under certainty. The aim is to achieve automatised network optimisation. However, these optimisation techniques cannot adapt to changing network status under uncertainty, unless they have the ability to learn from the real-time monitoring data [19].

Such uncertainties may come about if the system is very dynamic or complex. Due to current advances in the reconfigurability of optical networks, the PLIs are becoming path-dependent, configuration-dependent and load-dependent [6]. This makes many features challenging to predict. For example, the fibre nonlinearity is very complex phenomenon, and its status can alter quickly due to many effects such as power excursion, channel add-drops and temperature [20]. Simple monitoring cannot directly reduce the uncertainty. Network planning under such uncertainty may eventually result in resource over-provisioning, or potentially even network failure [2].

Given that direct knowledge from monitoring is impossible, we need to use learning tools to extract the desired information. Machine Learning (ML) has proven itself as a promising tool to make the most of the monitoring data wisely. ML can learn from the observed data, generate insightful information as knowledge, and help the control plane make further predictions and decisions on top of the knowledge. It serves as an automated reasoning tool to combat the aforementioned network knowledge uncertainty given the observed data.

In addition, most of the QoT models are both mathematically and computationally complex [7, 8]. They consume considerable computing resources and time to achieve the expected prediction performance. Even a tiny mistake in the model input parameters may lead to unacceptable prediction errors. Conversely, most ML models (especially supervised learning) are straight-forward statistical mapping algorithms between the system inputs and outputs. They have the potential to bypass the problems associated with complex traditional models and solve the prediction problem in a roundabout way using monitoring. Relevant research on this topic will be reviewed in Chapter 3. Therefore, given the network telemetry capability, intelligent learning agents can be built for high-performance control plane management.

1.3 Motivation for sustained learning

Although ML is a promising approach for combating network uncertainty, some problems still need to be addressed. Unlike fields such as Computer Vision (CV) [21] or Natural Language Processing (NLP) [22], in which the systems are too complex to formulaically analyse, the optical networks have well-proven analytical models that can capture comprehensive PLIs. If these models are completely replaced by ML [23, 24], the network planning process will become rather empirical. We refer an empirically designed system which only exposes its inputs and outputs, i.e., with no insights, as a black box system. In such a black box system, network engineers are blind to the PLIs that contribute to the observed system behaviour, hence making system diagnosis impossible.

Moreover, offline learning is another controversial issue. In the CV or NLP field, Deep learning (DL) models are commonly used. Abundant training data is available for the DL models, and these training data is not required to be real-time. For example, the state-of-the-art CV DL model has a training image data size of 1.2 million [21]. Such

amount of data is extremely hard to obtain in optical networks. Some research work uses historical data or hand-crafted data for training when relatively shallow neural networks are used [24, 25]. However, for the generation of hand-crafted training data, the network systems or the target devices have to be offline, i.e., not in service [24, 25]. This is not realistic for commercial network systems that are in sustained operation. For sufficient historical training data, the data collection period has to span many years of the network operational period. Such offline training ML models will be unadaptable to the changes in network conditions over time such as temperature. In other words, it lacks self-adaptability while the network is evolving. It is worth noting that the self-adaptability is not for the prediction of temperature or ageing, but the prediction of a target QoT under the impact of effects such as temperature and ageing. The learning agent is analogous to a robot which tries to explore the world based on the environment it perceives. The robot has to collect real-time sensory data in order to make predictions or decisions. Offline training cannot improve its learning ability once the environment changes.

For the reasons above, ML models are preferred to capture running, in-service optical network performance with real-time monitoring and online training capabilities. This can also be called Sustained Learning (SL). SL means that the real-time monitoring data can be dynamically used as the ML model training set for learning in the next time slot. Such SL capability is intrinsically adaptable to dynamic and variable systems like optical networks. Except for the design uncertainties that can be captured by offline learning, there are operational uncertainties during the network running period which are analytically intractable over time. ML models should serve as auxiliary tools on top of the off-the-shelf analytical models to minimise these operational uncertainties. We define this as SL-based network analytics. This solution realises adaptive network planning where ML model predictions are updated adaptively with the real-time monitoring data.

From a statistical point of view, SL aims to solve the problem arising from data distribution mismatch. In principle, the training data set used to predict a particular network performance needs to come from the same distribution as the test data set. However, as the network condition changes, the test set no longer belongs to the original distribution. SL works by updating the training set so that it matches again with the test set distribution. Another potential problem that can be easily neglected is that the training set itself may consist of data from different distributions given the very large sliding window. Therefore, either mismatching within the training set, or mismatching between the training set and the test set will be fatal to the learning performance evaluation procedure.

1.4 Challenges

As discussed, the challenges brought about by traditional offline ML models can be solved by online learning, or SL. However, SL also suffers from shortage of the online training data in optical networks. This problem still remains a big challenge for learning in the field of optical networks. One candidate solution is increasing the online training data size by expanding the data collection sliding window. For example, for the prediction of some PLIs such as the transceiver noise which does not change rapidly over time, the sliding window can span a longer period. Such balance needs specific optical domain knowledge to justify whether the expanded window will cause data distribution mismatch or not, as discussed earlier in this chapter. It is intrinsically a design trade-off between the training data size and the prediction performance.

In addition to increasing the training data size, another solution is generative methods. Due to the lack of monitoring data, learning agents are forced to make decisions based on incomplete information. Probabilistic Bayesian methods turn out to be a potential

solution to tackle such data size limitation problems when the agent is not omniscient. Unlike frequentist methods, such as neural networks which are deterministic, Bayesian methods are generative in nature and can generate more knowledge based on small data sets. In the network design, the prior system knowledge can easily be obtained from vendors or analytical models. It serves as the prior component of a Bayesian model. The monitoring data hence serves as the Bayesian model observation to update the prior knowledge. The updated knowledge is called posterior estimations [26].

In summary, Artificial Intelligence (AI) and ML methods are applied extensively in optical networking. Some of the challenges to be solved by AI and ML are addressed here. Firstly, as aforementioned, ML is used to reduce the ubiquitous uncertainty in the networks. ML models are expected to learn from monitoring data and generate updated knowledge of the uncertain parameters. The prediction accuracy is the most common KPI to assess the model performance. This learning capability forms the foundation for network diagnosis and reliability. Secondly, ML can be useful in optimising the control plane decision-making process. This is commonly achieved by generating a utility (cost) function and optimising it with uncertainty [27]. Thirdly, ML is a promising method for replacing traditional optimisation models, such as ILP, due to the high computational complexity. Although such applications sometimes sacrifice the learning accuracy, they can reduce the redundant computation and speed up the learning process, while maintaining acceptable levels of optimisation performance [28, 29]. Amongst all these challenges, the SL capability is critical for capturing the real-time performance of optical network systems.

1.5 Thesis overview and outline

This work applies the proposed SL-based network analytics extensively in optical networks. The overall aim is to combat the network knowledge uncertainty problems and consequently optimise proactive control decision-making. This work demonstrates a new way of bridging the gap between the control plane knowledge base and the underlying physical layer through learning. The SL model's self-adaptability is addressed here in contrast with offline learning. Bayesian learning is employed as the principal online learning method that is capable of learning under small dataset thanks to its generative nature.

The background knowledge needed to understand the subsequent chapters is described in Chapter 2. This chapter lays out the fundamental requirements and potential network architectures for optical network cognition and intelligence, the dominant PLIs affecting QoT performance, as well as the basic ML concepts. Comprehensive literature review of recent AI and ML approaches in optical networking is studied in Chapter 3. The review covers two main fields: physical layer design and control plane algorithms. It reviews up-to-date topics of AI-based network intelligence concerning solutions to network uncertainty, making accurate predictions and optimisation of control plane decision-making. In Chapter 4 Gaussian process is introduced to learn the receiver-DSP-computed SNR without any prior system knowledge and only depending on monitoring data. This work is further extended in Chapter 5 in which Bayesian inference is applied together with Gaussian process to form a hybrid supervised/unsupervised method. This method aims to learn physical layer hidden parameters in a network scale. Chapter 6 describes the idea of integrating in-band OSNR monitoring at network intermediate nodes for more in-depth network insights. This intermediate node monitoring is further extended in Chapter 7 as a monitoring-on-demand function. Bayesian optimisation is applied to reduce redundant monitoring trials at intermediate nodes. The method realises an

intelligent, "out-of-the-loop" monitoring strategy at per-link level. Finally, Chapter 8 summarises the whole thesis and proposes relevant pieces of future work.

1.6 Publications

The following conference proceeding and journal papers have been published during my PhD period.

1. (invited JOCN OFC 2018 special issue, top-download journal) **F. Meng**, A. Mavromatis, Y. Bi, S. Yan, R. Wang, R. Nejabati, and D. Simeonidou, 2019. Self-learning monitoring on-demand strategy for optical networks. Journal of Optical Communications and Networking, 11(2), pp.A144-A154.

2. (top scored) **F. Meng**, A. Mavromatis, Y. Bi, S. Yan, R. Wang, Y. Ou, K. Nikolovgenis, R. Nejabati, and D. Simeonidou, "Field Trial of Monitoring On-Demand at Intermediate-Nodes Through Bayesian Optimization," in Optical Fiber Communication Conference, OSA Technical Digest (Optical Society of America, 2018), paper M3A.2.

3. **F. Meng**, S. Yan, K. Nikolovgenis, Y. Ou, R. Wang, Y. Bi, E. Hugues-Salas, R. Nejabati, and D. Simeonidou, "Field Trial of Gaussian Process Learning of Function-Agnostic Channel Performance Under Uncertainty," in Optical Fiber Communication Conference, OSA Technical Digest (Optical Society of America, 2018), paper W4F.5.

4. (top scored) **F. Meng**, S. Yan, R. Wang, Y. Ou, Y. Bi, R. Nejabati and D. Simeonidou, "Robust Self-Learning Physical Layer Abstraction Utilizing Optical Performance Monitoring and Markov Chain Monte Carlo," 2017 European Conference on Optical Communication (ECOC), Gothenburg, Sweden, 2017, pp. 1-3.

5. **F. Meng**, Y. Ou, S. Yan, K. Sideris, M. D. G. Pascual, R. Nejabati and D. Simeonidou,

"Field trial of a novel SDN enabled network restoration utilizing in-depth optical performance monitoring assisted network re-planning," 2017 Optical Fiber Communications Conference and Exhibition (OFC), Los Angeles, CA, 2017, pp. 1-3.

6. (ECOC post deadline paper) Yan, Shuangyi; Khan, N. Khan; Mavromatis, Alex; Gkounis, Dimitrios; Fan, Qirui; Ntavou, Foteini; Nikolovgenis, Konstantinos; **Meng, Fanchao**; Salas, Emilio Hugues; Guo, Changjian; Lu, Chao; Lau, Alan Pak Tau; Nejabati, Reza; Simeonidou, Dimitra, "Field trial of Machine-Learning-assisted and SDN-based Optical Network Planning with Network-Scale Monitoring Database," 2017 European Conference on Optical Communication (ECOC), Gothenburg, Sweden, 2017, pp. 1-3.

7. Yanni Ou, Matthew Davis, Alejandro Aguado, **Fanchao Meng**, Reza Nejabati, and Dimitra Simeonidou, "Optical Network Virtualisation Using Multitechnology Monitoring and SDN-Enabled Optical Transceiver," J. Lightwave Technol. 36, 1890-1898 (2018)

8. Y. Ou, **F. Meng**, P. M. Anadarajah, S. Yan, A. Aguado, M. D. G. Pascual, R. Nejabati, D. Simeonidou, "Investigation of optical impacts on virtualization using SDN-enabled transceiver and optical monitoring," 2017 Optical Fiber Communications Conference and Exhibition (OFC), Los Angeles, CA, 2017, pp. 1-3.

9. R. Wang, **F. Meng**, R. Nejabati and D. Simeonidou, "A Novel Traffic Grooming Scheme for Nonlinear Elastic Optical Network," 2017 European Conference on Optical Communication (ECOC), Gothenburg, Sweden, 2017, pp. 1-3.

10. R. Wang, Y. Bi, Y. Ou, E. Hugues Salas, **F. Meng**, S. Yan, R. Nejabati, D. Simeonidou, "Coordinated Fibre Span Power Optimisation and ROADM Input Power Management Strategy for Optical Networks," 2018 European Conference on Optical Communication (ECOC), Rome, Italy, 2018.

11. Y. Ou, A. Aguado, **F. Meng**, S. Yan, B. Guo, R. Nejabati, D. Simeonidou, "Optical

network virtualization using multi-technology monitoring and optical virtualize-able transceiver," 2016 Optical Fiber Communications Conference and Exhibition (OFC), Anaheim, CA, 2016, pp. 1-3.

12. A. Mayoral et al., "First experimental demonstration of a distributed cloud and heterogeneous network orchestration with a common Transport API for E2E services with QoS," 2016 Optical Fiber Communications Conference and Exhibition (OFC), Anaheim, CA, 2016, pp. 1-3.

13. M. S. Moreolo et al., "SDN-enabled sliceable BVT based on multicarrier technology for multi-flow rate/distance and grid adaptation," 2015 European Conference on Optical Communication (ECOC), Valencia, 2015, pp. 1-3.

14. M. Svaluto Moreolo et al., "SDN-Enabled Sliceable BVT Based on Multicarrier Technology for Multiflow Rate/Distance and Grid Adaptation," in Journal of Lightwave Technology, vol. 34, no. 6, pp. 1516-1522, March15, 15 2016.

CHAPTER 2

BACKGROUND

This chapter contains the background architecture and knowledge for the subsequent chapters. The first section introduces three architectures applicable for optical network cognition and intelligence. The second section discusses the fundamental requirements for driving optical network intelligence. In particular, a knowledge defined network is described in the next section, which is a desirable feature adding to the requirements. Next, the network prediction performance is addressed as the most important factor driving low-margin and proactive optical network design. Subsequently the PLIs that affecting the optical network performance are introduced. The final section introduces the essential ML concepts needed for optimising optical networks. Particularly, Bayesian learning is proposed for sustained learning purpose.

2.1 Cognitive network architecture

For achieving optical networking intelligence, some cognitive network architectures can be utilised [10, 11, 28, 30] in support of the desired learning capability. Learning agents

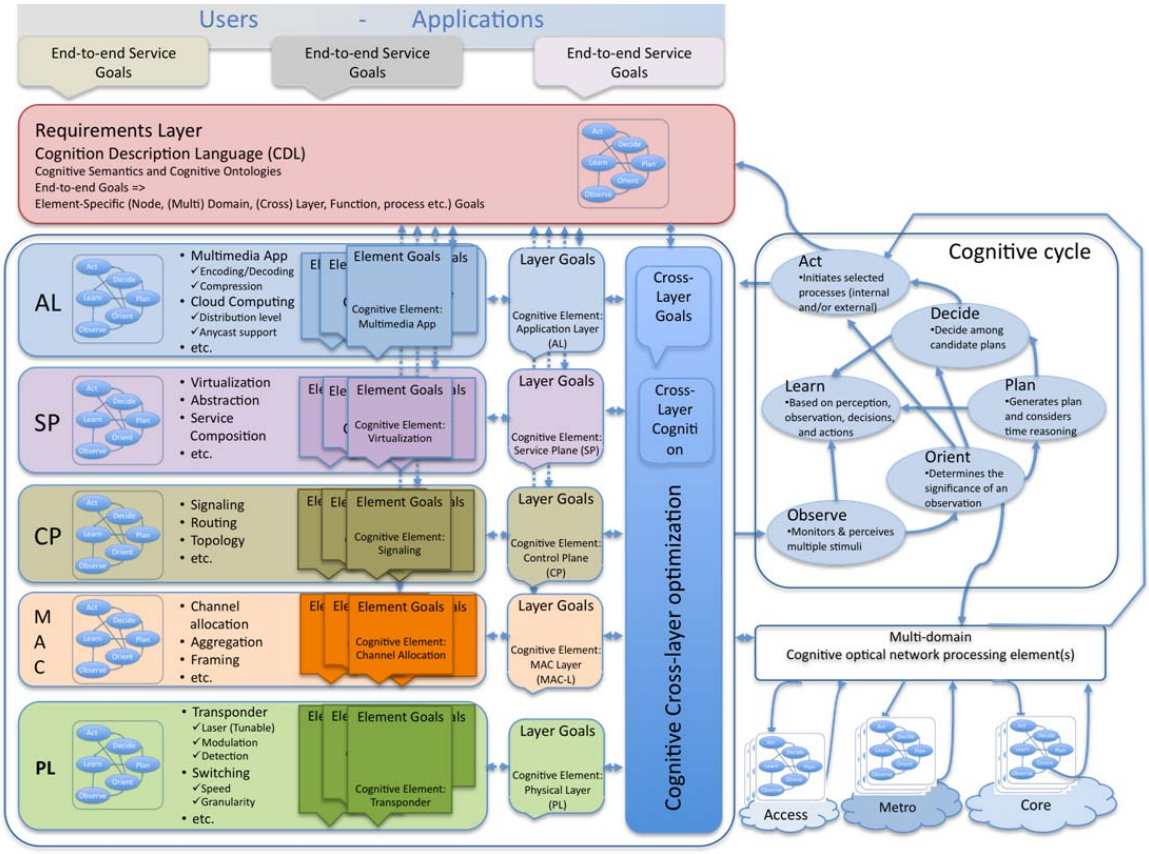

FIGURE 2.1. Schematic cognitive optical network architecture proposed by Zervas et al. [10].

adopting ML can be built either for single layer optimisation, or cross-layer optimisation. It is worth noting that the ML agents are preferred to be integrated in the cognitive architectures, nevertheless, they are not requisite for the architectures.

The first architecture uses a holistic framework in which all the network layers are cognitive [10]. Fig. 2.1 shows the overall architecture. The network consists of the physical layer, the Medium Access Control (MAC) layer, the Control Plane (CP), the service plane, and the Application Layer (AL). Cross-layer optimisation is applied to the holistic architecture for delivering end-to-end performance. The monitoring capability is emphasised to allow for dynamic adaptation of physical layer parameters on demand. The proposed

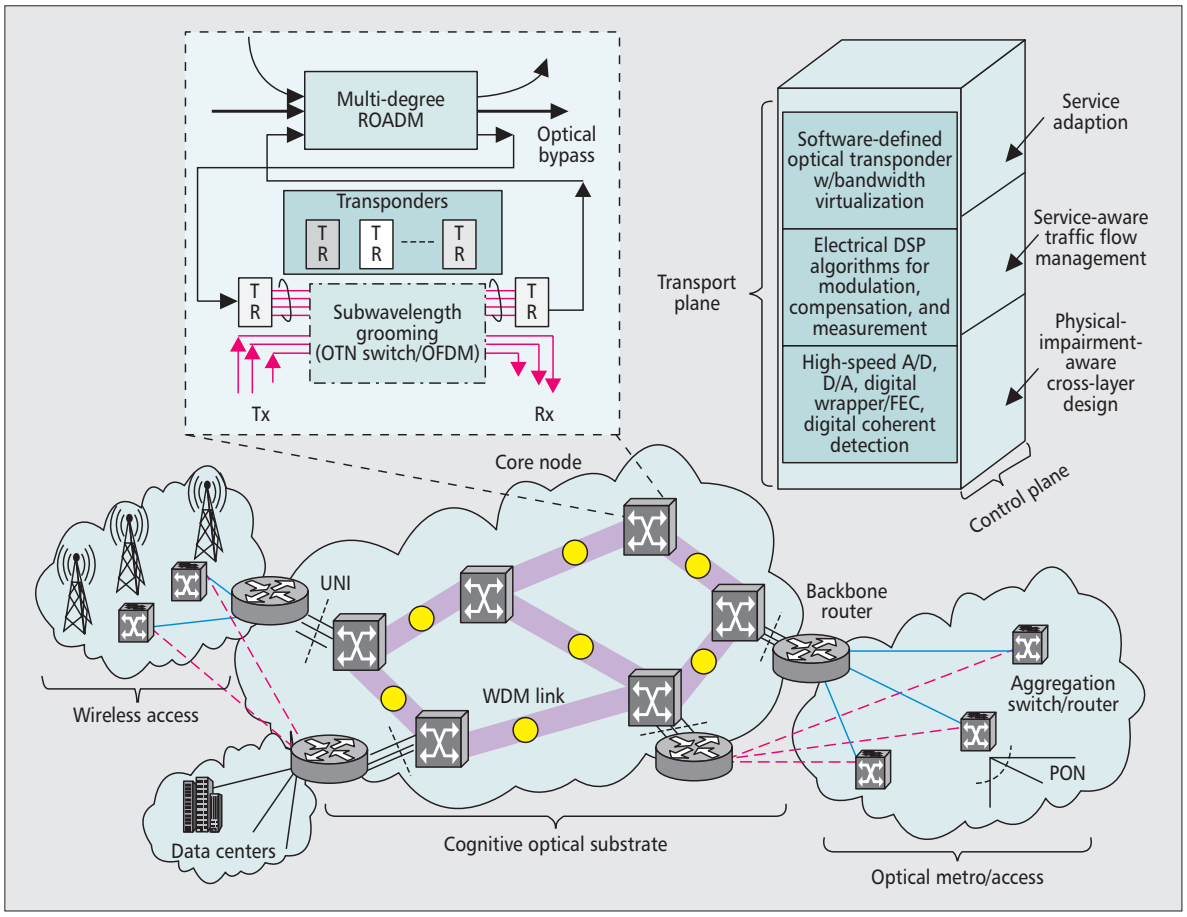

FIGURE 2.2. Schematic cognitive optical network architecture proposed by Wei et al. [11].

architecture is service-oriented thanks to its top-to-bottom design approach. However, the cognitive cycle is represented in the state-space. This is not a good representation in the AI sense. There are too many states and transitions to acquire and reason with. A large change to the state representation is needed even a small change to the model is introduced. Adding another feature means changing the whole representation. For example, to model the traffic demand level so that the network can perform adaptive slicing, every state needs to change. An alternative representation can be feature-based in which the feature values in the next state serves as a function of the feature values of

the previous state and the action [19]. Also, there is no transition going out of the "learn" state in the figure, which makes no sense. Moreover, the multi-domain information exchange can be complex since the control plane design is distributed.

On the other hand, a software-defined cognitive optical network framework is also proposed [11] as shown in Fig. 2.2. The framework consists of the Data Plane, the CP, and the AL. In the data plane, the optical transceivers are programmable and the optical grid is flexible. Impairment compensation modules are available and the monitoring capability is ubiquitous across the network. The CP is responsible for cross-layer traffic management and PLI-aware RWA. The AL employs a client-service-aware approach. It aims to deliver bandwidth on-demand leveraging the network programmability. Compared to the first architecture, this proposal emphasises the device programmability and flexibility. However, the preceding two frameworks do not have a knowledge-based block to convert raw information into useful network knowledge so that the control plane can easily utilise. There is no learning module designed as the "engine" for making decisions.

Moreover, an European project Cognitive Heterogeneous Reconfigurable Optical Network (CHRON) [28, 30] proposes a centralised architecture for cognitive optical networks. Fig. 2.3 shows the schematic architecture. The cognitive decision system forms the most significant part of the framework which makes decisions based on the knowledge bases and learning modules. The learning modules process the data collected from the monitoring systems and generate network knowledge based on ML or data mining algorithms. Various decisions can be made according to the updated knowledge base. For example, decisions such as traffic grooming, virtual topology reconfiguration, RWA, etc.

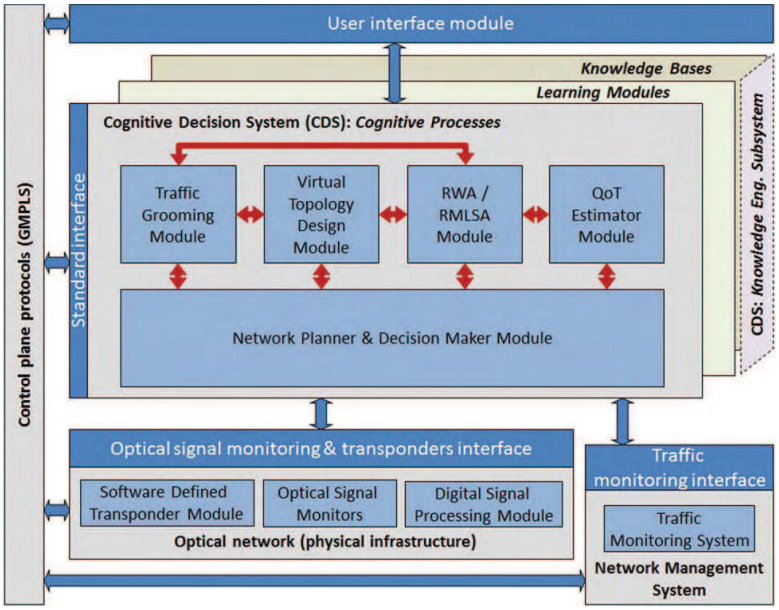

FIGURE 2.3. Schematic cognitive optical network architecture from CHRON [28].

2.2 Requirements for optical network intelligence

Although there are different cognitive architectures for optical networks, some features are in common which form the prerequisites for driving network intelligence.

The first is the monitoring capability, or network telemetry as introduced in Chapter 1. These information are critical for real-time network forecasting and decision-making tasks where ML algorithms are extensively applied. The modern transmission technologies adopt coherent transceivers [31] for beyond 100 Gb/s transmission. Monitoring from the coherent DSP units is available for the key PLIs such as OSNR, Bit Error Rate (BER), CD, PMD, etc. Except for the end-to-end performance monitoring, intermediate node (e.g., amplifiers, ROADMs) monitoring is also proposed as a desired feature to provide more in-depth network information [16, 17, 32]. For example, the authors in [32] proposes a SDN-enabled intermediate node OSNR monitoring to get straight-forward link-level QoT information. In addition, active monitoring with measurement probes [33] is also

proposed in situations where passive monitoring data is not enough. It is anticipated that the learning agent performance can be significantly improved with the ubiquitous monitoring capabilities.

Another prerequisite is device programmability. Software-defined elements are essential to allow optimal decision making based on learning [28]. These programmable elements offer much higher level of flexibility compared to fixed elements. They are capable to be controlled autonomously to adapt to the changing requests. Without such flexibility, it will be challenging for the network to allocate adaptable resources to service demands even intelligent predictions can be made. For example, the software-defined optical transceivers can alter the modulation formats, bandwidth, frequencies, etc. to adapt to the predicted traffic demands. Thus, the QoS and optimum use of the network resource are guaranteed. The device programmability converts the state-of-the art optical modules into cognitive-enabled optical systems [10].

A control mechanism is also essential for driving network intelligence. Both centralised and distributed control mechanisms are applicable. In the centralised design, all the components are under the management of a single cognitive entity. In the distributed design, the cognition capability is distributed among each of the network nodes, efficient exchange of the distribution information is required. Whichever design is used, a control plane is needed to configure the optical devices based on the network status. It serves as the bridge between the real-time network status and the resulting reconfiguration [28].

Last but not least, carefully designed ML algorithms are predominant for network intelligence. It will be discussed in more details later in this chapter.

2.3 Knowledge defined networks

Previous research proposes a Knowledge Plane (KP) for intelligent networks [34] based on ML. KP is also proposed in the CHRON architecture in the form of a knowledge base [28]. The KP offers the opportunity to realise automated network reasoning capability by collecting results from the learning agents. However, KP has not been realistically deployed in optical networks due to the complexity. This remains a big challenge in distributed networks where each node only has a partial view of the entire network. Knowledge that learnt from one domain of the network is very hard to be applied to other domains. Therefore, the Software-Defined Networking (SDN) [35] architecture is preferred to support KP and the learning agents for centralised control. It offers much less complexity due to the common Application Program Interface (API) programmability and separation of the control plane from the data plane [34]. The logically centralised controller serves as a logical single point with knowledge of the whole network. The KP can use various ML approaches to gather knowledge about the network, and exploit that knowledge to control the network using logically centralised control capabilities. SDN is also vendor-technology agnostic which makes the knowledge transfer between different network domains much simpler.

2.4 Network prediction

Given all the criteria described above for driving intelligent optical networks, the dominant factor is the performance of the learning models. A robust learning performance should have high fidelity in making inference on existing data, or predictions on new unseen data. The prediction accuracy is regarded as the most significant KPI for ML models. It benefits many aspects of the optical network design. For example, the design of a low-margin optical network [2].

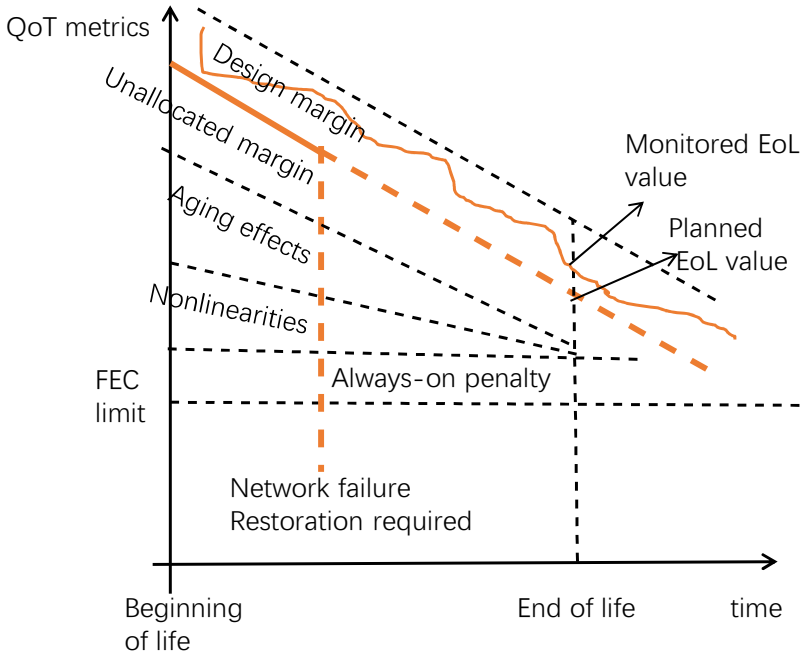

FIGURE 2.4. Margin design of optical networks. The design margin is due to uncertainty, and should be minimised.

As shown in Fig. 2.4, at the Beginning of Life (BoL), the network has many different margins designed for penalties. The always-on penalties refer to the PLIs that are fast time-varying such as PMD, Polarisation Dependent Loss (PDL), etc. The nonlinearity margin is not used at BoL, but as channels are loaded to the network, this margin will be utilised at the network End of Life (EoL). The same applies to the ageing effects. The unallocated margin refers to the difference of capacity/reach between the demand and that of the equipment. It results from the discrete datarate and reach granularity of commercial transmission equipment [36]. Finally, the design margin results from the uncertainty of the network. It is desired that the design margin can be reduced as much as possible.

Due to uncertainty, the network planning models have poor estimation or prediction performance. Reducing the design margin is equivalent to reducing the uncertainty to

improve the model prediction performance. Fig. 2.5 describes the mechanism to reduce uncertainty by monitoring. The inputs to the planning models (typically RWA) contain uncertainties $\epsilon \sim \mathcal{N}(\mu,\sigma)$ (the traffic demand uncertainty results from service heterogeneity). After lightpath provisioning, the uncertainty is updated due to the change of network status (e.g., ϵ_H to ϵ'_H). Then monitoring is used to reduce the uncertainties by proposing new $\epsilon'_{H'}$, ϵ'_D, ϵ'_T. All these uncertainties can be used for quantified design margin evaluation through some models $f = M(\epsilon_H, \epsilon_D, \epsilon_T)$. These new proposals are expected to reduce the design margin, i.e., $f = M(\epsilon'_{H'}, \epsilon'_D, \epsilon'_T) < f = M(\epsilon'_H, \epsilon_D, \epsilon_T)$. Otherwise network failure may happen due to inaccurate prediction. ML models can be used to propose new ϵ, more details can be found in Chapter 5. According to the last figure of [2], up to 50% of the total number of regenerators (depending on the network load) can be saved given accurate prediction performance.

Except for the low-margin design, proactive network design also benefits from model prediction performance. "Proactive" means that rigorous inspection of the network is carried out to look for the causes of a failure before that failure occurs. Many research work exists in the literature which adopts ML for proactive network design. For example, the authors in [25] propose deep learning to predict power excursion in cascaded Erbium-doped Fibre Amplifier (EDFA) systems. It uses the prediction for proactive wavelength assignment. More related work can be found in Chapter 3.

2.5 PLIs affecting optical performance

Prediction for QoT needs to take the PLIs into account. For beyond 100Gb/s transmission, linear impairments such as CD, PMD, etc. can be fully compensated in the coherent receiver DSP unit [31, 37]. Thus, SNR dominates the evaluation of the lightpath QoT. There are three sources of noise that contribute to the SNR degradation: transceiver

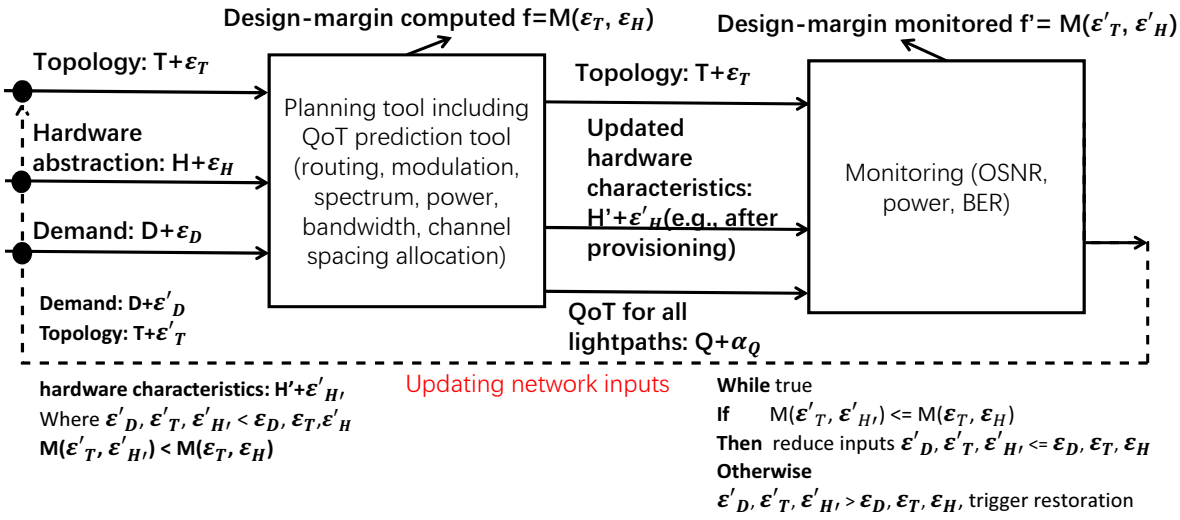

FIGURE 2.5. Reduction of design margin. ϵ represents the uncertainty, mathematically ϵ can be in the form of Gaussian noise $\mathcal{N}(\mu,\sigma)$.

noise, EDFA ASE noise, and nonlinear noise.

Fig. 2.6 shows the relevant noise sources in a transmission system. The linear noise is dominated by ASE noise which is generated by optical amplifiers such as EDFA. The EDFAs are commonly employed in optical networks to compensate for the transmission power losses. The nonlinear noise is due to interference and crosstalk between different optical channels or the channel itself when the signal launch power exceeds a certain limit. Stimulated Brillouin Scattering (SBS), Stimulated Raman Scattering (SRS), Four-Wave Mixing (FWM), Self-Phase Modulation (SPM), Cross-Phase Modulation (XPM) are the most common fibre nonlinearity phenomenon [38]. Operation in the nonlinear regime has become popular in current high capacity optical networks due to advanced modulations and higher bandwidth utilisation [20]. Besides ASE and nonlinear noise, the transmitter and receiver noise also contributes to the total SNR degradation. Transceiver noise comes from Digital-to-Analogue Converters (DAC) and Analogue-to-Digital Converters (ADC) in the transmitter and receiver respectively. The

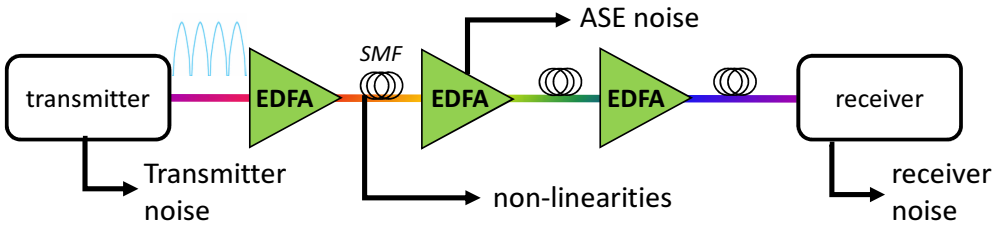

FIGURE 2.6. Noise affecting system SNR performance, SMF: single mode fibre.

achievable SNR performance is upper bounded by the inherent transceiver noise [39].

Gaussian Noise (GN) model has been well proven for its robust prediction performance for nonlinearities [8, 40]. So in this thesis, unless otherwise stated, GN model is used as the analytical model for SNR prediction. In the expression for calculating SNR performance, the total SNR after DSP compensation is

$$SNR_{total} = \frac{P}{\eta P^3 + P_{ASE} + \kappa P} \tag{2.1}$$

where η is the NonLinear Interference (NLI) coefficient in the GN model [8], P_{ASE} is the ASE noise power from all the amplifiers and $\kappa P = {\sigma_{TR}}^2$. By definition the transceiver SNR_{TX} is the maximum achievable SNR a transmission system can have in the absence of ASE and NLI noise. It is quantified as $SNR_{TX} = \frac{1}{\kappa}$. The ASE noise degrades the SNR of the optical signal. The power of ASE is quantified by [8]

$$P_{ASE} = h \cdot v \cdot NF \cdot G \cdot B \tag{2.2}$$

where h is Planck's constant ($6.626 \times 10^{-34} Js$), v is the optical carrier frequency, G is the amplifier gain, B is the noise bandwidth, NF is the Noise Figure (NF). So the ASE power is largely dependent on NF. NF can be influenced by numerous factors such as temperature, input power, pumping current, etc. [41, 42]. η quantifies the intra and inter channel nonlinear noise. The basic assumption is that the signal disturbance generated

by the NLI manifests itself as Additive Gaussian Noise (AGN) [8]. The effective span length is

$$L_{eff} = \frac{1 - \exp(-2\alpha L_s)}{2\alpha} \tag{2.3}$$

where α is the fiber loss coefficient, L_s is the span length. The total nonlinear noise can be computed as the coherent Gaussian noise

$$\begin{aligned} G_{NLI}(f) = \frac{16\gamma^2}{27} \int\int \frac{sin^2(2N_s\pi^2|\beta_2|L_s f_1 f_2)}{sin^2(2\pi^2|\beta_2|L_s f_1 f_2)} * \\ |\frac{1 - exp(-2\alpha L_s) exp(j4\pi^2|\beta_2|L_s f_1 f_2)}{2\alpha - j4\pi^2|\beta_2|f_1 f_2}|^2 L_{eff}^{-2} * \\ G_{tx}(f_1 + f_2 - f) G_{tx}(f_1 + f) G_{tx}(f_2 + f) df_1 df_2 \end{aligned} \tag{2.4}$$

where γ is the fibre nonlinearity coefficient, N_s is the total number of spans, β_2 is the absolute fibre dispersion value, $G_{tx}(f)$ is the power spectrum density and f is the central frequency of the target channel. This equation is defined as the Gaussian Model Reference Formular (GMRF) in its original paper [43]. It represents the power spectral density of NLI noise at the end of a link and it assumes that the spans are identical and the power loss of each span is fully compensated. This equation is derived by modelling a WDM signal as a suitable Gaussian random process whose spectrum is composed of arbitrarily many spectral lines, then using proper ensemble averaging and perturbative techniques. Further details can be found in [44]. Equation 2.4 physically describes the beating of each thin spectral slice of the WDM signal with all others through a FWM process. The term $\rho(f_1, f_2, f) = |\frac{1 - exp(-2\alpha L_s) exp(j4\pi^2|\beta_2|L_s f_1 f_2)}{2\alpha - j4\pi^2|\beta_2|f_1 f_2}|^2 L_{eff}^{-2}$ represents the normalised FWM efficiency of the beating of three pump frequencies $f_1, f_2, f_1 + f_2 - f$. This beating creates an interfering signal at frequency f. The factor $\chi(f_1, f_2, f) = \frac{sin^2(2N_s\pi^2|\beta_2|L_s f_1 f_2)}{sin^2(2\pi^2|\beta_2|L_s f_1 f_2)}$ quantifies NLI accumulation along the link. The term $G_{tx}(f_1 + f_2 - f) G_{tx}(f_1 + f) G_{tx}(f_2 + f)$ governs the power spectral density that each of the three pumps carries.

Equation 2.4 is commonly simplified into the closed form as follows, where P_{ch} is the launch power per channel.

$$P_{NLI} = \eta P_{ch}^3 \tag{2.5}$$

2.6 Machine learning

ML is a cross-discipline subject covering Mathematics, data science and computer science. It teaches a computer program to "learn" from data by optimising its model parameters. Fig. 2.7 shows a schematic overview of ML. As there are too many algorithms, here just a few of them are listed. More algorithms can be found in [45]. ML can be divided into supervised learning (labelled training data is provided as a "teacher" to train the model before making real predictions), unsupervised learning (no labelled data is provided and the model has to find the data structure itself) and reinforcement learning (making software agents to take actions or make decisions based on historic action feedback). Each of the sub-field has a great impact on applications such as CV, NLP, gaming, advertisement, logistics, etc. ML is especially useful when the system is complex, variational and with uncertainties. In this case, performance prediction and network planning become analytically intractable. In optical networks where uncertainties indeed exist, ML algorithms can be empowered by the network monitoring capability to reduce the uncertainties, or the model complexities.

2.6.1 Supervised learning

Supervised learning is a sub-field of machine learning where each given data set is clearly labelled as inputs and outputs. These data is then used to train a typical regression or classification model for future predictions. Fig. 2.8 shows the process of supervised learning, the input training data set is used to teach the learning algorithm to learn a good approximate hypothesis h(x) so that it can predict new y given new x. In regression

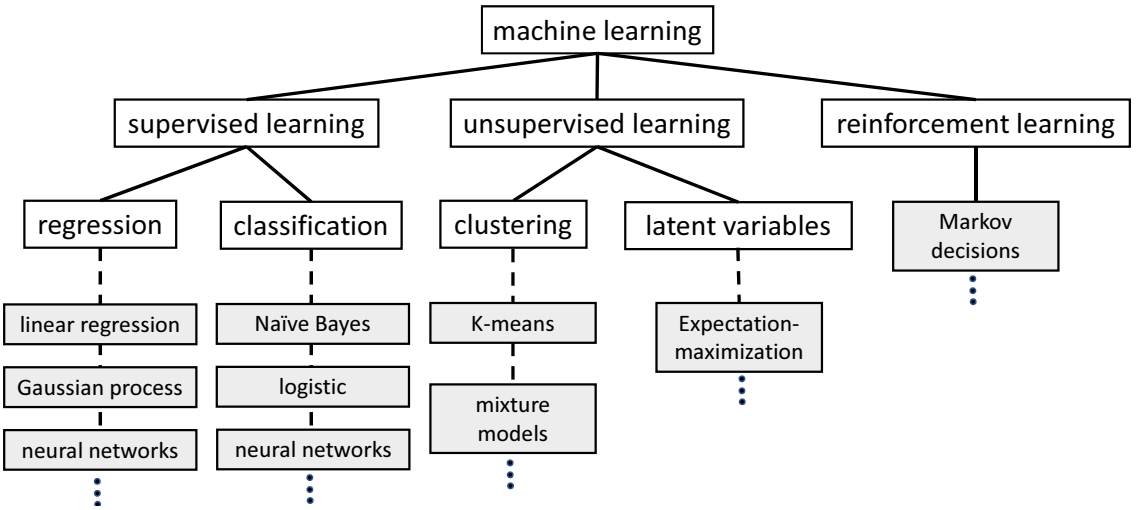

FIGURE 2.7. Conceptual machine learning algorithm overview

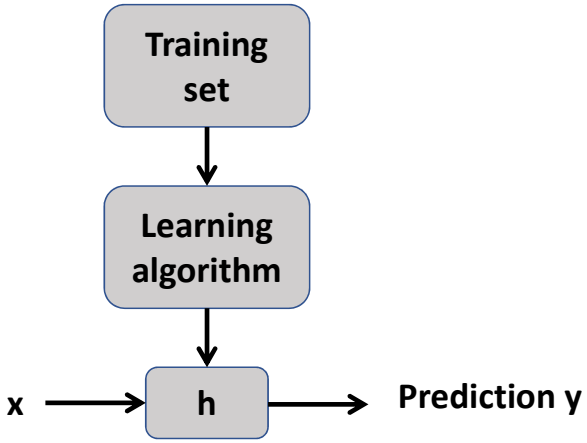

FIGURE 2.8. The process of a supervised learning: given a training set, the learning algorithm is trying to learn a function h so that h(x) is a good predictor for the corresponding value of y.

problems, we are trying to predict a target value in a continuous way, which means we need to map each input feature to some continuous functions. In classification problems, the mapping is made from each input feature to discrete categories. Commonly used supervised learning models are linear regression [46], Artificial Neural Network (ANN) [47], Support Vector Machine (SVM) [48], etc. Supervised learning is particularly useful

for network prediction purposes. Lots of optical network research work adopts this technique. For example, The authors in [7] use neural networks to predict whether the unestablished lightpath Q-factor will exceed a pre-defined threshold or not. The training data input has many attributes such as path length, number of EDFAs, wavelength, etc. The output is just a binary indicator which is 1 if the QoT is sufficient, and 0 otherwise. This is intrinsically a binary classification problem. More related work can be found in Chapter 3.

Supervised learning is particularly useful for prediction purposes and when the training data size is large. If the network can generate large amount of monitoring data, supervised learning is a straight-forward method to reduce traditional model complexity while delivering even much better prediction performance. However, it may suffer from rapid system variation which leads to data distribution mismatch as mentioned in Chapter 1. Its black-box feature is also undesired for system diagnosis.

2.6.2 Unsupervised learning

Unsupervised learning aims to infer a function to describe the hidden structure from a group of unlabelled data. There is no training phase for unsupervised learning and no feedback based on the prediction results, so it allows us to solve problems where there is little or no idea what the result should look like. Clustering [49] is the most common model of unsupervised learning. There are many other algorithms such as principal component analysis [50], Bayesian inference [26], etc. Unsupervised learning is also very useful for optical networks. As an example, the authors in [51] propose a clustering algorithm to autonomously identify the modulation format such as Quadrature Phase Shift Keying (QPSK), 16Quadrature Amplitude Modulation (QAM) without the need to get additional information from the control plane. The digitised I & Q (in-phase and quadrature) samples are used as unlabelled data. K-means clustering algorithm is

applied to identify the modulation by counting the number of clusters in the data set.

Unsupervised learning benefits for tasks such as receiver DSP pattern recognition where the structure of the observed data set needs to be identified. For example, nonlinearity or modulation format identification can benefit from unsupervised learning. It can also make inference of some uncertain network parameters. Since there is no training phase needed, the inference process is on-the-fly which is exactly the desired feature for online, real-time SL. However, unsupervised learning often depends on probability, it may be extremely hard to improve a certain unsupervised model performance because it does not depend on the size of the data.

2.6.3 Overfitting and underfitting

Supervised learning aims to find a target function f which maps the input X to the output Y. An important issue with supervised learning is the model generalisation performance to new data. Generalisation measures how well a supervised learning model can be applied to predict the data that has never seen before. Overfitting and underfitting are the two biggest causes for the poor performance of supervised learning algorithms. If a model has very large training error, i.e., it cannot capture the features of the training data. Then the model is underfitting the training data. Conversely, if the model perfectly matches each of its training data, then it has small training error, but it will not generalise well on new data. So this model is overfitting the training set.

A typical underfitting and overfitting example is shown in Fig. 2.9. Both overfitting and underfitting will cause generalisation error of a ML model. Commonly, underfitting means a model with large bias, while overfitting means a model with large variance. There is a fundamental trade-off between overfitting and underfitting. If the learning model is too simple or has too few parameters, then it is likely to have large bias

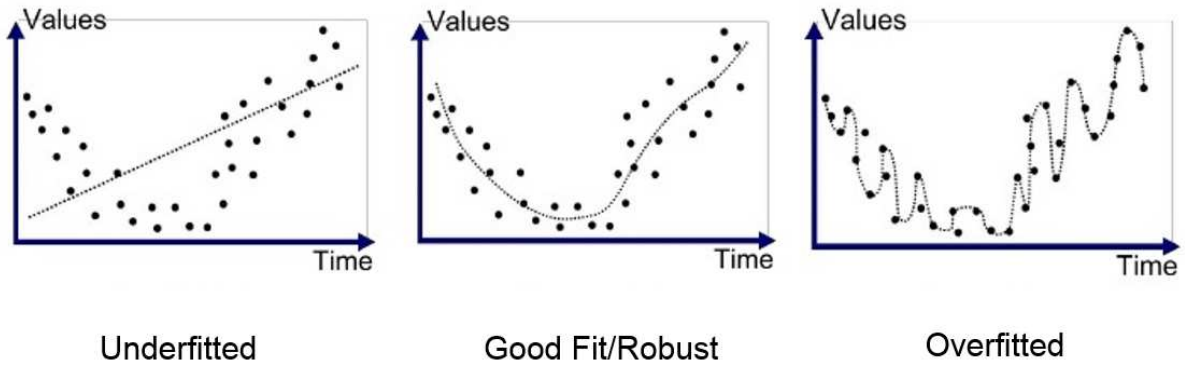

FIGURE 2.9. The left hand side figure is underfitting the data, or with high bias, conversely, the right hand side figure is overfitting the data, or with high variance. The middle figure captures the data best.

(underfitting). If a learning model is too complex and has too many parameters, then it may suffer from high variance (overfitting) [52]. Cross-validation is a prevalent method for rectifying the bias and variance of a learning model. It randomly splits the training data into k subsets, then the randomly chosen $k-1$ subsets are used to train the model, and the remaining one subset is used to calculate the development error or validation error. This is process is repeated until the lowest development error is found.

When designing a supervised learning model for network prediction purpose, it is important to assess its bias-variance or generalisation performance. It directly affects the accuracy of the model. Model selection is the research field to tackle this problem, however, it is beyond the scope of this thesis.

2.6.4 Bayesian statistics

There are always debates about the frequentist and Bayesian models in the ML field. In the frequentist point of view, the parameters of a learning model are fixed. It just

happens to be unknown, and the job of the supervised learning is to estimate the unknown parameter using methods such as Maximum Likelihood Estimation (MLE). An alternative way is to take the Bayesian view. In Bayesian methods, the parameters of a model are randomly distributed. After updating "belief", they follow some probability distributions. Often a prior knowledge of our "belief" about the parameters should be given. After some observations, we can compute the posterior distribution of the parameters. Bayes' Theorem is the fundamental theory that supports Bayesian statistics. It is often expressed in conditional probability

$$p(\theta|y) = \frac{p(y|\theta)}{p(y)} \tag{2.6}$$

where p(.) denotes a probability distribution, p(θ) is the prior distribution, p($y|\theta$) is the likelihood distribution, and p($\theta|y$) is the posterior distribution. Most of the times, the so called Maximum A Posteriori (MAP) estimate value is used for a single value estimation:

$$\theta_{MAP} = \arg\max_{\theta} \prod_{i=1}^{m} p(y^{(i)}|x^{(i)},\theta)p(\theta) \tag{2.7}$$

where $p(\theta)$ is the prior. In practice, the prior is often assumed to be Gaussian distributed $\theta \in \mathcal{N}(0, \tau^2 I)$. This choice of prior will result in smaller norm than MLE, which makes Bayesian MAP less susceptible to overfitting. In this thesis, Bayesian methods are the main methods used for sustained learning purposes due to its less requirement for large dataset and less susceptibility to overfitting.

CHAPTER 3

LITERATURE REVIEW

This chapter reviews recent published work on applying AI and ML algorithms in optical networking. Fig 3.1 shows a summary of published AI and ML techniques applied to optical networking. The application can be roughly divided into two categories: the physical layer domain and the network control domain. The goals for applying AI and ML models in these domains are, firstly, to make predictions combating the increasing uncertainties of the system in which many non-deterministic factors take place. Secondly, to make optimal decisions in some complex cases that have to depend on data. Thirdly, to recognise certain patterns which are subject to dynamic changes.

3.1 Physical layer domain

This section describes AI applications in the physical layer of optical networks. This involves characterising QoT performance as well as the device operation performance.

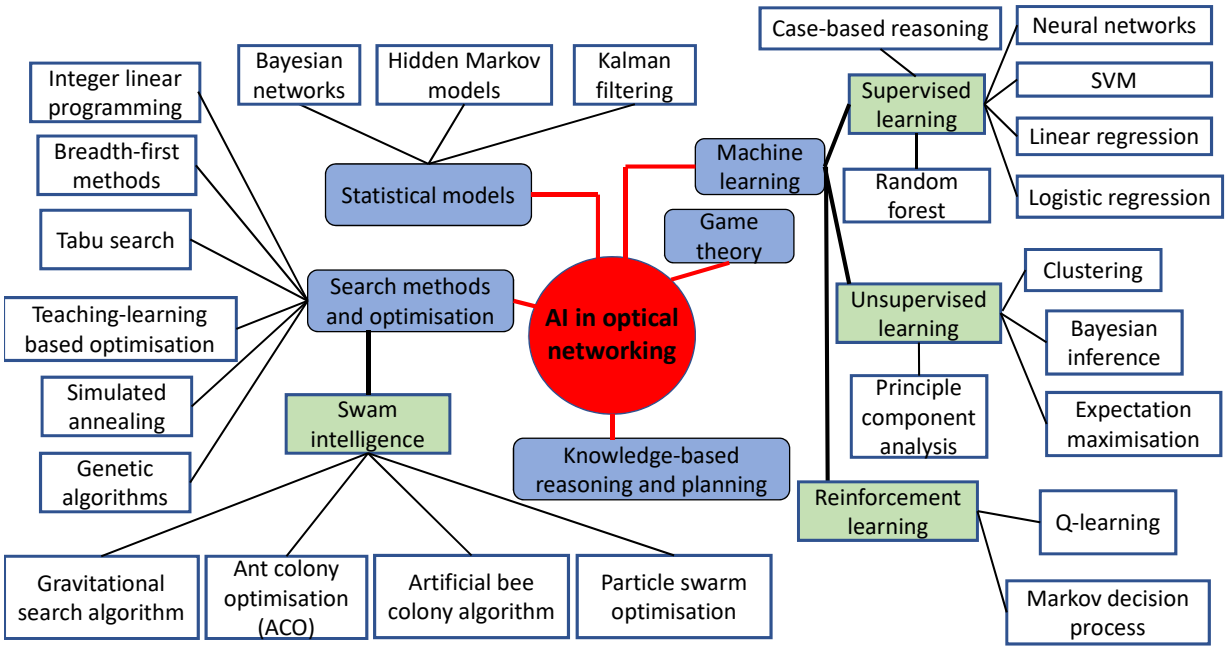

FIGURE 3.1. Schematic diagram of AI techniques applied in optical networking, the machine learning branch will be the focus of this thesis.

3.1.1 Optical performance monitoring

Optical Performance Monitoring (OPM) is essential for real-time device-level and network-level control applications. The field of OPM has embraced extensive ML approaches. Most of the work is done at the receiver side for estimations of the target features such as OSNR, CD, PMD, etc. In particular, Artificial Neural Network (ANN) is well suited for estimating the target value due to its ability to learn the complex mapping between the received samples and optical transmission parameters. The authors in [53] present a comprehensive method using the ANN model to simultaneously identify the OSNR, CD and PMD from eye-diagram parameters in 40 Gb/s On-Off Keying (OOK) and DPSK systems with high correlation coefficients. This transforms the receiver side DSP problem into pure pattern recognition tasks in computer vision. With the advances of deep learning, it is anticipated that traditional ANN models will be replaced by the state-of-the-art

deep learning models. In particular, Convolutional Neural Network (CNN) [21] is a good candidate to reach the ultimate goal.

The input feeding to the ANN model can come from different sources to predict target features. The power eye-diagrams such as Q-factor, closure, variance, root-mean-square jitter and crossing amplitude are applied in [54–58] as the inputs, two-dimensional eye-diagram and phase portrait are used as the inputs in [58], the authors in [56] use the asynchronously sampled amplitude histogram as the ANN input. As the ANN hidden layer is shallow, the model is easy to be trained because a small number of training data is sufficient. Another approach is to pass the samples at symbol level and to use Deep Neural Network (DNN) [23], this will require a large number of training data (at million level). As aforementioned, such number of training data is difficult to obtain, especially for SL.

A DNN method to predict OSNR in the coherent receiver DSP unit is proposed in [59]. The model takes asynchronous sampled dataset from ADCs as the input for training the DNN. The model has at least five hidden layers and needs to be trained with at least 400,000 training samples to achieve target OSNR prediction accuracy. Although not mentioned in the paper, more than 10,000 parameters (ReLU) need to be tuned during training. Such complex training phase results in the model with little scalability to other systems. The poor scalability also becomes serious as the network changes because the model has to be trained from scratch.

Apart from using ANN or DNN model for optical feature estimations, the authors in [60] propose Kalman filter for carrier phase tracking, polarisation tracking and estimation of the first-order PMD. It is further shown in [61] that Kalman filtering can track and compensate nonlinear noise such as XPM. However, most of the above mentioned ML-based OPM techniques need prior knowledge about the signal such as its data rate

for modulation format, this requires additional cross-layer communication to obtain this information from upper-layer protocols which can significantly increase the node complexity. A technique is proposed in [62] for simultaneous multi-impairment (OSNR, CD and PMD) monitoring and autonomous bitrate and modulation format identification. The key algorithm that enables such flexibility is Principal Component Analysis (PCA)-based pattern recognition. Given a set of images represented in a high-dimension image space, PCA finds a small set of orthonormal eigenvectors spanning a subspace. In this way, PCA can reduce the dimensionality of an image space without losing much information. This method is beneficial for real-time, online physical layer autonomous monitoring. Further work can be carried out to integrate such autonomous monitoring capability into the aforementioned cognitive or SDN architectures.

3.1.2 QoT estimation

The capability of QoT prediction for a new lightpath prior to provisioning is essential to guarantee proactive and low-margin network design [2]. Existing analytical models are able to provide accurate QoT prediction results, but they come with very high computational complexity [8]. Some solutions have lower computational complexity, but they often over-estimate the QoT penalties leading to under-utilisation of network resources [2, 27]. Under such motivation, ML models are introduced to balance this complexity and accuracy problem.

A cognitive Case-Based Reasoning (CBR) method is proposed in [63] to estimate QoT based on historically observed data. It uses a knowledge database to store all the historical information of a lightpath including Q-factor, route, wavelength, total length, number of co-propagating channels in a link, etc. A new request QoT is determined by computing the similarity (Euclidean distance) between the new channel's information and the

database through CBR-based classification. The optimisation process of the knowledge database is further studied in [28] to trade-off the database size and computational complexity. In practice, the use of CBR is not restricted to QoT prediction. CBR can also be used for converged learning purpose for different networks due to its domain knowledge agnostic nature. For example, the knowledge learned from wireless networks can be mapped to the optical domain to solve new but abstractly similar problems. Ontology [64] is essential to abstract the correct network knowledge for such purpose.

A similar database oriented ML approach is also proposed in [24] where a Network-scale Configuration and performance Monitoring DataBase (NCMDB) is used to store all the offline monitored network metrics such as laser info, EDFA gain, power, OSNR, etc. A Multi-Layer Neural Network (MLNN) is used to predict any future request QoT based on offline training. However, the relatively small training data size and the offline training mechanism are hard to capture the dynamicity of modern optical networking systems. Also, the MLNN used in the paper only have one hidden layer, which is too shallow to capture a complex system behaviour. It is anticipated that more hidden layers and more training data will help to improve the prediction performance.

MLNN based QoT prediction has drawn significant attention recently due to the well-proven power of deep-learning in other fields such as CV [65] and NLP [22]. The authors in [7, 66] propose feed-forward Neural Network (NN) to predict whether future request QoT will exceed a pre-defined system threshold or not based on metrics such as path length, the number of EDFAs, maximum link length, wavelength, etc. Training techniques are emphasised to prevent over-fitting by using mini-batches, dropout, etc. An end-to-end deep learning solution is proposed in [23] to model the Intensity Modulation/Direct Detection (IM/DD) communication systems which are commonly used in data-centre and metro networks. The model uses a block-based transmitter design to allow massive parallel processing of the single block messages. Each message is encoded

into a single one-hot vector and fed into a single MLNN. These MLNNs are then connected to the transmission link. The receiver side uses reversed MLNN architecture of the transmitter side to decode the message. The model is shown to achieve BER of below the 6.7% Hard-Decision Forward Error Correction (HDFEC) threshold and information rate of 42Gb/s can be transmitted beyond 40km. Although these work could be a good trial exploring end-to-end deep learning applications in optical networking, such method tends to treat the whole optical communication system as a black box and ignore any prior system models. This is a great waste in terms of prior system design knowledge. More importantly, the final communication system represented by deep learning model will be very hard to inspect. Engineers have no idea what is happening inside the system because of its end-to-end black box nature. Such an empirical system design without any optical domain knowledge is not preferred.

Apart from NN based approach, other ML methods are also proposed. A Gaussian Process (GP) based OSNR regression technique is demonstrated in a field trial [67] to combat the noise spectrum non-uniformity problem across a broad wavelength range. GP samples stochastic functions of the transmission link conditioned on monitored SNR data. Two important features of GP make it suitable to predict QoT. First, because the data monitoring process is inherently noisy in which the data output fluctuates around its mean value, GP models the noisy monitoring data by adding additive Independent and Identically Distributed (IID) Gaussian noise to the mean value. Given this IID noise, the final regression curve does not necessarily pass through each training point. Second, the kernel assumption of GP measures the similarity or correlation between any training points by using the kernel matrix. For example, if two wavelengths are close to each other, their SNR performances should be nearly identical given their lightpaths are the same. If two wavelengths are far from each other, their performances are less correlated. This work forms the fundamental work supporting multi-link QoT computation in optical

networks. Unlike other offline training ML models, GP is inherently an online training model. This means the learning model can take as input the real-time monitoring data and easily adapt to any system variation while the network is evolving.

A "learning, living" network is proposed in [68] by monitoring the link-level BER performance of selected wavelength and performing linear regression to estimate new service request OSNR. The model can learn path-level OSNR performance by summing up link-level performance. However, there could be a problem with this model. The per-span OSNR update rule is likely to spread one particular span OSNR degradation to multiple spans. In other words, when a single link fails (introducing large noise), the learning process will average this penalty to each traversing link. This is not a practical way to solve the operational uncertainties in the network. It can lead to under-estimation of per-span (or per-link) OSNR performance. Moreover, using linear regression to estimate new service OSNR can easily underfit the training data. This work intrinsically only utilises monitoring without any ML methods. Another QoT estimation work is proposed in [69] to apply Random Forest (RF) classification algorithm to predict the probability of whether an un-established lightpath BER will exceed a pre-defined threshold or not. The input of the RF model includes the length of the path, span numbers, baud rate, modulation format, bandwidth. Several combinations of the input features are considered and the algorithm identifies the ones that will be most likely to meet the BER requirements. However, attention should be paid to the computational complexity of RF when the number of sub-trees increases.

In addition to passive monitoring, active probe based monitoring is also used to assist ML models. The authors in [70] and [71] propose Network Kriging (NK) and norm L2 minimisation as the theoretical algorithm for improving the network knowledge gain with as few monitoring trials as possible. These techniques are further applied in [72, 73] for network-scale lightpath QoT prediction. NK and L2 norm help to select the most

informative monitoring path and minimise the number of active probes by using linear algebraic matrix computation. However, as active probe method sends additional signals without carrying meaningful service data, the method tends to increase network blocking probability and occupy valuable bandwidth resources. The trade-off between placing the probing signals and the prediction accuracy is studied in [74]. Moreover, the assumption in [72] that the impairments are flat across the transmission spectrum is not always true [75]. Such uncertainty problem will be addressed in Chapter 7. Last but not least, the computational complexity of NK is high for large-scale networks [76], an alternative way is intermediate node monitoring [6, 77].

3.1.3 EDFA control

EDFA is one of the fundamental components enabling optical long-distance transmission thanks to its low induced ASE noise. Completely characterising the operation performance of EDFA needs a huge amount of fine-grained offline measurements which is time-consuming. To combat the uncertainties brought by temperature, pump power, loading states, ageing, etc., the performance of EDFA is extensively modelled by ML algorithms which can interpolate the mapping function over points that are not pre-tested. A Kernel-Based nonlinear Regression (KBR) method is proposed in [78] to model the power excursion of a cascaded EDFA system. The model takes as the input all the combination of channel allocation with 20 slots, and it outputs the standard deviation of the power excursion with respect to a new input combination. Given a new network loading state, it can predict the power excursion from how similar the loading state is with the training data (kernel assumption). As this work is done with only fixed grid, to make it more adaptable to flex-grid networks in which dynamic defragmentation is often applied, the authors of [79] further extends this work by formulating a Ridge Regression (RR) model together with a logistic classification model to determine the contribution of each

spectral granularity to the post-EDFA discrepancy. According to the prediction model, intelligent pre-adjustment strategies can be applied for spectrum defragmentation and wavelength assignment. Moreover, a multilayer perceptron neural network is proposed in [80] to achieve intelligent adjustment of EDFA operating point for optimising both the EDFA NF and the ripple of the frequency response of the system. This idea is originated from the cognitive EDFA control concept proposed in [81]. Such concept is further used in [25] which proposes a deep NN to predict the power dynamics of a 90-channel ROADM system. The learning model uses the most advanced deep-learning training techniques such as ReLU activation function (to overcome gradient vanishing problem), batch gradient descent (to overcome slow training), etc. The model is shown to enhance power excursion prediction with 0.1dBm mean squared error in a 90-channel Dense Wavelength Division Multiplexing (DWDM) transmission system including eight EDFAs, hence allowing rapid wavelength switching operations. All these work aims to achieve proactive network decision-making utilising the robust model prediction performance. However, these models lack self-adaptability as they are trained in an offline fashion. Online learning is hard especially for the deep learning model proposed in [25] due to the lack of data.

In addition to characterising EDFA output power performance, the authors in [82] uses MLNN model to map the EDFA input/output power to NF and gain flatness. It demonstrates MLNN can be used as an auxiliary tool to characterise EDFA while eliminating large number of pre-testing points. The method results in a gain prediction error as low as 0.1dBm. Unlike other black box methods, this work studies the insights of the EDFA device characteristics leveraging ML, which is a great advantage for system design in the optical domain.

Instead of offline training and testing, the CBR model is applied in [83] in dynamic network scenarios. Upon arrival of a new lightpath request, a knowledge database is

created which stores the amplifier gains of established lightpaths corresponding to the lightpath information such as OSNR, number of links, total length, etc. CBR retrieves the entries of the database with the highest similarity compared to the incoming lightpath. The vectors of gains of respective EDFAs are temporarily chosen and a new choice of gains is generated by perturbation of such values. Then, the OSNR value that would be obtained with the new vector of gains is estimated by simulation. The vector associated with the highest OSNR is considered for tuning the amplifier gains when the new lightpath is established. This method is inherently an online learning mechanism that can robustly combat system operational uncertainty. Since OSNR only accounts for the linear regime, further work should be focused on addressing nonlinearity.

It can be seen that in the studies of EDFA, frequentist methods are used mostly while Bayesian methods are rarely used. It is due to the fact that EDFA power excursion problem has no theoretical models that can be used as likelihood function. Therefore, even there is prior knowledge about the EDFA (gain flatness or NF), the posterior estimation is unavailable under uncertainty.

3.1.4 Receiver nonlinearity mitigation

The information capacity of current high-speed optical long-haul transmission systems is limited by the nonlinear noise mainly due to the fibre Kerr effect. Huge research effort has been focused on mitigating the nonlinear noise [37]. Traditionally, detecting and compensating for nonlinear noise is done by analytics or deterministic information of the fixed fibre link. For example, the digital back-propagation [84] or stochastic digital back-propagation [85]. But due to the computational complexity, these methods are difficult to be practically implemented in real networks.

To combat the complexity issue of analytical methods, ML methods are investigated in

the receiver DSP to enhance symbol detection and mitigate nonlinearities. The authors in [51, 62] propose a cognitive DSP based receiver which is able to identify the modulation format such as QPSK, 16QAM without the need to get additional information from the control plane. Unsupervised clustering algorithms and PCA based dimension reduction are used to achieve this automation. Moreover, Bayesian filtering and Expectation Maximisation (EM) together with state-space models are proposed in [61] in which the underlying physics and optical components are taken into consideration during the formulation of DSP algorithms. The method achieves carrier recovery, XPM induced polarisation scattering and nonlinear phase noise mitigation. However, as the training of the EM algorithm depends on the state-space transmission link characteristics, the method is difficult to be practically used in dynamic optical networks under uncertainty.

Classification algorithms are also used to mitigate nonlinearities. Support Vector Machine (SVM) classifier is implemented in [86] in the coherent receiver DSP to mitigate NonLinear Phase Noise (NLPN) which affects detection of M-ary phase shift keying (M-PSK) signals. The SVM model is used to identify nonlinear decision boundaries that allow bypassing the errors induced by nonlinear impairments in the constellations of M-PSK signals. The optimised system has improvements in both launch power dynamic range and maximum transmission reach. However, as a binary classifier, the proposed SVM model cannot deal with higher order modulation formats. Further work should be carried out using multi-class SVM.

To make the ML model independent of transmission link characteristics and modulation formats, an unsupervised K-Nearest Neighbour (KNN) model is demonstrated in [87]. Only a small labelled data set is needed to learn the link properties and make decisions on the nonlinear boundaries. By performing multi-class classification, the model can simultaneously detect multiple kinds of modulation formats. Maximum transmission distance and nonlinear mitigation improvements are demonstrated in a 16QAM coherent

transmission. Following this, [88] proposes a non-symmetric demodulation technique in the coherent receiver DSP based on k-means clustering algorithm. The model mitigates the effect of time-varying impairments such as the imbalance of in-phase and quadrature signals, bias drift and phase noise. The demodulator is shown to be computationally efficient and transparent to the nonlinearity source. Recent research [89] further extends this method in more advanced systems with Coherent Optical Orthogonal Frequency Division Multiplexing (CO-OFDM) technologies. The proposed approach uses a nonlinear equaliser SVM of reduced classifier complexity to mitigate inter-subcarrier nonlinear crosstalk effects which further allows larger launch power. To mitigate nonlinearity in OFDM systems, the authors in [90] uses ANN for nonlinear equalisation. Each subcarrier is trained and detected by one ANN where the number of neurons is equal to the number of symbols. As the training process is computationally too expensive for so many ANNs, an Extreme Learning Machine (ELM) equaliser is proposed in [91]. ELM solves the computation complexity issue by using a generalised matrix inversion to compute the neuron weights without needing any weight optimisation step (such as gradient descent and back-propagation). ANN is also proposed in [92] for jointly estimating both linear and nonlinear noise. The input to the ANN has features such as the normal and tangential components of the noise variance, CD, number of channels. etc. The output consists of two neurons for linear and nonlinear SNR values. This work is particularly useful to separate linear and nonlinear noise. It forms the foundation for in-depth network diagnose and nonlinearity aware RWA tasks [93].

The learning performances of different ML models, e.g., SVM, ANN, KNN, etc., need to be compared in terms of complexity, data size requirement and accuracy. It is also interesting to study the impact of deep learning on nonlinear mitigation because it has already revolutionised many other fields [21, 22].

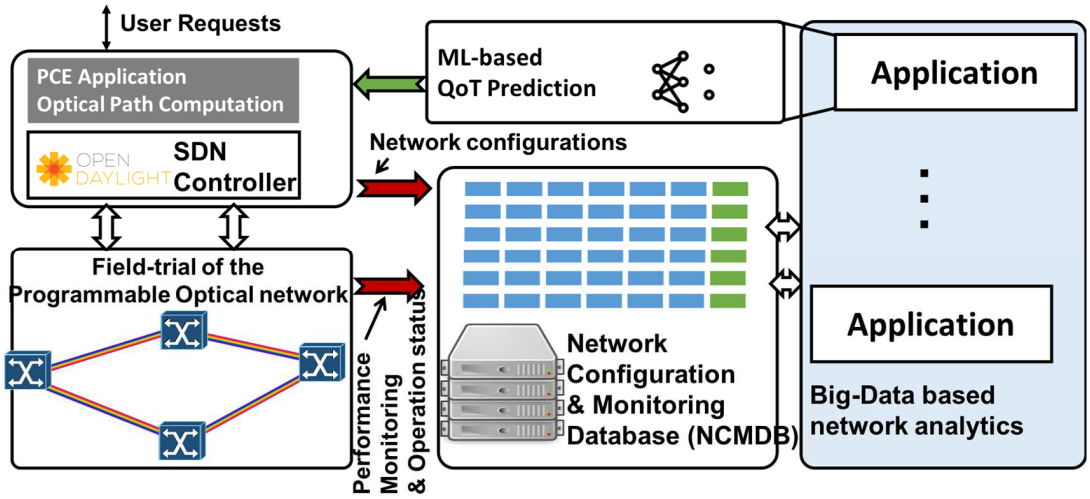

FIGURE 3.2. Schematic diagram describing the function of SDN control plane comprising AI algorithms and policies for intelligent optical networks planning.

3.2 Networking domain

Learning agents can serve as the control plane management applications for network optimisation. Various ML models and policies can be dependent on the application use cases. Therefore, as shown in Fig. 3.2, the next generation optical networks control plane is expected to have a large scale learning agent repository containing different ML algorithms and policies. For efficient global network optimisation, SDN is preferred [94]. The control plane acts as the brain of the network that regularly interacts with the underlying data plane such as transponders, EDFAs, ROADMs, etc. This is to automate operations and make intelligent decision making during dynamic control and management of network resources.

3.2.1 Traffic prediction for virtual topology design

Traffic prediction is an important capability enabling flexible virtual resource allocation and dynamic network planning. Virtual topology is the set of lightpath connections in the

optical network. It can be dynamically reconfigured to adapt to changing traffic demands subject to QoT constraints, delay requirements, etc.

A supervised learning method, Auto-Regressive Integrated Moving Average (ARIMA), is proposed in [95, 96] for traffic forecasting. The algorithm is applied to the time-series data which is the real-time traffic matrix observed over a window of time just prior to the current period. Accurate short-time traffic prediction is used to perform virtual topology reconfiguration. The authors also propose Network Planner and Decision Maker (NPDM) module to support the ARIMA. The NPDM interacts with other modules to do virtual topology reconfiguration. The relatively low computational complexity of ARIMA makes it attractive for real-time prediction purposes. However, the model performance is not compared with other learning methods, for example, NN model. Hence it is hard to justify that ARIMA is the most effective method. To tackle the same problem, i.e., virtual topology reconfiguration, NN model is proposed in [97, 98]. A decision maker module is proposed to take the input from the prediction of the source-destination traffic matrix for the next time period which is based on the output of the NN model. The decision maker determines whether the current Virtual Network Topology (VNT) needs to be reconfigured or not based on the matrix. Because of the better prediction accuracy (less than 3% error) and adaptability to changes in input traffic, NN model is preferable than other models. However, as traffic patterns become heterogeneous, the size of the NN model needs to increase in terms of its hidden layers, the number of neurons, etc. For example, deep Recurrent Neural Networks (RNNs). This will leads to increasing demand for larger training dataset. The training phase will become too computationally complex to meet the real-time prediction requirement.

Except for supervised learning, unsupervised learning, such as Bayesian inference, is also proposed [99] for VNT reconfiguration. The authors develop a VNT reconfiguration framework without the need for the traffic demand matrix. A set of "good" virtual

networks are memorised, each of which works well for a certain traffic situation. One of the candidate virtual networks is retrieved for the current traffic pattern through Bayesian inference. The results demonstrate that Bayesian inference can identify the traffic situation using the incoming/outcoming traffic at edge routers which is easier to get access to than the traffic demand matrix. This method is inherently a reactive way of performing VNT reconfiguration, which is less preferred to the proactive way using prediction.

Besides designing VNT reconfiguration algorithms, the framework that supports such capability is also proposed. To formalise the infrastructure of ML-based traffic prediction for VNT reconfiguration, the authors in [100] proposes a cognitive network management module correlated to the Application-Based Network Operations (ABNO) framework. The proposed big data network management architecture can support VNT adaptability based on traffic prediction by applying data analytics to the monitored traffic data. Focused on the same cognitive idea but without monitoring, a multi-objective Genetic Algorithm (GA) for virtual topology design in which the principle of reinforcement learning is applied in [101, 102]. The authors use previous solutions of the GA for virtual topology design to update the fitness function for future solutions. This analytical and learning hybrid method can "teach" the control plane to achieve better decision-making performance. The genetic algorithm is a search heuristic for optimisation tasks which does not belong to ML. However, for proactive VNT provisioning, traffic prediction capability is essential in which ML serves as the fundamental method. The prediction is often built with time series data.

Recently there are concerns about whether the modern ML and DL methods will perform better than traditional time series forcasting methods such as ARIMA. Recent study [103] has demonstrated that traditional time series forcasting methods outperform complex and sophisticated methods, such as decision trees, Multilayer Perceptrons (MLP), and

Long Short-Term Memory (LSTM) network models. This finding could have a great impact in field of VNT.

3.2.2 Failure and anomaly detection

This area of application aims to use ML models to localise, identify and predict a certain network failure in terms of location, time, or type of failure. In [70, 104], network kriging is proposed to localise the exact position of malfunction along network links. This method uses the monitoring information at the receiver side of already established lightpaths route, when the exact localisation cannot be computed, active probes may be sent to provide the lacking information. The way of choosing the probe signal is by maximising the rank of the routing matrix. Depending on the network loading status, the number of monitoring nodes necessary to ensure unambiguous localisation is evaluated. The necessity to introduce network kriging is because intermediate node performance is unknown such that link performance is sometimes ambiguous. Network kriging aims to solve such problem by indicating the minimum number of effective monitoring probes in order to minimise the ambiguity or maximise the network knowledge gain. As aforementioned, intermediate node monitoring can be a good alternative to obtain the lacking information. More details can be found in Chapter 6 and 7.

A combined ML solution in [105] comprising clustering algorithm and Bayesian networks is proposed to identify and localise failures in VNT that can lead to an unacceptable QoS. Experimental characterisation of several causes of failure is clustered to train the Bayesian network which is further used to identify and localise the most probable cause of failure impacting a given service. The authors in [105] applies Bayesian network which can identify whether a fault is occurring along the lightpath. If so, the type of the fault (such as tight filtering or channel interference) can also be detected. The input of the Bayesian network consists of time series measurement of BER and received power

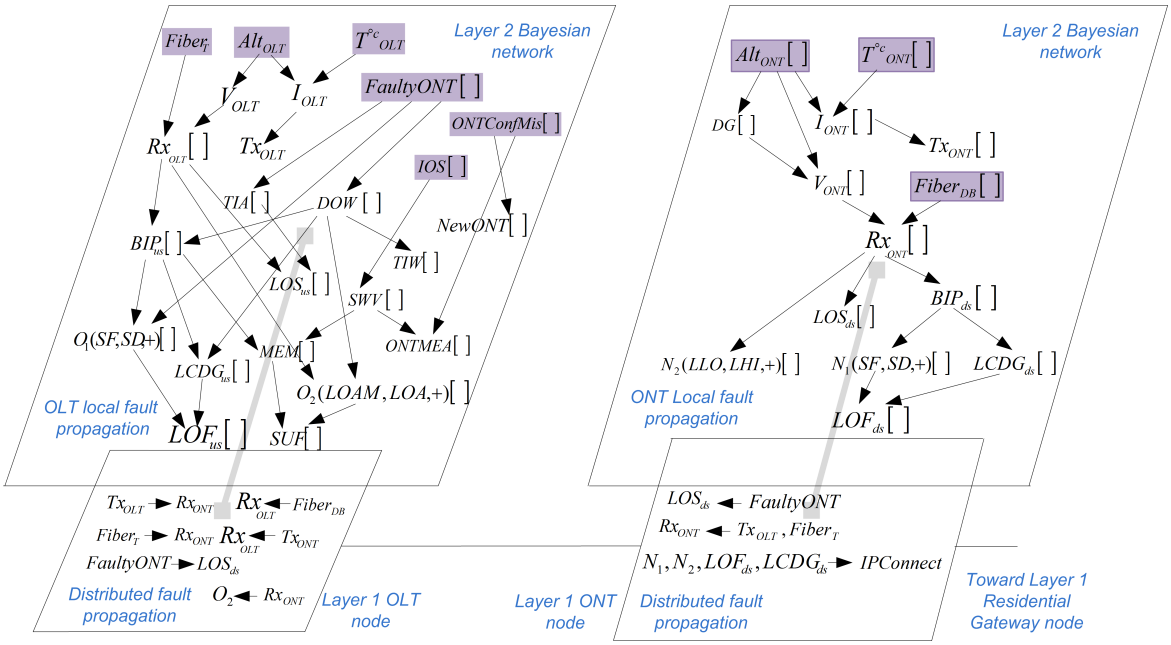

FIGURE 3.3. The GPON-FTTH model based on Bayesian network. The figure is taken from [106], detailed explanation of the abbreviations can be found in [107].

at lightpath end nodes. An identification decision is made based on the monitoring patterns such as maximum, average and minimum values, presence and amplitude of steps. Experimental results show that the classification error of Bayesian network is only 0.8%. However, the method needs previous offline training data available in order to locate different causes of failures. As the soft failures such as frequency drift may not happen frequently, the training data is often unavailable.

Other Bayesian methods are also proposed to infer and detect faults in optical networks. As in [106, 108], a self-diagnosis solution using EM algorithm and Bayesian network is proposed for Gigabit Passive Optical Network-Fibre To The Home (GPON-FTTH) access network. The GPON/FTTH network is modelled as a layered Bayesian Network as shown in Fig 3.3. Layer 1 of the system is the physical network topology of Optical Line Terminals (OLT), Optical Network Terminals (ONT) and fibre. Fault propagation between

different network components is modelled in layer 2 using a set of Directed Acyclic Graphs (DAG) interconnected through layer 1. The strengths of dependencies between layer 2 nodes with conditional probability distributions are quantified to estimate the fault propagation uncertainties. To cope with the missing data due to improper measurements, EM algorithm is used in which the missing data is inferred such that the estimation maximises the expected log-likelihood function (maximum likelihood). As can be seen in Fig 3.3, the Bayesian network has lots of dependencies between each other, errors may easily propagate along the network which may lead to inaccurate estimation. Such error is very hard to be detected due to the model complexity.

Besides Bayesian methods, other ML methods can also be used for network diagnosis. Supervised learning methods such as regression and classification are proposed in [109] for anomaly detection. A BER anomaly detection algorithm is proposed to detect any abrupt changes in BER. It takes as input the historical BER information, BER threshold and real-time BER per lightpath. The anomaly detection is deployed at each network node, the output of the algorithm denotes whether the BER is out of a certain threshold or within a predefined boundary. The output is further fed into another ML algorithm together with historical BER and historical received power to detect the most likely failure cause from a set of failure classes. The inputs are encoded into features that can be quantified by time series, namely received power above the reference level, BER periodicity and BER positive trend. The classification algorithm maps these feature probabilities to failure probabilities. The regression algorithm makes prediction for a short time based on the historical BER data, however, this method may not work for rapid BER changes due to hard failure. In such case, this method becomes reactive.

A soft failure localisation algorithm for optical networking is proposed in [110]. The authors apply two techniques for active monitoring during commissioning testing and passive in-operation monitoring. The latter relies on specifically designed low-cost Optical

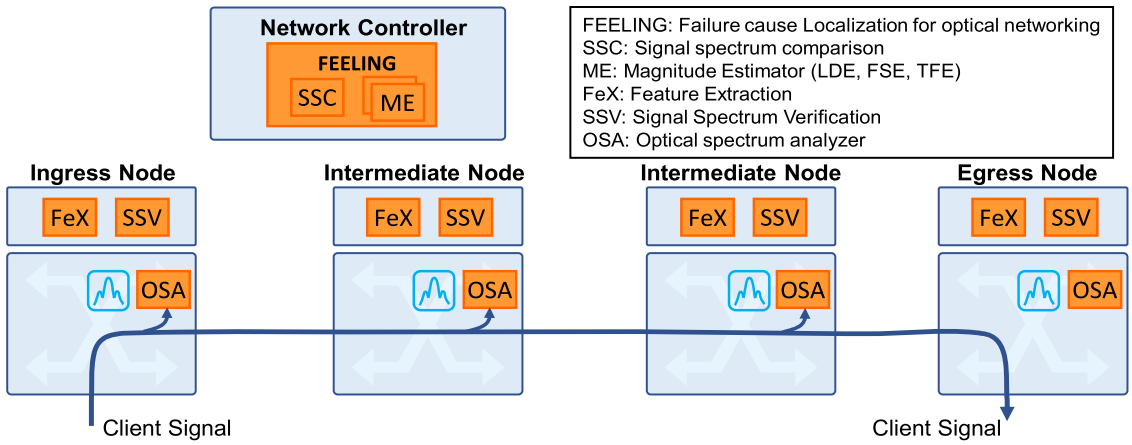

FIGURE 3.4. OSA passive monitoring for in-operation failure localisation, the figure is taken from [110]

Testing Channel (OTC) modules and Optical Spectrum Analyser (OSA). Two algorithms are proposed: Testing optIcal Switching at connection SetUp time (TISSUE) and FailurE causE Localisation for optIcal NetworkinG (FEELING). TISSUE is used to localise soft failures by assessing the estimated BER values provided by the OTC module with monitored BER. FEELING uses decision tree and Support Vector Machine (SVM) to classify and localise soft failures impacting a lightpath using OSA, the monitoring setup is shown in Fig. 3.4. The input data set in the form of paired frequency and power measured by OSA is transformed into a set of features such as central frequency power, power around other offset points of the entire spectrum, etc. These features are further fed into a decision tree which is a multi-class classifier to predict whether a soft failure belongs to 'Normal', 'LaserDrift' or 'FilterFailure'. If the soft failure is determined as a 'FilterFailure', a SVM-based classification is further applied to determine whether the filter failure is due to FilterShift or TightFiltering. This method needs OSA to be deployed at each intermediate node for power measurment. However, as OSA is a very expensive device, such investment for the infrequent soft failures is not realistic.

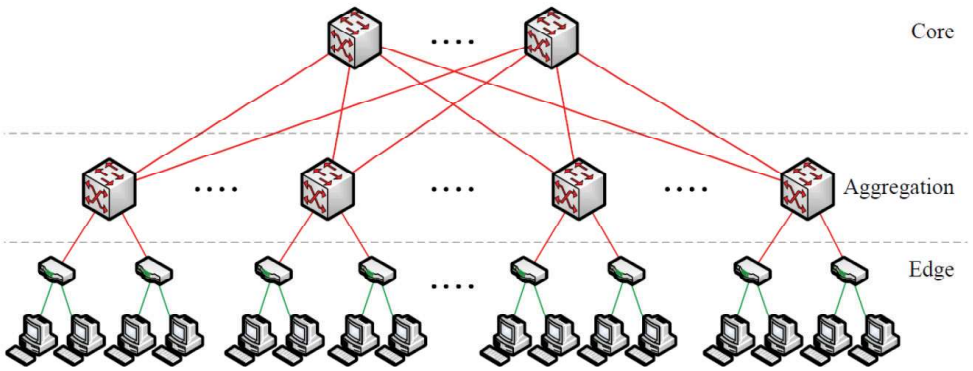

FIGURE 3.5. A typical intra-datacentre tree-like interconnection topology, the figure is taken from [111]

3.2.3 Intra-datacentre networking

Intra-Data Centre (DC) networking field also embraced many ML methods applied to improve the performance. For example, in DCs with hybrid-switching architecture where an optical circuit-switched network exists together with an electrical packet-switched network, ML-based network traffic flow classification can be a good candidate solution to provide rapid and accurate network control and management. Fig. 3.5 shows a typical data centre interconnection topology involving various sizes of electronic switches. The authors in [112] propose multi-layer ANN to assign network resources to Transmission Control Protocol (TCP) flows with their corresponding requirements. Because of the robust optical channel bandwidth aggregation performance and accurate flow classification performance, the method obtains 54.7% network throughput improvement compared to a random classification baseline. In addition to this work, an ANN-based flow classifier is proposed in [113] at the edge of the network whose output is utilised by an SDN controller in order to optimise global network resources. ANN allows for rapid and accurate traffic classification at the edge of the network without compromising the server computing resources. SDN is a promising architecture to deliver such learning capability in correspondence with application requirements from a global view.

In [114], the authors propose an adaptive end-to-end Markov scheduling policy which makes decisions for every time slot and determines the time to reconfigure the transmission schedule according to the most recent queue length information. Such method aims to solve the problems in all-optical DC networks where there is no buffer for optical packets, and the reconfiguration delay is non-zero. So decisions have to be made in advance and adaptively. From all these work, it can be seen that proactive decisions have to rely on learning from monitoring data. The model adaptability is critical in dynamic networks.

3.2.4 Passive optical networks

Passive Optical Networks (PON) are systems that bring optical signals to end consumers. Depending on where the signals terminate, PON can be in the form of Fibre-To-The-Curb (FTTC), Fibre-To-The-Building (FTTB), or Fibre-To-The-Home (FTTH). AI methods are also applied in the research of PON. The authors in [115] proposes using GA to optimise PON design and planning in terms of topology searching and splitter placement. The authors use street-map graph representation scheme to formulate and minimise the amount of optical cabling, number of splitters and power budget. GA is also used in [116] to optimise the first and secondary PON nodes (where the signal power is split) in terms of nodes position, their split levels, the association of customers to secondary nodes, and the association of secondary nodes to the primary nodes. GA is widely used as an alternative to traditional searching algorithms due to its reduced computational complexity. However, GA does not guarantee to find the optimal solution. This feature needs to be addressed when the network resource is scarce, or the cost is expensive.

Besides GA related algorithms, other methods are also used in PONs. A teaching-learning based optimisation algorithm is proposed in [117] with the aim to reduce the number of Optical Network Units (ONU). It ensures connectivity among wireless routers and

ONUs in a Fibre-Wireless (FiWi) network. Simulation work is carried out for various grid size of the geographical area as well as wireless routers. The result shows that the number of required ONUs is reduced compared to previous random and deterministic approaches. Therefore the proposed method can be a great potential solution for designing cost-efficient FiWi network.

Research works using AI methods are also focused on the autonomous diagnosis of PONs. For instance, EM algorithm is proposed in [106] for optical access network self-diagnostics. The method is based on Bayesian networks which are parameterised by conditional probabilities. The conditional probabilities come from a database of alarms collected on a GPON-FTTH access network. Self-diagnosis is performed to detect the root cause of alarms by probabilistic Bayesian inference. The performance of the proposed method is evaluated with respect to an expert system currently used by the Internet access provider. This raises the issue that most network-wide diagnostic research has to rely on real network data rather than data from the lab. This renders most of the network diagnostic research difficult. Another work [118] proposes a hybrid (optical/wireless) architecture in which SDN is used for collecting and providing traffic-status information. It modifies the Long-Term Evolution (LTE) radio uplink-downlink configuration using a proposed learning scheme. The learning scheme predicts the configuration of the next LTE frame based on the collected real-time uplink and downlink data together with previous LTE frame data. This allows for an improvement in the packet latency and jitter performance in a global network view by computing a proactive configuration based on the prediction. So traffic prediction is also very important in PONs.

Delivering QoS and resolving MAC issues in PONs are another area of research where AI methods can be applied. Again, GA is proposed to cope with these problems. The authors in [119] propose GA to balance asymmetric traffic load and reduce congestion among ONUs in PON networks. Through simulation with actual traffic amount of 120

sample users, the algorithm successfully reduces the traffic load of each ONU and the asymmetric behaviour of burst data for a PON system. A dynamic excess bandwidth allocation algorithm based on GA is proposed in [120] for a converged hybrid PON with wireless, optimal solution can be achieved with the proposed method in assigning excess bandwidth. In addition, the authors in [121] use a Genetic Expression Programming (GEP) algorithm together with the limited packet transmission strategy to predict QoS, the result shows that the proposed algorithm can optimise traffic queue variation and reduce the delay of high priority traffic.

Research efforts are also made to integrate Proportional-Integral-Derivative (PID) control with GA or ANN in PON optimisation. For example, in [122] the authors provide PON delay guarantees and manage to keep the mean packet delay of high priority services lower than a maximum threshold by designing an autonomously tuning proportional controller based on GA. Moreover, they increase the efficiency of the global algorithm when facing self-similar traffic by adding a dynamic admission control module to transmit or drop packets. In addition, a PID control strategy is proposed in [123] to control QoS requirements based on ANN-assisted parameter tuning in Ethernet Passive Optical Network (EPON). The simulation result shows that the proposed method can ensure the minimum guaranteed bandwidth levels (QoS) to every profile faster than GA-assisted PID control scheme. The feedback control loop used in these work guarantees that the inputs to the optimisation models are accurate which enhances the model awareness and adaptability.

3.3 Summary

Optical networks have long been studied using AI methods such as GA, CBR, convex optimisation, etc. for searching and optimisation tasks. However, these solutions only

perform well given the model inputs are accurate. Very few research work addresses the performance of these optimisation solutions under network uncertainty. ML is proven to be an effective method to reduce the uncertainty through monitoring. It is anticipated that ML and AI methods should be applied in a hybrid way for ultimate network intelligence.

CHAPTER 4

SNR PREDICTION WITH GAUSSIAN PROCESS

This chapter [1] reports the use of OPM and a ML method Gaussian Process (GP) to combat system noise uncertainty for SNR prediction. In later chapters it will be shown that GP forms the fundamental method that supports most of the extended research.

4.1 Motivation

OPM has been extensively applied in optical networks not only reactively where network restoration is triggered after failure detection [32], but also proactively where monitoring data is treated as the training set to train the system model and further predict QoT for future connections. One challenge in predicting unestablished lightpath performance by learning from the existing connections is model selection. A common choice would be regression method in a weight-space view [68, 124]. However, the EDFA gain spectrum and NF are wavelength dependent while the link loss is wavelength independent, hence

[1] This work is published in OFC conference proceeding [67]

channels with distant wavelengths are less SNR-representative than neighbour ones. This gain/loss wavelength discrepancy results in severe SNR non-uniformity across the C-band after passing through a cascade of EDFAs. Even under static power equalisation [125], the unstable EDFA gain excursion and NF perturbation issues due to ageing, loading, temperature, etc. still exist [126, 127]. In addition, each channel will experience sophisticated fibre nonlinear distortions due to intra-channel and inter-channel interference. The induced nonlinear noise is also unobservable and hard to formulaically analyse. The compound effect on SNR performance will vary severely among channels and is very difficult to be theoretically parameterised in real-time, especially in the case of sparse channel distributions because of add-drops.

Due to the compound uncertainty of EDFAs, fibres and nonlinearities, traditional SNR prediction with static GN model becomes intractable. Given there is no prior knowledge of what the prediction model is, i.e., function-agnostic, any arbitrarily chosen weight-space model will result in under-fitting or over-fitting issues. These issues can further lead to network failure or margin over-provisioning due to poor QoT estimations. Fortunately, In contrast to the weight-space view method, GP is a stochastic probability distribution over functions (function-space view) [128], any inference takes place directly in the space of functions that derived from the data. So rather than claiming the optical link SNR model against wavelength to be linear, cubic, etc. GP can represent the model obliquely, but also rigorously by letting the monitoring data "speak" more.

There are many other regression methods such as neural network or SVM which can also tackle nonlinear regression problems. However, the power of neural network only works given sufficient training data and model size, finding a suitable neural network architecture (with specific hyperparameters such as number of hidden layers, number of neurons, learning rate, optimisers, etc.) for online learning tasks with restricted dataset size is difficult. A well-tuned neural network model is hard to scale to other systems.

Moreover, the non-Bayesian methods intrinsically carries no estimation confidence intervals which can be used later as the decision-making input. GP is a less-parametric method with very few hyperparameters to tune, and hence more scalable to new dataset. It also computes estimation confidence intervals as the generated posterior knowledge given insufficient dataset. So GP as a Bayesian method under small dataset is preferred in this online learning setting.

4.2 System modelling

As uncertainties happen during the network operation, offline training ML models [24, 129] are not suitable to capture the online system characteristics. In this case, GP is considered for such small data set online learning task. Online learning means the system can take the real-time monitoring data as the training set to achieve "sustained learning" throughout the network lifecycle. The training phase is on-the-fly and based on the monitoring data. Fig. 4.1 shows the flow chart of the overall learning algorithm. The controller updates its database and iterates through the process every time a new channel is lit. To fit the GP model, the monitoring data (SNR vs λ) of the existing channels is seen as the training set, a new channel SNR performance is seen as the test set. It is assumed that lightpaths are established one by one. So each time a new lightpath is established, its monitoring data is taken into the training set for prediction of the next single channel establishment.

The monitoring data is intrinsically noisy because the OSNR readings fluctuate around the mean value over time. GP models additive IID Gaussian noise ϵ to the mean value

$$Q(monitored) = Q(mean) + \epsilon \tag{4.1}$$

$$\epsilon \sim \mathcal{N}(0, \sigma_Q^2) \tag{4.2}$$

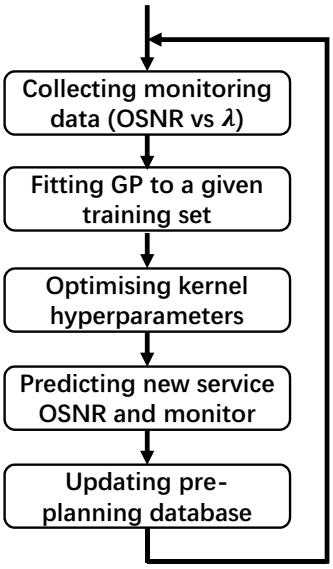

FIGURE 4.1. GP learning flow chart. Note that the data collection step is always running to achieve sustained learning.

where Q(mean) is the mean SNR value and σ_Q^2 is the measurement noise variance. So all future inferences are made by taking the measurement noise variance into account. The final fitted GP curve does not necessarily pass through each training point, but is always within the variance range σ_Q^2. Fig. 4.2 shows an example of the measurement reading noise when computing the OSNR using power monitoring.

Fig. 4.3 shows the graphical model explanation for GP. The inputs λ_i (wavelength) and outputs Q_i (monitoring SNR) of the training set are known data while the function node f_i is unknown. Each monitored data Q_i is conditionally independent of all other nodes given the latent variable f_i. To predict a new test channel SNR Q_*, GP samples functions for the corresponding function f_* that is conditioned on λ_* and the given training set. The feasibility of applying GP relies on the kernel assumption which is also applicable in optical transmission systems: given the same route, if two channels are close to each other, their noise performances should be more correlated (GP similarity kernel reaches maximum). Or more formally, any subset drawn from the SNR monitoring data set

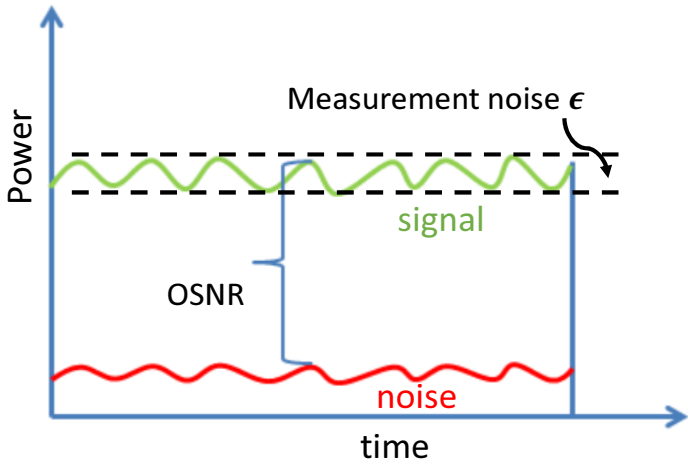

FIGURE 4.2. Additional measurement Gaussian noise ϵ is added to the training set.

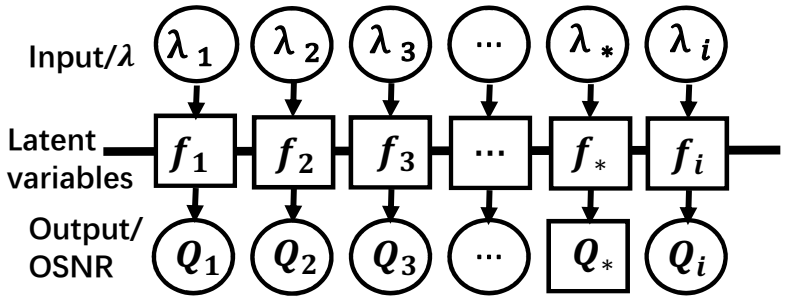

FIGURE 4.3. Function-space sampling of GP, the function f is also called latent variable.

follows a multivariant Gaussian distribution.

We model the similarity kernel (covariance function) using the squared exponential kernel, or the so-called Radial Basis Function (RBF) [130]

$$k(\lambda,\lambda') = \sigma_f^2 \exp\left(\frac{-(\lambda-\lambda')^2}{2l^2}\right) + \sigma_Q^2 \delta(\lambda,\lambda') \tag{4.3}$$

where σ_f^2 (signal variance) and l (length scale) are hyperparameters that affect the shape and smoothness of GP, $\delta(\lambda, \lambda^{'})$ is the Kronecker delta function. The kernel function value $k(.,.)$ is a scalar which measures the similarity between two channels. We use cosine similarity to measure correlation. If two channels are too far away, then $\lambda - \lambda^{'}$ goes to infinity. Thus the kernel becomes 0 ($exp(-infinity) = 0$), which means these two channels have little correlation (k becomes closer to 0). In other words, closer channels offer more information to the OSNR estimation of the target channel than distant channels. It is worth noting that there exist about 20 choices of kernels, for example, polynomial kernel or exponential kernel [131]. The motivation behind the choice of a particular kernel can be very intuitive. However, the Gaussian kernel (RBF) used in here is well known to give smooth sampling functions compared to others. This coincides with the fact that there should not be any abrupt ascends or falls of the OSNR spectrum, i.e. the smoothness assumption. One interesting future work can be exploring the most suitable kernel for a particular task.

If there are m channels used as the training points, a m-by-m covariance kernel matrix $\mathbf{K}$ (throughout the chapter matrices are shown in **bold** font) can be constructed as

$$\mathbf{K} = \begin{bmatrix} k(\lambda_1, \lambda_1) & k(\lambda_1, \lambda_2) & \cdots & k(\lambda_1, \lambda_m) \\ k(\lambda_2, \lambda_1) & k(\lambda_2, \lambda_2) & \cdots & k(\lambda_2, \lambda_m) \\ \vdots & \vdots & \ddots & \vdots \\ k(\lambda_m, \lambda_1) & k(\lambda_m, \lambda_2) & \cdots & k(\lambda_m, \lambda_m) \end{bmatrix} \tag{4.4}$$

The diagonal elements of $\mathbf{K}$ measure the self-similarity of each channel and are hence equal to 1. The amount of the correlation between the training and test channels follows a joint multivariant Gaussian distribution which is computed from the training data $\mathbf{Q}$ and test data Q_* according to the prior (initial belief of the sampled hidden function)

[132]

$$\mathbf{K}* = \begin{bmatrix} k(\lambda_*, \lambda_1) & k(\lambda_*, \lambda_2) & \cdots & k(\lambda_*, \lambda_m) \end{bmatrix} \tag{4.5}$$

$$\mathbf{K}_{**} = k(\lambda_*, \lambda_*) \tag{4.6}$$

$$\begin{pmatrix} \mathbf{Q} \\ Q_* \end{pmatrix} \sim \mathcal{N}\left(\mathbf{0}\ , \begin{bmatrix} \mathbf{K} & \mathbf{K}_*^{\mathbf{T}} \\ \mathbf{K}_* & \mathbf{K}_{**} \end{bmatrix} \right) \tag{4.7}$$

where $\mathbf{K}_*$ is a 1-by-m matrix, $\mathbf{K}_*^{\mathbf{T}}$ is the transpose of $\mathbf{K}_*$. The posterior OSNR estimation of the test set Q_* conditioned on the training set and test input λ_* hence follows the Gaussian distribution [132]

$$Q_*|(\mathbf{Q}, \lambda, \lambda_*) \sim \mathcal{N}(\mu_*, \sigma_*) \tag{4.8}$$

$$\mu_* = \mathbf{K}_* \mathbf{K}^{-1} \mathbf{Q} \tag{4.9}$$

$$\sigma_* = \mathbf{K}_{**} - \mathbf{K}_* \mathbf{K}^{-1} \mathbf{K}_*^{\mathbf{T}} \tag{4.10}$$

The pseudocode that summarises the GP algorithm fitting to transmission system is shown in Algorithm 1. The "\" operation means matrix division. The hyperparameters are optimised by maximising the log marginal likelihood $\log[p(Q|\lambda)]$ (maximum likelihood). It is maximised by seeking partial derivatives with respect to σ_f^2 and l.

An important feature of GP is that it computes the Estimation Confidence Interval (ECI) that forms critical constraints for control decision making [27]. ECI quantifies posterior prediction uncertainty which goes high where there is no monitoring data, and goes low where there is sufficient monitoring data. 95% pointwise ECI is a common choice which is computed by

$$ECI = \overline{Q_*} \pm 1.96\sqrt{\mathrm{Cov}[Q_*]} \tag{4.11}$$

Input:
λ - - training channel (established connections) wavelength;
$\mathbf{Q}$ - - training channel (established connections) OSNR;
$\mathbf{K}$ - - kernel function;
σ_Q^2 - - monitoring data noise or variance;
λ_* - - test channel (unestablished connection) wavelength;
Target:
Q_* - - unestablished connection OSNR prediction;
Algorithm:
$\mathbf{L} := Cholesky(\mathbf{K})$; [133]
$\mathbf{A} := \mathbf{L}^T \backslash (\mathbf{L} \backslash \mathbf{Q})$ - - intermediate computation;
$\overline{Q_*} := \mathbf{K_*^T A}$ - - posterior OSNR mean;
$\mathbf{B} := \mathbf{L} \backslash \mathbf{K_*^T}$ - - intermediate computation;
$\mathrm{Cov}[Q_*] := \mathbf{K}_{**} - \mathbf{B}^T\mathbf{B}$ - - posterior OSNR variance;
$\log[p(\mathbf{Q}|\lambda)] := -\frac{1}{2}\mathbf{Q}^T\mathbf{A} - \sum_i^n \log \mathbf{L_i} - \frac{n}{2}\log 2\pi$ - - log marginal likelihood to be maximized during hyperparameter tuning;
Return:
$\overline{Q_*}$, $\mathrm{Cov}[Q_*]$, $\log[p(\mathbf{Q}|\lambda)]$

Algorithm 1: GP learning of SNR spectrum

4.3 Experimental setup

Fig. 4.4 shows the field trial testbed setup using part of the UK National Dark Fibre Infrastructure Service (NDFIS) [http://www.ndfis.org/] which connects three geographical nodes: University of Bristol, Brandley Stoke and Froxfield. 15 equalised 50GHz-spaced (50GHz grid ITU) 32Gbaud DP-QPSK signals (training data, wavelength ranging from 1545nm to 1565nm) are generated at the transmitter side. The I and Q modulator branches are driven independently by two uncorrelated 32-Gbaud Pseudo-Random Bit Sequences (PRBS) of length $2^{15} - 1$ produced by the PPG. Polarisation Division Multiplexing (PDM) is achieved by splitting the signal through a Polarisation Beam Splitter (PBS) into two branches, delaying one branch, and recombining the signal through a Polarisation Beam Combiner (PBC). The signal is then amplified to 0 dBm at the launch side. Commonly the optimum launch power would range between -4dBm and

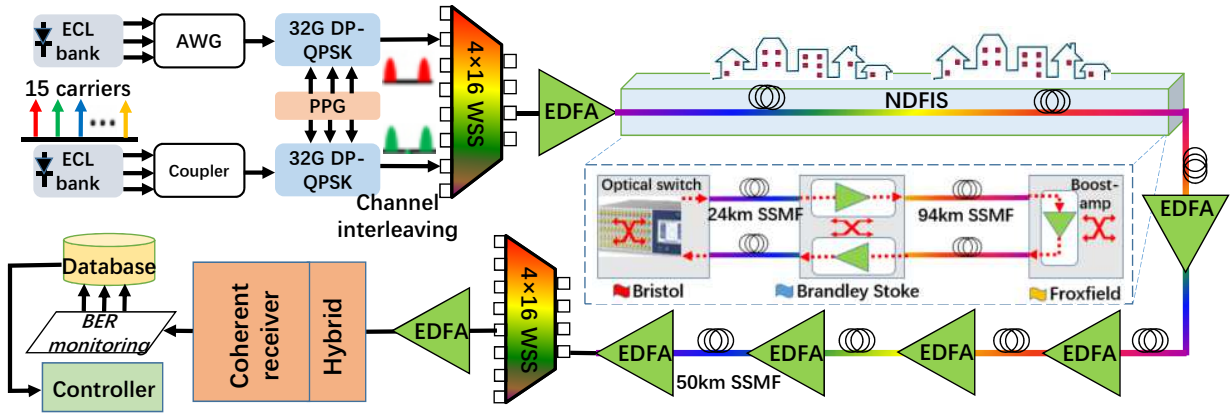

FIGURE 4.4. Field trial UK testbed with NDFIS, ECL (external cavity laser), AWG (arrayed waveguide grating), PPG (pulse pattern generator), DP-QPSK (dual polarisation quadrature phase shift keying), SSMF (standard single mode fibre), BER (bit error rate).

4dBm depending on the system [16, 40, 68]. We did not optimise this launch power since the target of this work is to examine the advantage of the learning method rather than searching for the OSNR performance limit. A Wavelength Selective Switch (WSS) is used both as an equaliser and interleaver to avoid crosstalk, WSS filter bandpass bandwidth is set to 50GHz/wavelength. Fig. 4.5 shows the equalised channels at transmitter side. All the other 32 channels' SNR values within the wavelength range are treated as the test data. The SNR test data is measured by setting up a single test channel at each of the empty wavelength slot, it is torn down once the monitoring value is recorded.

Launch SNR is kept identical among the 15 channels by conducting back-to-back Error Vector Magnitude (EVM) based BER monitoring using an Optical Modulation Analyser (OMA) device. The NDFIS loop-back link gives 236km effective transmission length. At each site, a boost amplifier is used to completely compensate the span loss. Another 200km fibre link is added after the loop-back (giving 436km in total) where signals are amplified for every 50km before being coherently received. Some of the pre-tested EDFAs

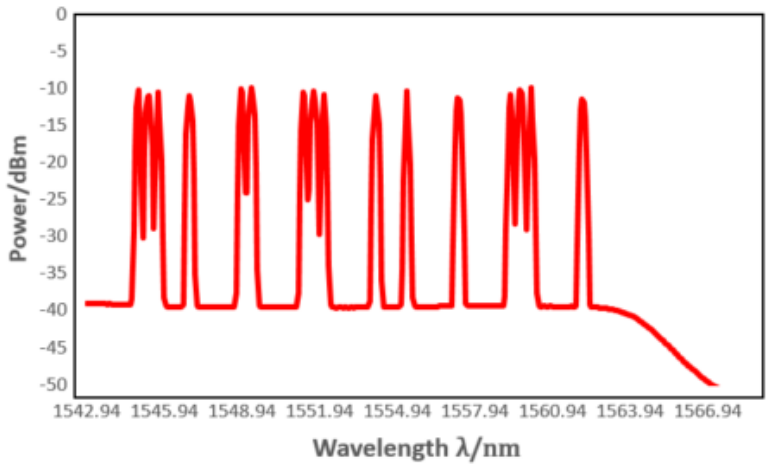

FIGURE 4.5. Launch channels with power equalisation using WSS at the transmitter side.

introduce unexpected noise excursion because of ageing.

In the coherent receiver, absolute BER is monitored at 5 minutes/channel interval and stored in a local database, the BER is further converted to SNR by

$$SNR_{QPSK} = [\text{erfc}^{-1}(2 \cdot BER)]^2 \cdot 2R_s/B_n \tag{4.12}$$

where the operator "/" means division operation throughout the thesis. R_s and B_n are the signal baudrate and noise level bandwidth respectively.

4.4 Results analysis

To exemplify the GP learning model performance, we transmit 15 equalised DP-QPSK signals from the transmitter side to the coherent receiver, resulting in 436km transmission distance in total. The SNR monitoring data of these 15 channels is used as the training data for GP. To emulate the situation in which channels are sparsely distributed (channel fragmentation) due to intermediate node add-drops, the 15 training channels are randomly distributed across the wavelength band. As an example, the received

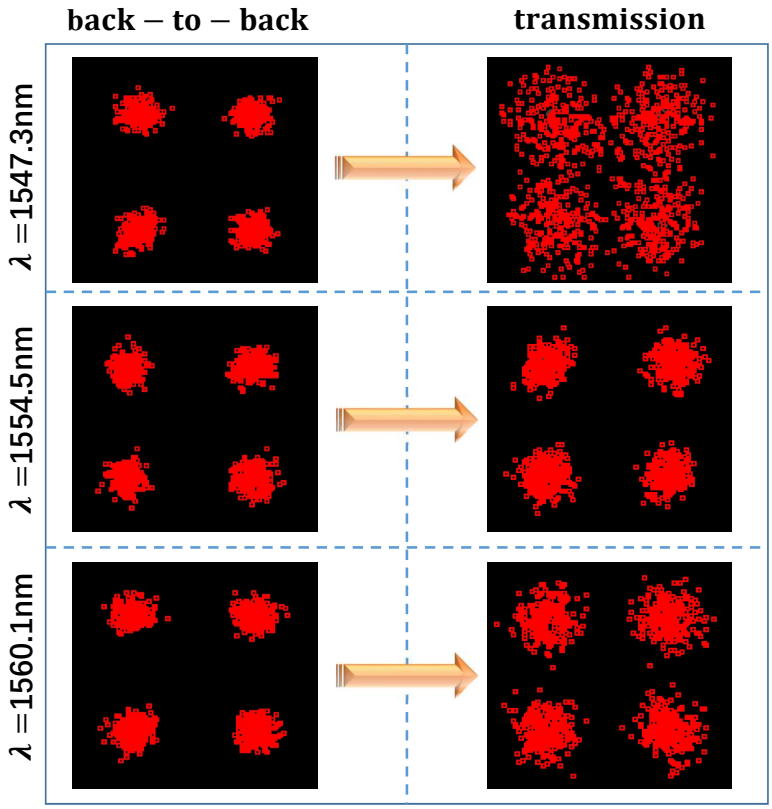

FIGURE 4.6. Receiver side constellation diagrams of three DP-QPSK channels with different wavelengths before (back-to-back) and after 440km transmission. The more scattered constellation means signals with higher noise.

constellation diagrams are recorded for visualising the noise uncertainty. Fig. 4.6 shows the received constellation diagrams of three training channels at different wavelengths 1547.3nm, 1554.5nm and 1560.1nm. Their launch Back-To-Back (BTB) performances are identical. After transmission, it can be seen that their constellation performances show various noise degradations.

We model this non-uniformity problem with GP regression as shown in Fig. 4.7. The GP curve represents the posterior mean estimation for the target channel given all the training set. In dynamic cases, all the real-time monitoring data is fed to the training set

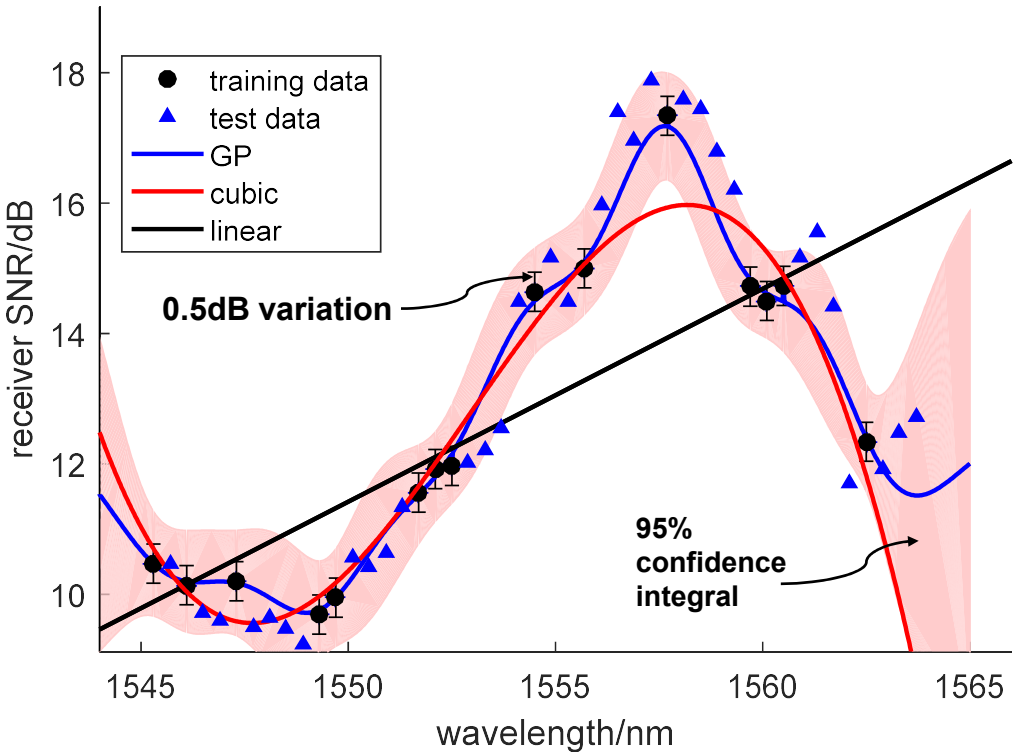

FIGURE 4.7. Regression lines based on 15 training data points (black dots), blue line is from GP, red line is cubic polynomial, black line is from least square linear regression, red shaded regions represent 95% confidence integral of GP.

for the next step prediction purpose. The process iterates throughout the lifecycle of the optical network.

We add IID measurement Gaussian noise variance σ_Q^2 = 0.5dB (as indicated by the black bar in the figure) to tolerate the intrinsic SNR reading noise. The exponential kernel hyperparameters σ_f^2 and l are optimised to be 2.07 and 1.53 respectively by MLE of the log marginal likelihood. The 95% pointwise ECI indicates the posterior prediction uncertainty which goes low where training data is sufficient, and goes high where there is no training data. For example, the high uncertainty case is shown on the most right-hand side of Fig. 4.7 with large red ECI area. It can be seen from the figure that only 4 test

data points fall outside of the confidence integral while 88% of the test data is captured by GP with 95% confidence. It is worth noting that ECI can be taken into account as one constraint of control plane wavelength assignment. This constraint is used for allocating more wavelengths to unexplored regions in order to minimise the prediction uncertainty in those areas.

As Fig. 4.7 indicates, channels with wavelength around 1557nm present the best SNR performance (global maximum) while channels with the worst SNR performance (global minimum) locate around 1548nm due to unpredictable accumulated noise. To evaluate the performance of GP, three other estimation methods are used as baselines. The first is Least-Square Linear Regression (LSLR): the overall fitted line minimises the sum of squares of residuals/errors. In other words, it is the line that makes the vertical distance from the data points to the regression line as small as possible. LSLR is seen as the most common weight-space method in machine learning. This method has been used in many research works such as [68]. The second method is similar to LSLR, but it is not a straight line. From the distribution of the training set in Fig. 4.7, it is intuitively possible that a cubic function may fit. So least-square cubic regression is used. The third prediction baseline is Neighbour Average (NA). This method averages SNRs of the adjacent training channels located at both sides of the target channel. Such manipulation is commonly used in out-of-band OSNR computation where the noise power level is computed by averaging the noise power at both sides out of the target channel spectrum band. LSLR and cubic regression methods are plotted in Fig. 4.7. The LSLR line has the gradient of 0.3048. It can be seen that neither of the methods can capture the training data very well because they are not flexible enough and tend to underfit the training set. It can be deduced that by increasing the order of the polynomial function will likely to cause overfitting.

The prediction error using different methods are plotted in Fig. 4.8. The error is defined

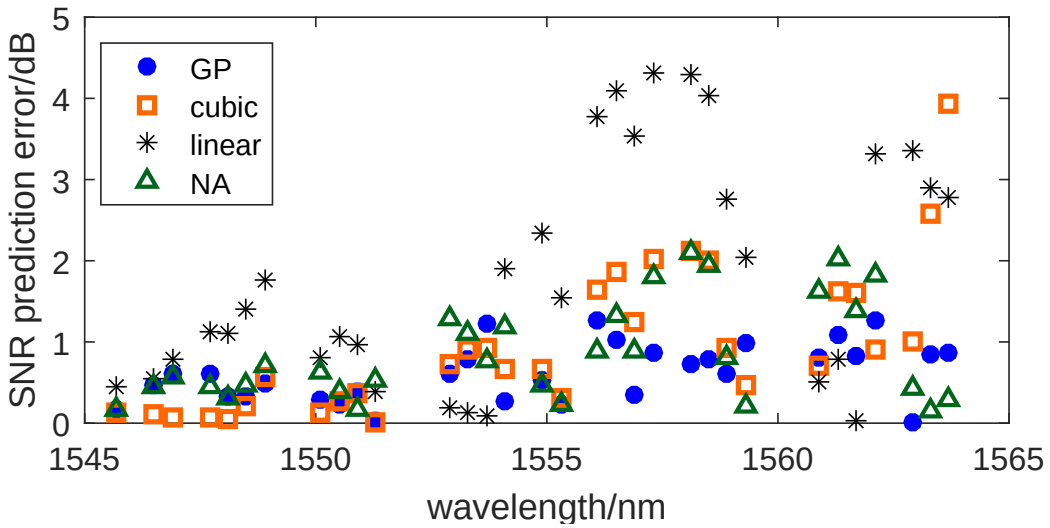

FIGURE 4.8. SNR prediction error plot using different methods (GP, cubic, linear, and neighbour-average (NA))

as the absolute value subtracting the monitoring data from the prediction data. The figure indicates that GP has the smallest prediction error mean and variance. We use Root Mean Squared Deviation (RMSD) to quantify the mean error, and the maximum error value to quantify error range. It is further summarised in Fig. 4.9 that GP outputs the lowest RMSD with 0.7dB and the lowest MAXimum (MAX) prediction error with 1.2dB. GP has the MAX error reduction of 73.3% compared to LSLR (2.5dB RMSD and 4.5dB MAX). This demonstrates that GP is an accurate SNR (QoT) prediction method compared to others.

To explore the impact of the training set position on the GP performance, we randomly select three different sets of training data, each consists of 15 training channels. To simplify the process, we index the wavelength from 1545nm to 1565nm into sequential numbers from 1 to 50 at 0.4nm/channel scale. According to Table 4.1, for the first row where the channels are uniformly distributed, GP returns the lowest RMSD prediction error (0.5dB) compared to the next two rows (0.8dB and 0.6dB). In row 2 and row 3

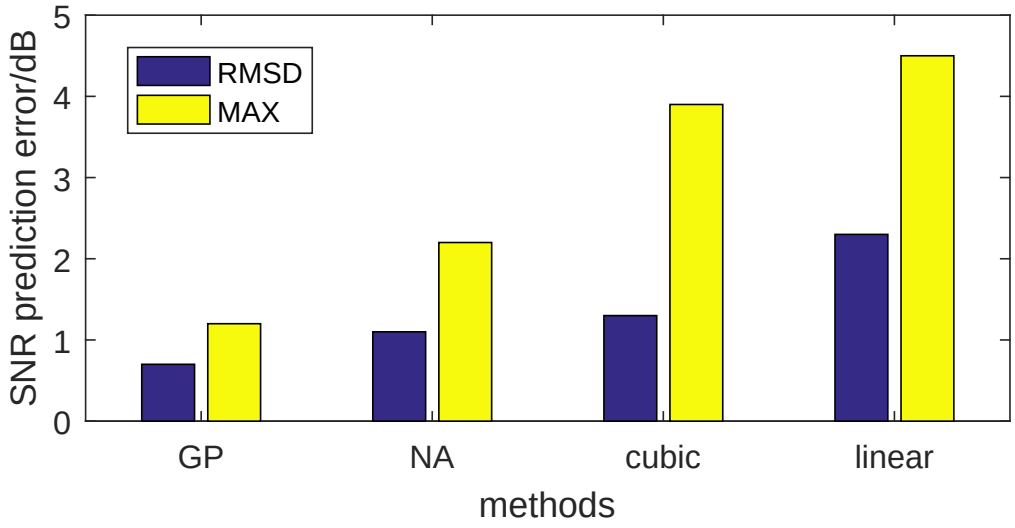

FIGURE 4.9. RMSD and MAX of SNR prediction error of the four methods. The RMSD error for GP, NA, cubic regression and LSLR respectively is 0.7dB, 1dB, 1.3dB and 2.5dB, MAX error is 1.2dB, 2.2dB, 4dB, 4.6dB respectively.

where channels are not uniformly distributed, GP has a slightly worse RMSD error but is always better than NA and LSLR methods.

The number of available monitoring channels will also influence the learning performance. Similarly, Table 4.2 shows the impact of the number of monitoring channels on the prediction performance of the three methods. 15, 10, 8, 6, 4 and 2 training channels are shown in the table with the corresponding rows. It can be seen that, generally, the performance of each of these three methods degrades with the decrease of the number of training/monitoring channels. When the number of training channels is fewer than 6 (row 4), GP and NA have very close prediction performance. This indicates that when there is only a few monitoring data available, it is preferred to use the NA method for prediction since it has much lower computational complexity than GP (GP kernel matrix dimension is proportional to the number of training channels).

Impact of monitoring channel position on prediction performance			
training channel index	GP	NA	LSLR
2, 8, 11, 14, 22, 23, 28, 30, 31, 33, 39, 42, 45, 48, 50	0.5dB	1.2dB	2.3dB
1, 4, 5, 9, 15, 16, 17, 20, 22, 25, 29, 33, 35, 39, 44	0.8dB	1.1dB	2.8dB
9, 15, 16, 22, 24, 30, 33, 34, 35, 40, 41, 44, 45, 47, 49	0.6dB	1.4dB	2.8dB

Table 4.1: The RMSD performance of GP, NA and LSLR under different 15 training set situations.

Impact of the number of monitoring channels on prediction performance			
training channel index	GP	NA	LSLR
2, 8, 11, 14, 22, 23, 28, 30, 31, 33, 39, 42, 45, 48, 50	0.5dB	1.2dB	2.3dB
8, 11, 14, 22, 28, 31, 39, 42, 48, 50	0.9dB	1.3dB	2.7dB
8, 14, 22, 28, 31, 39, 42, 48	0.9dB	1.4dB	2.5dB
8, 22, 28, 31, 39, 48	1.1dB	1.4dB	2.7dB
8, 22, 39, 48	1.5dB	1.5dB	2.6dB
8, 39	1.6dB	1.8dB	2.9dB

Table 4.2: The RMSD performance of GP, NA and LSLR under different number of training set situations.

4.5 Conclusion

We configured a cognitive, network-scale testbed in which signals are transmitted through the NDFIS system to introduce sufficient uncertainties in the network. We have shown that by applying GP regression with SNR monitoring, while without any prior system knowledge, we can make performance predictions with high fidelity using online passive monitoring data. With GP learning, 1.2dB MAX SNR prediction error and 0.7dB RMSD error are achieved across a large wavelength range which demonstrates that GP outperforms other methods. GP model also allows estimating SNR prediction uncertainties by computing estimation confidence integrals. This quantified prediction uncertainty feature can be potentially leveraged as control plane algorithm constraint to further optimise global SNR uncertainty. For example, the monitoring on-demand application which will be introduced in Chapter 7.

During the dynamic network planning and design process, SNR margin saving is essential to optimise the network resource utilisation which needs an accurate QoT estimator. The proposed GP learning model is shown to accurately estimate QoT by enabling a "self-learning" network using monitoring. It can allow network to run close to its performance limit and save significant margins under noise uncertainties.

CHAPTER 5

LEARNING OF NETWORK HIDDEN PARAMETERS

This chapter [1] describes the work on the inference process for the hidden optical network parameters under uncertainty. Current optical networking has evolved into fully reconfigurable and dynamic era. However, such complicated network system unavoidably comes with ubiquitous physical layer uncertainties in amplifiers, fibres, switches and transceivers. While active diagnostics exist, they are either invasive or offline. Online knowledge acquisition of the hidden parameters that abstract amplifier and fibre nonlinear impairments is indispensable but remains a big challenge under such uncertainty. The limited amount of online monitoring data further makes most offline-training machine learning solutions infeasible. We present hybrid supervised/unsupervised Bayesian inference leveraging limited online monitoring data to circumvent this problem. Our proposed approach uses the Gaussian noise model as the likelihood function. The posterior estimations of the hidden parameters are refined with quantified estimation probability through simultaneous exploration and exploitation of a field-trial network. Such intelligent network analytic is shown to provide accurate

[1] This work is published and top scored in ECOC conference proceeding [134].

physical layer insights and minimise real-time impairments uncertainties under small data set restriction. It forms a reliable foundation for network control and management.

5.1 Introduction

In current coherent optical networks, QoT is largely determined by OSNR or SNR when nonlinearity is considered. ASE noise and fibre NLI noise are two dominant impairments contributing to SNR degradation [6, 8, 40, 135]. The modern advances of network scalability and reconfigurability [136, 137] result in these noise induced impairments being network state dependent and subject to changes of environment. In such dynamic networks, operational noise uncertainties are ubiquitous in network components such as EDFA, fibre links, and optical switches [2, 126, 129] due to add-drop, ageing, temperature, pump power, etc. Moreover, different signals with diverse modulation formats and bit rates will suffer different noise degradation. Utilising OPM (or network telemetry) can to some extent obtain information about the network status, but it still cannot provide direct knowledge of the hidden parameters that abstract the transmission induced impairments. Two main hidden and unobservable parameters are EDFA NF and GN model NLI coefficient η_{NL} which determine ASE and NLI impairments respectively [8, 138]. Traditional optical network planning models assuming theoretical computation of these impairments cannot take into account such operational uncertainty.

Several ANN models are proposed [23, 24, 139] to achieve autonomous SNR predictions which aim to replace traditional planning models. Unfortunately, the offline training process using artificial training data only considers offline design uncertainties hence it is intrinsically unadaptable to operational uncertainties over time in a living, in-operation network. Moreover, the proposed ANN models tend to disregard prior analytical models and treat the system as a black box to learn from scratch. This will result in transmission

impairments being untraceable over time which consequently leads to blindness of system noise behaviour. Therefore, to capture real-time knowledge of noise induced impairments and minimise dynamic operational uncertainties, learning models should utilise real-time online monitoring data for deeper network insights.

Online learning also suffers from the shortage of training data in running optical networks where the number of in-service channels is limited. Learning under such restricted data size still remains a big challenge for optical networking. Fortunately, unlike frequentist methods such as ANN that neglects any off-the-shelf transmission knowledge and only relies on OPM data which is far from enough, we propose a hybrid supervised/unsupervised Bayesian learning architecture to combat such online small data set restriction [140]. Our proposed Bayesian method combines OPM data with given prior knowledge from device vendors and analytical models to leverage all the information available. For online supervised learning, probabilistic methods can be used to compensate for data shortage issue and infer the target value with certain amount of probability. Since there is no training needed for unsupervised learning, online knowledge of physical layer ASE and NLI impairments can be refined in real-time with statistical scales of estimation uncertainty. Such real-time hidden parameter tracking is otherwise impossible through direct monitoring especially under small data set limitations. It is a brand new way of carrying out optical network analytics utilising hybrid probabilistic and generative learning model which differs from traditional pure deterministic models. It is "hybrid" not only in the supervised/unsupervised way, but also in the analytic/learning way.

In this chapter we propose and demonstrate a hybrid learning-assisted network analytic solution that autonomously extracts physical layer hidden knowledge with high fidelity in a network-scale field trial. SDN architecture [141] is used to collect and process the OPM data. SDN is a suitable candidate for realising such learning capability because

it is vendor technology agnostic and its global-wide network view allows information from various network parts to be effectively collected for centralised control. Due to the well-proven theoretical accuracy, GN model is used to abstract the physical layer ASE and NLI noise with EDFA NF and NLI coefficient η_{NL} respectively. These parameters are fed into the GN model to predict candidate path SNR performances. Learning is performed both horizontally and vertically (H/V) throughout the network. Horizontal "system surface" exploration (H-step) is done by supervised Gaussian Process (GP) learning using online SNR monitoring data. The learning process of GP has already been described in Chapter 4. On top of the GP returned information, vertical parameter exploitation (V-step) using unsupervised Markov Chain Monte Carlo (MCMC) inference is performed to refine the distribution of the hidden parameters NF and η_{NL} at network level. NF knowledge error is shown to be reduced by 15% compared the prior, the final learning-assisted GN model is shown to have a 70% reduction of SNR prediction error compared to the static case, this further proves the accuracy of the inference process for both ASE and NLI impairments. Such hybrid H/V learning of hidden network knowledge provides deep insights into physical layer uncertainties and guarantees dynamic network self-awareness for proactive control.

5.2 Scheme for hybrid optical network learning

Fig. 5.1 shows a general 5-node optical network where each node represents a Reconfigurable Optical Add-Drop Multiplexer (ROADM). Services are provisioned dynamically across different nodes, the end-to-end SNR monitoring information is available at each node receiver side. SNR in combination with synchronised span power information are collected and stored in a database for hybrid learning-assisted analysis. H-step GP learning (online supervised learning) is performed to learn any unestablished lightpath SNR as the QoT metric. On top of the SNR estimations, the V-step link parameter inference

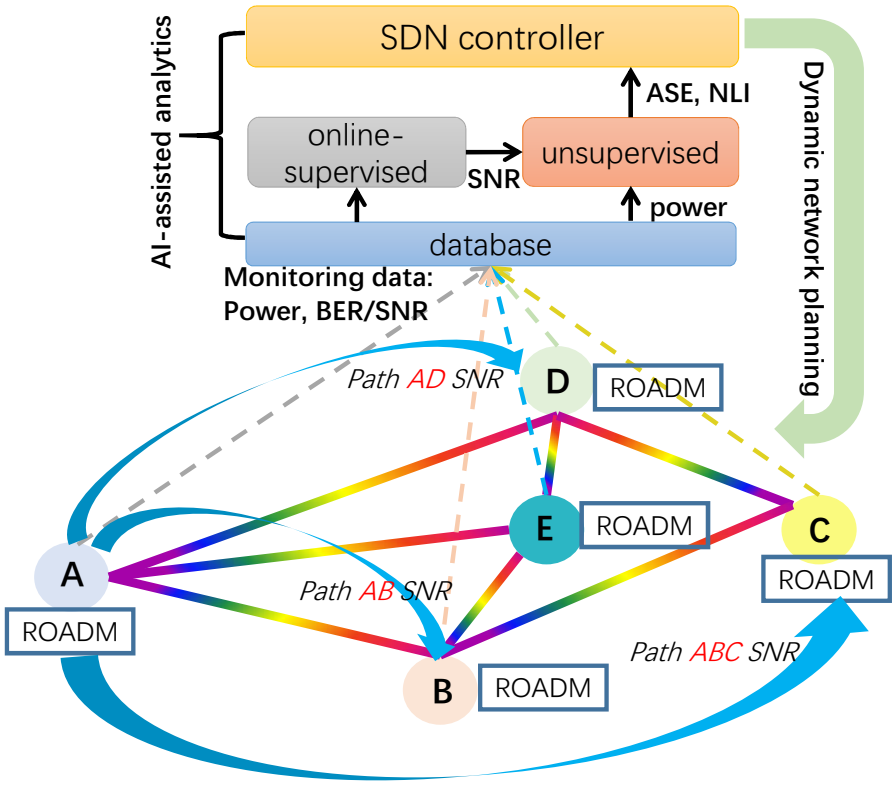

FIGURE 5.1. Proposed hybrid learning-assisted network analytic architecture in a general optical network. Each of the node represents a ROADM which can dynamically transmit and receive signals. The power and SNR monitoring data is stored in database for online supervised and unsupervised learning. The updated physical layer knowledge is used by the controller for dynamic network re-planning.

(unsupervised learning) is performed to evaluate the corresponding link parameters that affect the QoT.

More specifically, Fig. 5.2 illustrates the detailed network control scheme assisted by learning. The system is separated into three blocks: model parameter inputs, system models and observation/monitoring. Information such as data rates, source-destination pairs, etc. are treated as control plane requests (inputs). The inputs for physical layer QoT estimation are (1) GN model nonlinear distortion coefficient η_{NL}; (2) filter wave-

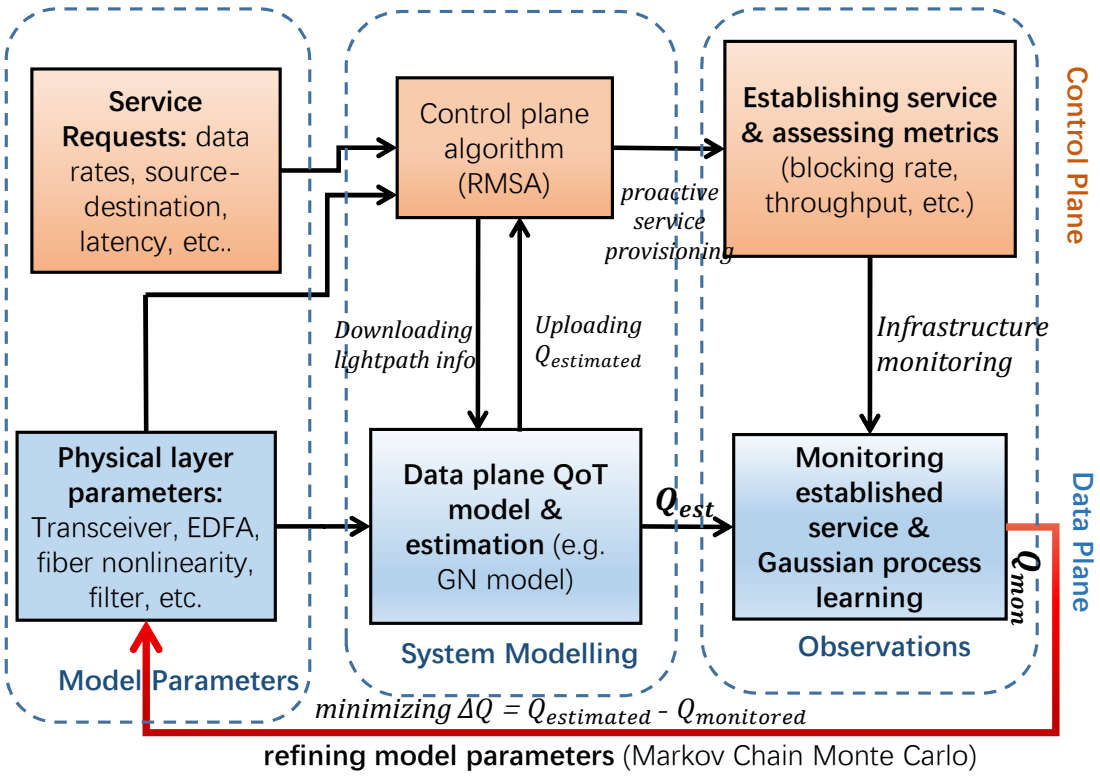

FIGURE 5.2. Schematic view of the learning architecture. Control plane decisions are made to efficiently satisfy the network requests based on network knowledge. Data plane QoT model serves as a lower level abstraction of the physical layer. Because of network uncertainties the model estimation output does not fit the monitoring data. Unsupervised learning MCMC inference can be applied to re-optimise those feeding parameters which can be verified by the difference between the new output and monitoring data. Online supervised GP is used to estimate the missing SNR information in a network scale.

length detuning $\delta\lambda$; (3) EDFA gain characteristic G (gain » 1); (4) EDFA NF. Any other parameters influencing the QoT performance are neglected [138]. The QoT estimation together with physical layer parameters are fed to the control plane as constraints to meet heterogeneous service requests. Due to operational uncertainties of the physical layer model parameters, after service provisioning the estimated SNR does not match the monitoring value. Based on the end-to-end monitoring data (SNR, power) and prior

knowledge of the lightpath, unsupervised inference MCMC (V-step) is applied to refine the model parameters until the estimation and monitoring data converge. It is worth noting that due to the power monitoring capability (e.g., Optical Channel Monitor (OCM) deployed ubiquitously across the network, the wavelength detuning $\delta\lambda$ and EDFA gain are seen as observable parameters, thus the real-time knowledge of these two parameters do not require inference. The final QoT estimation after learning is used for proactive network planning.

However, such unsupervised inference can only learn path-level physical layer parameters given the end-to-end path SNR monitoring data is available. To enable inference at network level where sometimes there is no signal available for path monitoring, online supervised learning (H-step) can be applied. For example, in Fig. 5.1, a set of λ_1 is sent through path A-B-C, another set of λ_2 is sent through path A-B, to apply V-step inference for path B-C at a new wavelength λ_3, online supervised GP regression for both path A-B-C and path A-B are performed to estimate path B-C SNR in order to do further unsupervised inference, i.e., inference over inference.

5.3 Data monitoring and system pre-testing

As a key enabler to such self-learning capability, autonomous collection and processing of the ubiquitous monitoring data across the network is required. Fig. 5.3 depicts the SDN-enabled monitoring platform implemented for network self-learning which is also an experimental implementation of Fig. 5.1. The UK NDFIS is used for field trial loopback transmission, NDFIS runs through different geographic nodes across the country serving as a real transmission network, hence offering sufficient uncertainties to the system. Monitoring data from transmitter (node A), link EDFA, optical spectrum analyser (OSA) deployed at intermediate node [27] (node B) and coherent receiver (node C) is collected

and synchronised in a MongoDB cloud database [24].

The monitoring database serves as the centralised information hub to collect all the remote monitoring data, it also interfaces with network control applications and SDN controller. There are mainly three sources of information: transmitter, optical path and receiver. The transmitter information includes modulation format, wavelength, power, bandwidth, baud rate. Optical path information includes EDFA I/O power, gain, EDFA pump laser status, temperature. Receiver side information includes CD, PMD, SNR, power, etc. For each connection request, a unique record ID is generated to connect all the affiliated data in parallel. JavaScript Object Notation (JSON) is used as the file format in the database, data is synchronised through unique time stamps. The monitoring data is updated once per minute. The SDN-based applications query the selected record ID which is the key for traversing the data tree.

16 equalised 50GHz-spaced 32Gbaud DP-QPSK channels are generated at the transmitter side with wavelength ranging from 1545nm to 1565nm (relative EDFA gain flat region). Perfect filtering is assumed in all filters. CD and PMD are fully-compensated in the DSP. Each EDFA fully compensates the span power loss to ensure each channel launch power per span is 0dBm, this is controlled by passive EDFA I/O monitoring and OSA spectrum information. In this case, the EDFA gain is seen as an observable parameter. Some of the pre-tested EDFAs introduce unexpected additional ASE noise due to device ageing. The signal SNR is computed by averaging the BER monitored in the receiver optical modulation analyser (OMA) using [68]

$$SNR_{QPSK} = [\text{erfc}^{-1}(2 \cdot BER)]^2 \cdot 2R_s/B_n \tag{5.1}$$

where R_s and B_n are the signal baudrate and noise level bandwidth respectively.

The received signals are first filtered by a WSS with 0.4nm band pass filter and then pre-amplified to 3dBm for coherent detection. We use Keysight N4391A OMA which

consists of a 40GHz dual polarisation coherent receiver with local oscillator followed by a DSP unit. BER monitoring is performed using the built-in BER_{actual} counting software. The Pseudo-Random Bit Sequences (PRBS) length is $2^{15} - 1$ at transmitter side PPG, 50 sequences are counted for each epoch, yielding a minimum detectable BER of 6.1E-7 per epoch. Smaller BER detection is applicable for necessary cases by counting more PRBS per epoch. CD and PMD are fully compensated in the DSP by assuming dispersion of 16ps/(nm·km).

During network planning, GN model is used to predict system performance due to its well-proven robustness for nonlinear noise estimation. GN model also serves as lower level abstraction of the physical layer from which we can draw posterior parameter estimations. SNR is predicted by the GN model with [40, 135]

$$SNR_{rx} = \frac{k \cdot P}{\sum_{i=1}^{N} P_i^{ASE} + P^3 \cdot \eta_{NL} + \kappa \cdot P} \tag{5.2}$$

where P is per span launch power, k is the calibration coefficient, N is the number of spans, P_i^{ASE} is the ASE noise power in span i, η_{NL} is the NLI coefficient, $\kappa = (SNR_{TX})^{-1}$ is the inverse of the transmitter and receiver subsystem noise. P^{ASE} can be further expanded as [138]

$$P_{ASE} = h \cdot v \cdot NF \cdot G \cdot B \tag{5.3}$$

where h is Planck's constant, v is the optical carrier frequency, G is EDFA gain, B=50GHz. Equation 5.3 is under the assumption that G>>1. It is worth noting that strictly the gain term should be G-1. Since the gain is usually set to 15dB, this results in 3% error which is regarded negligible.

Among these model parameters, the channel power and EDFA gain can be directly monitored in real-time by reading the EDFA I/O power. SNR_{TX} is characterised before service provisioning and assumed constant due to its negligible variation over time

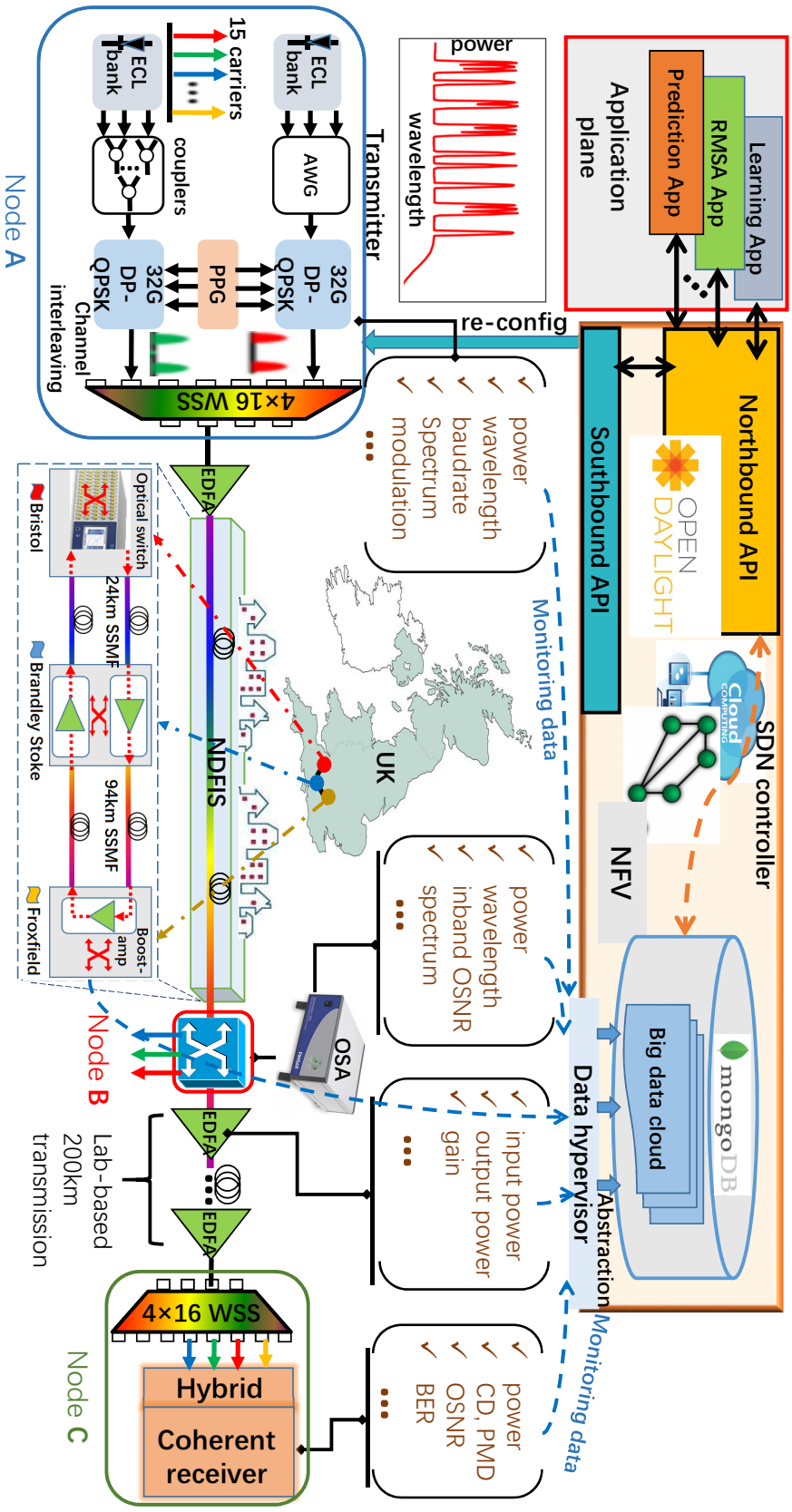

FIGURE 5.3. Caption on the next page.

FIGURE 5.3. SDN-based network-scale monitoring testbed. At node A transmitter side, 16 equalised 50GHz-spaced 32Gbaud DP-QPSK signals are interleaved and transmitted through NDFIS field trial, 4x16 WSS is used as interleaver and filter to avoid crosstalk. NDFIS connects three national geographical nodes: Bristol, Brandley Stoke (25km), Froxfield (95km). Signals are transmitted to Froxfield and looped back giving 240km effective transmission length. In each site, EDFA is used to fully compensate the span loss. Channel launch power per span is set as 0dBm, launch OSNR is kept identical among the 16 channels by conducting back-to-back EVM based BER monitoring. A 1x4 WSS is connected after loop-back as node B (intermediate node), serving for gain flattening filtering and channel add-drop. 4x50km (amplified per 50km) lab-based transmission is made after node B before signals are coherently received at node C. monitoring data from all devices is uploaded to SDN database for application plane use where machine learning algorithms are implemented. API: application programming interface, ECL: external cavity laser, PPG: pulse pattern generator, DP-QPSK: dual polarisation quadrature phase shift keying, AWG: arrayed waveguide grating, BER: bit error rate, WSS: wavelength selective switch, SSMF: standard single mode fibre, UK: United Kingdom

[2]. Back-to-back (BTB) measurement is carried out by connecting node A to node C and monitoring BTB BER performance versus OSNR to calculate SNR_{TX} as shown in Fig. 5.4. OSNR is controlled by coupling additional white Gaussian ASE noise into the system. Both the theoretical line without transceiver noise and the experimental line are plotted. The disparity of the two lines is because that the transceiver noise exists in the denominator of the SNR computation. As the OSNR is small, the linear ASE noise is relatively large compared to the transceiver noise. Given the transceiver noise is negligible, the measured SNR/BER value becomes nearly identical to the theoretical value (without transceiver noise). The measurement and theoretical SNR/BER values diverge with the increase of OSNR (equivalent decrease of ASE noise). SNR_{TX} can be computed by substituting a best fit point from the experimental line. As there is no BTB nonlinear noise, The OSNR degradation only accounts for ASE noise. SNR_{TX} is found to be 19.3dB using equation 5.1 and 5.2.

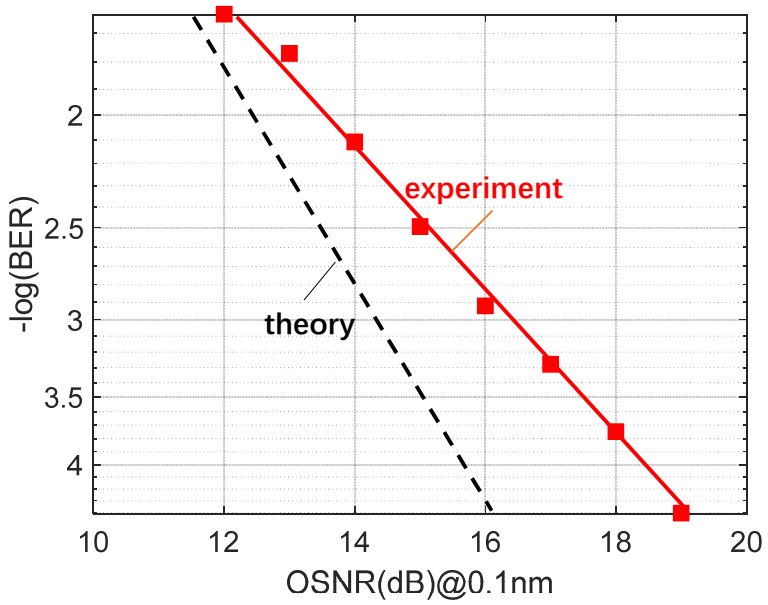

FIGURE 5.4. BTB characterisation of transceiver BER versus OSNR performance. Red solid line represents experimental regression line, black dashed line represents theoretical performance in the absence of transceiver noise.

5.4 Unsupervised MCMC inference (V-step)

As power can be monitored ubiquitously across the network by EDFAs, Optical Channel Monitor (OCM) or OSAs, the uncertainties are most likely to happen to the knowledge of EDFA NF and NLI coefficient η_{NL} which are the key parameters abstracting transmission linear and nonlinear noise respectively. We do vertical inference to learn deep into these hidden parameters.

Fig. 5.5 shows the flow chart of the network parameter learning process. After loading the pre-defined parameters, path SNR estimations are computed to compare with the monitoring value. If they are identical, then the pre-defined parameters are correct, otherwise the parameter tuning process has to be performed as a Monte Carlo process until the estimation error is minimised. The detail of the Monte Carlo process is described

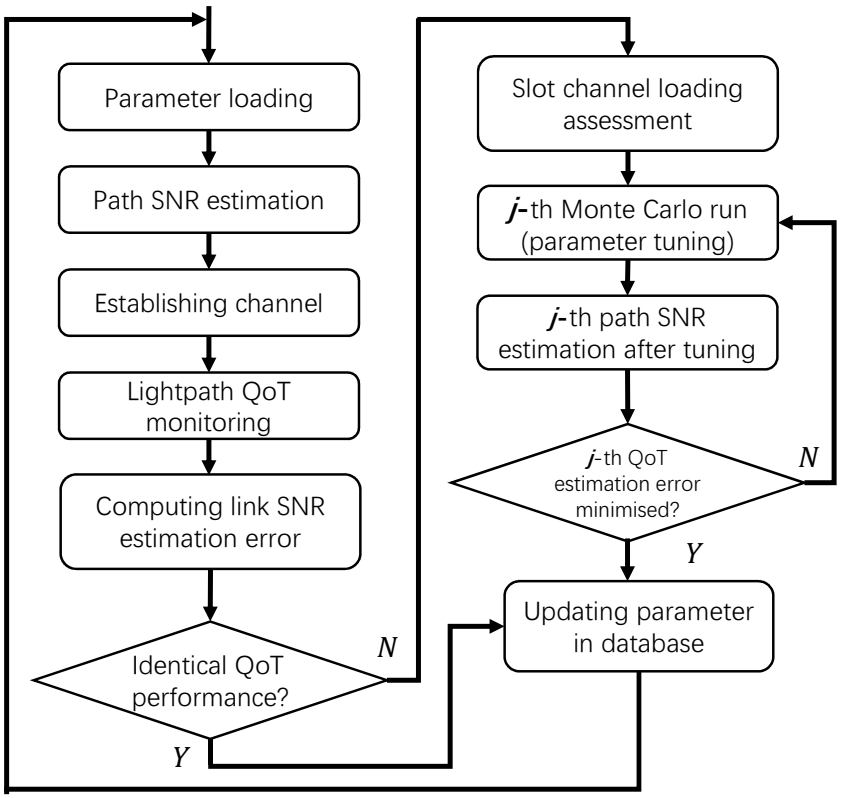

FIGURE 5.5. Flow chart of the parameter tuning process.

as the following.

Given the direct/observable knowledge of the target probability distributions of NF and η_{NL} is unavailable, we fit the GN model containing the uncertain parameters as the Bayesian likelihood function $P(Q_{monitored}|NF,\eta_{NL})$, we define our prior knowledge $P(NF,\eta_{NL})$ (ideal distribution) placed on NF and η_{NL} as Gaussian distributions

$$NF,\eta_{NL} \sim \frac{1}{\sqrt{2\pi\sigma^2}}\exp(-\frac{([NF,\eta_{NL}]-[NF,\eta_{NL}]_0)^2}{2\sigma^2}) \tag{5.4}$$

for which the priors $[NF,\eta_{NL}]_0$ come from data sheet information (NF) and GN model nonlinearity computation (η_{NL}) respectively. The posterior estimation (actual distribu-

tion) of the parameters can be determined with

$$P(NF,\eta_{NL}|Q_{monitored}) = \frac{P(Q_{monitored}|NF,\eta_{NL})P(NF,\eta_{NL})}{P(Q_{monitored})} \tag{5.5}$$

where $P(Q_{monitored})$ is a normalisation constant that is very hard to determine explicitly. By applying MCMC on top of GN model, we can ignore $P(Q_{monitored})$ and directly draw samples from the posterior

$$P(NF,\eta_{NL}|Q_{monitored}) \propto P(Q_{monitored}|NF,\eta_{NL})P(NF,\eta_{NL}) \tag{5.6}$$

MCMC calls for a likelihood function to maximize. Due to improper prior assumptions placed on $[NF,\eta_{NL}]$, the GN model QoT prediction $Q \sim NF,\eta_{NL}$ will be inconsistent with the monitoring value $Q_{monitored}$. We model the likelihood function $P(Q_{|}NF,\eta_{NL})$ based on the difference between $Q \sim NF,\eta_{NL}$ and $Q_{monitored}$ by mapping the error to 0-1 probability with Gaussian exponential

$$P(Q|NF,\eta_{NL}) = \exp(-k(Q_{monitored} - [Q \sim NF,\eta_{NL}])^2) \tag{5.7}$$

where k is a normalising coefficient. Hence the likelihood is maximised when the prediction and monitoring data converge. This also allows a closed-form expression for the posterior distribution (equation 5.5) given the Gaussian conjugate priors [142] placed on NF and η_{NL}. Sampling of the NF is in the unit of dB whereas using its absolute value should be more appropriate. The sampling range is controlled to be no less than 0, whereas for optical amplifiers, the more efficient range would be no less than 3dB. Inference of such bi-variate MCMC is conditioned on the network loading status which is fully-observable in the SDN controller: as more channels are loaded, sampling of η_{NL} is constrained to be no less than its previous value. Specifically, we define the channel of interest to be centred at a 7-slot window. The choice of 7 slots is because placing more than 7 channels around the target channel will not increase its nonlinearity further. Sampling

under any loading status is only considered to be performed given the corresponding window state and bounded by an upper-threshold for the worst case from historical inference data. Sampling for the entire window is performed so that in equation 5.7 the sum of the squared norm residuals $\sum \left\| Q_{monitored} - [Q \sim NF, \eta_{NL}] \right\|^2$ reaches minimum (equivalently maximising the likelihood).

Specifying proposed distribution:
$\theta = NF, \eta_{NL}$ - - definition
$q(\theta) \sim \mathcal{N}[\theta|\mu, \sigma]$ - - Gaussian proposal distribution;
$p(x) = textexp(-kx^2)$ - - squared exponential likelihood mapping;
$q(\theta_j|\theta_{j-1}) = q(\theta_{j-1}|\theta_j)$ - - symmetric random walk;
Sampling process:
for $i = 1 : N$ **do** - - N is the number of channels in the 7-slot window
Monitoring path SNR_i;
Specifying prior for θ according to datasheet;
for $j = 1 : M$ **do** - - M is the total number of MCMC iterations (sampling trials)
sampling $u \sim U[0, 1]$ - - uniform distribution from 0 to 1;
sampling $\theta \sim q(\theta_j|\theta_{j-1})$ - - Monte Carlo sampling for the next guess that depends on the current guess with Gaussian;
substitute new θ_j to estimate new SNR_j
$error_j = \left\| SNR_{est_j} - SNR_{monitored} \right\|$
If $u < F(\theta_j, \theta_{j-1}) = min[1, \frac{p(error_j)}{p(error_{j-1})}]$
$\theta_j = \theta_j$
else
$\theta_j = \theta_{j-1}$
end if
$error_j = error_{j-1}$
end for
updating θ in database
end for
Return:
θ, SNR

Algorithm 2: Pseudocode of CWMH algorithm to infer network hidden parameters.

Component-Wise Metropolis-Hasting (CWMH) sampling is adopted [143]: we assume Gaussian distribution for the component (parameter of interest) centred at the previous

accepted sample to be our proposal distribution. The next stochastic sample guess $q(NF', \eta'_{NL})$ is drawn from the current Gaussian

$$q(NF', \eta'_{NL}) \sim \mathcal{N}[(NF_0, \eta_{NL0}), \sigma^2] \tag{5.8}$$

where σ^2 is the variance that depends on the component, i.e., the optical parameter. The Monte Carlo sampling process follows symmetric random walk. A new sample pair NF', η'_{NL} is accepted if the likelihood $P(Q'|NF', \eta'_{NL})$ increases, otherwise there is a probability of P_{rej} that the jth sample pair is rejected where

$$P_{rej} = 1 - \frac{P(Q_j|NF_j, \eta_{NL_j})}{P(Q_{j-1}|NF_{j-1}, \eta_{NL_{j-1}})} \tag{5.9}$$

The pseudocode of MCMC inference is shown in Algorithm 2, CWMH is used so that the components NF and η_{NL} are updated in turn instead of simultaneously during each sampling process. First order Markov chain is used so that the next guess only depends on the current guess (Gaussian distributed) and ignores all the historical samples

$$P(\theta_n|\theta_{n-1}, ..., \theta_2, \theta_1) = P(\theta_n|\theta_{n-1}) \tag{5.10}$$

5.5 Performance of MCMC

Fig. 5.6 shows the joint bivariant Gaussian distribution approximated by CWMH sampling for a single channel transmission at $P_{launch} = 0dBm$, $\lambda = 1556nm$ from node A to node C (Fig. 5.3). In the case where spans are not of the same length, for computational convenience, the composite NF_{comp} is used to represent the equivalent average noise figure of all the cascading EDFAs (n) along the lightpath [144]

$$NF_{comp} = NF_1 + \frac{NF_2}{G_1} + \frac{NF_3}{G_1 G_2} + ... + \frac{NF_n}{G_1 G_2 ... G_{n-1}} \tag{5.11}$$

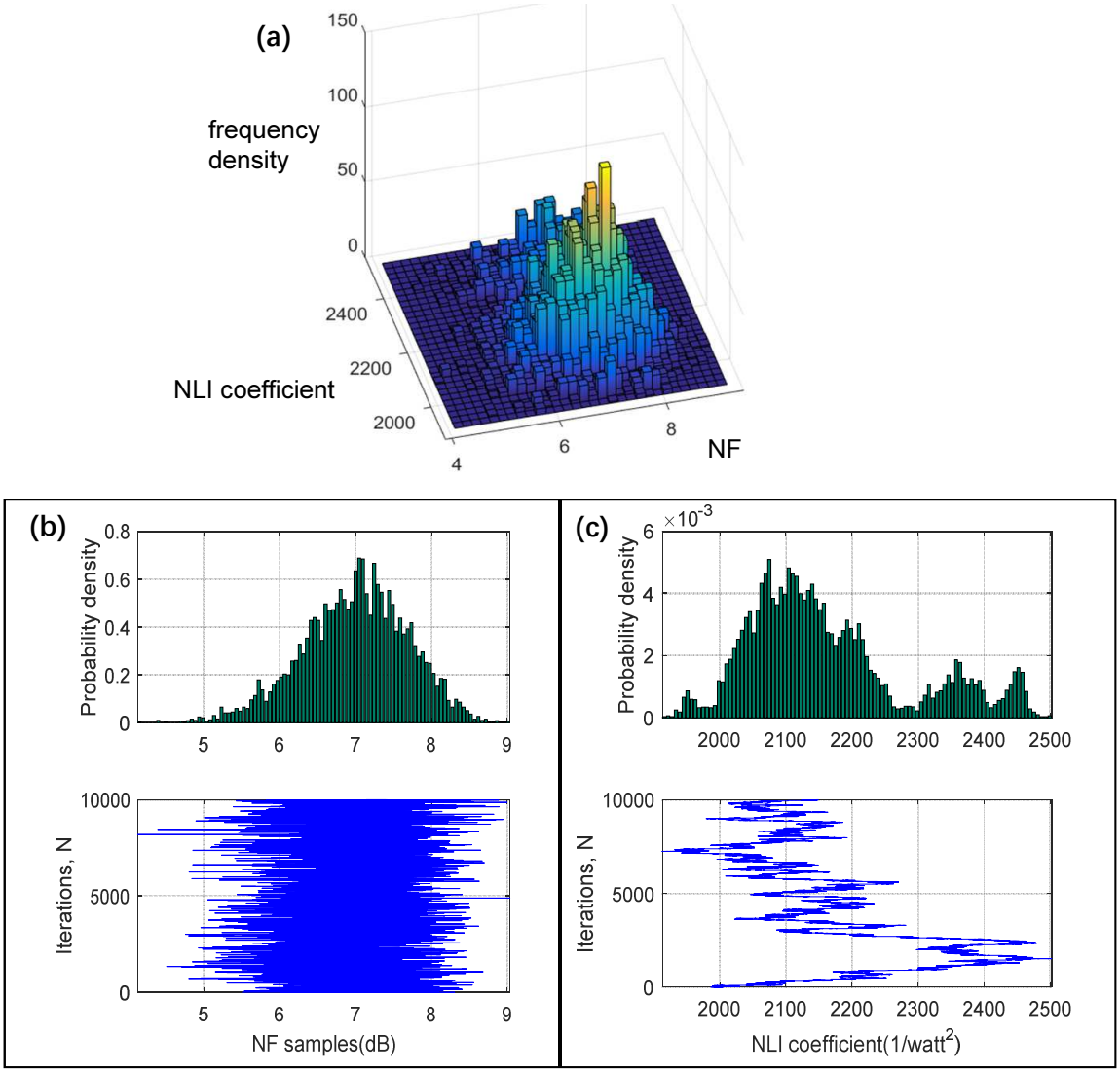

FIGURE 5.6. (a) Joint bi-dimensional frequency density distribution of single-channel transmission noise figure and NLI coefficient posterior inference. (b) Noise figure Probability Density Function (PDF) following a Gaussian distribution centred at 7.1 and its sampling iteration path including burn-in period. (c) NLI coefficient PDF following a Gaussian distribution centred at 2100 and its sampling iteration path including burn-in period.

where G is the span loss or the EDFA gain. η_{NL} represents the sum of all spans NLI coefficients along the path [8]

$$\eta_{NL} = \sum_{i}^{n} \eta_i \tag{5.12}$$

All the EDFAs I/O power are monitored to ensure complete compensation of all span loss. The mean of the Gaussian distribution is located where the actual value is most likely to be, i.e., the Maximum A Posteriori (MAP) estimation conditioned on the prior and monitoring data. The projections of the joint distribution are further shown in Fig. 5.6 (b) and (c), each representing the PDF of the posterior estimation of NF_{comp} and η_{NL} respectively. The priors placed on NF_{comp} and η_{NL} are 5.5dB and $1950W^{-2}$ respectively. As Fig. 5.6 (b) and (c) indicate, the iterations of the sampling guess for NF_{comp} and η_{NL} start from the prior values, after a burn-in period, they converge to the MAP with the highest sampling frequency, representing the highest probability. Finally we capture the MAP estimation to be 7dB and $2100W^{-2}$ respectively. The closed-form expression for the NF posterior distribution is

$$NF \sim \mathcal{N}(\theta|MAP,\sigma^2_{NF}) = 0.66\exp[-\frac{(\theta-7)^2}{0.72}] \tag{5.13}$$

In particular, the NLI parameter η_{NL} distribution exihibits relatively higher densities in other regions far from the MAP, this is due to its less contributed weight on the total noise performance in this setting compared to NF.

To verify the robustness of the inference process, we load 4 more adjacent channels in the 7-slot window to introduce more nonlinear noise to the target channel. We perform MCMC again for the new loading state. Fig. 5.7 shows the resulting posterior joint distribution and its projections for NF_{comp} and η_{NL} of the target channel. The MAP estimation for NF is 6.8dB which is very close to the previous estimation. It is worth noting that due to previous inference knowledge, the prior placed on NF is 7dB instead of 5.5dB, the iteration starts from 7dB and converges to 6.8dB. However, η_{NL} is theoretically independent of launch power but dependent of loading state, hence the prior placed on η_{NL} will not come from previous MAP but needs additional GN model simulation. As shown in Fig. 5.7(c), the iteration starts from $\eta_{NL} = 3800W^{-2}$ (prior from simulation) and

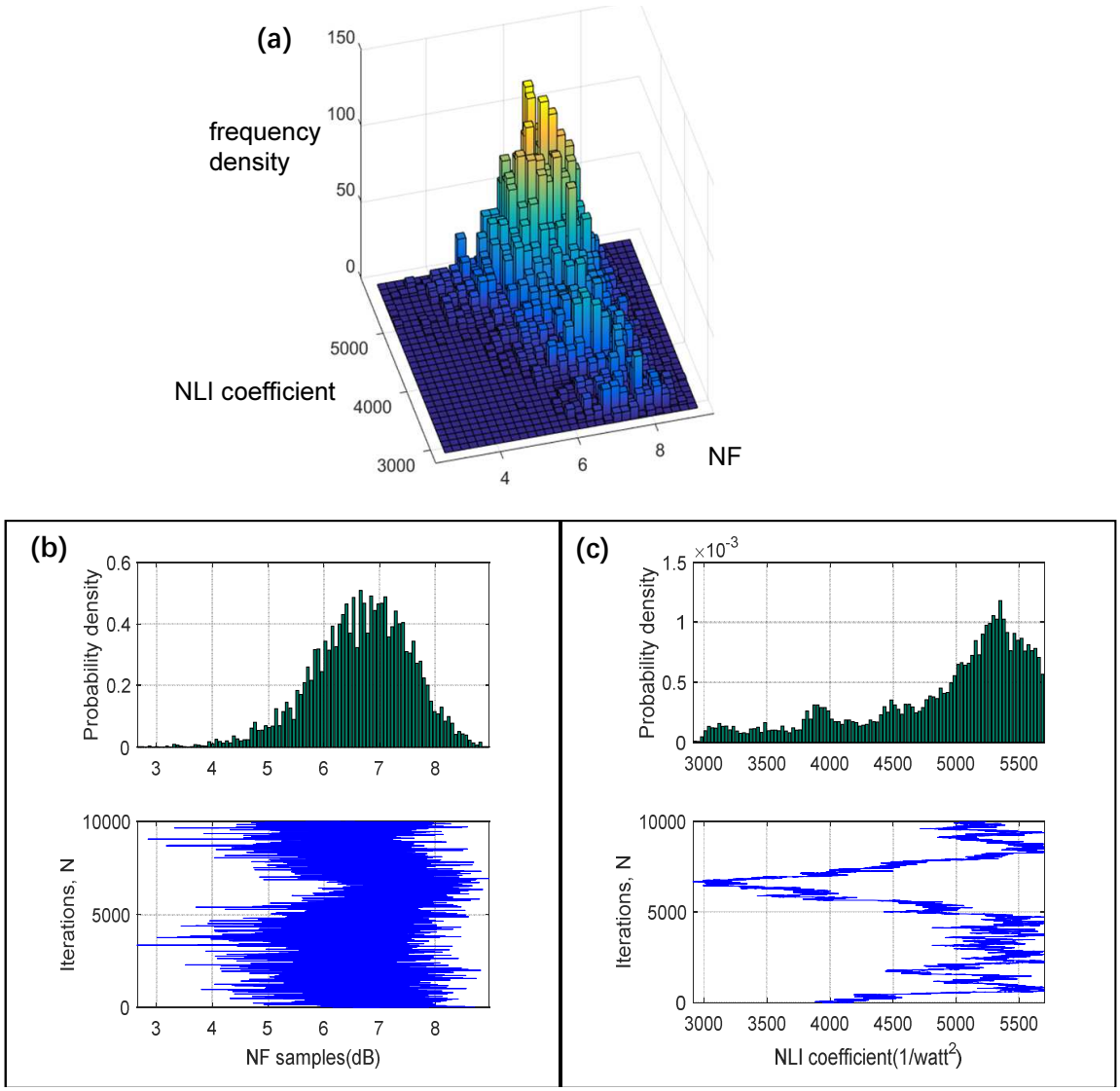

FIGURE 5.7. Joint bi-dimensional frequency density distribution of 5-channel transmission noise figure and NLI coefficient posterior inference. (b) Noise figure PDF that follows a Gaussian distribution centred at 6.8 and its sampling iteration path including burn-in period. (c) NLI coefficient PDF following a Gaussian distribution centred at 5300 and its sampling iteration path including burn-in period.

converges to the MAP estimation $5350W^{-2}$. In other cases where signal launch power is changed while loading state keeps the same, the prior knowledge placed on η_{NL} should

come from previous inference instead

$$P_n(\eta_{NL}) = P(\eta_{NL}|Q_n) = \frac{P(Q_n|\eta_{NL})P_{n-1}(\eta_{NL})}{P(Q_n)} \tag{5.14}$$

where $P_{n-1}(\eta_{NL})$ is the prior knowledge from the previous inference result.

We examine the true value of each inline EDFA NF_i by doing offline NF measurement with an OSA. The additional noise introduced by laser is avoided by interpolation and is subtracted from the total noise emitted by the EDFA. We keep the input power and gain in each EDFA identical as the online case. The laser source spontaneous emission (SSE) noise is subtracted from the total noise emitted by the EDFA according to [145]

$$NF_{dB} = 10\log(\frac{P_{ASE}}{GhvB_0} + \frac{1}{G} - \frac{P_{SSE}}{hvB_0}) \tag{5.15}$$

where P_{ASE} is the total noise spectral density at 0.1nm including SSE at the signal wavelength, P_{SSE} is the 0.1nm SSE spectral density at the signal wavelength, B_0 is the effective noise bandwidth of the OSA, G is the optical gain, v is the optical frequency, h is Planck's constant. All the measurements are carried out using an OSA with 0.1nm resolution. Fig. 5.8 shows the SSE noise measurement before passing EDFA.

Fig. 5.9 shows the offline NF testing result at $\lambda = 1556nm$, the composite NF calculated from the test values is 6.7dB which is very close to the inference value. Prior data sheet knowledge of $NF_{prior} = 5.6dB$ is also shown as a reference, due to the Gaussian conjugate prior placed on the NF, the posteriori estimation follows Gaussian distribution hence 95% CI can be computed. The prior sits out of the CI range of the inference while the offline measurement mean sits right within the range, indicating there is 95% chance the true composite NF average will fall close to our inference value. Taking the offline measurement mean value as benchmark, inference dramatically decreases our knowledge error of NF from 1.1dB (prior knowledge) down to 0.1dB (MCMC).

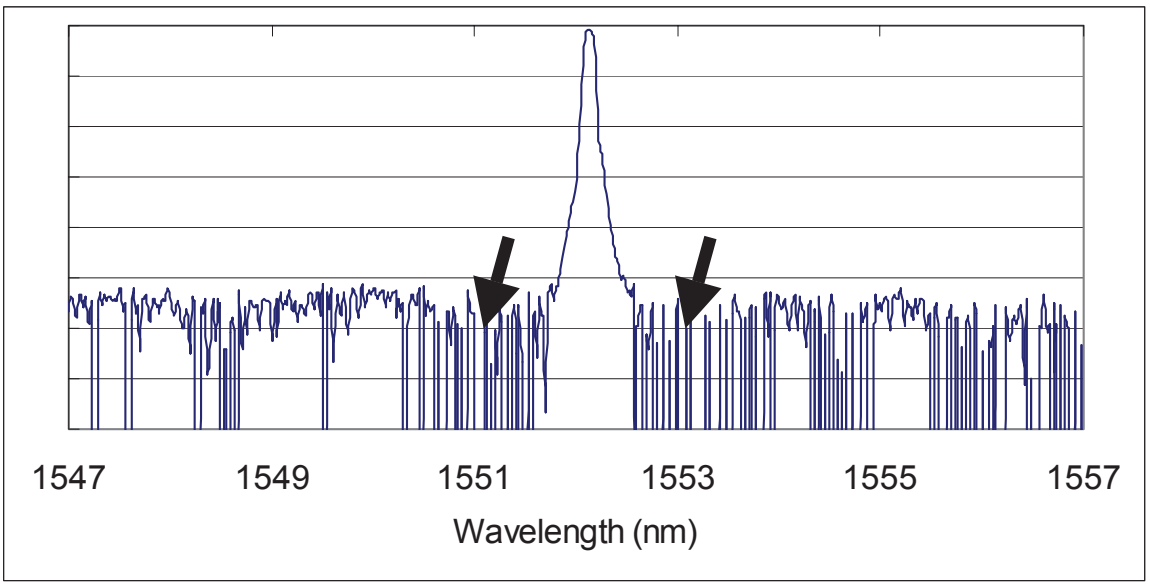

FIGURE 5.8. Measurement of SSE power levels with 1nm on both sides of signal wavelength. This is the signal before amplification.

As the number of channels increases, inference of both NF and NLI coefficient is shown in Fig. 5.10. The theoretical η_{NL} is computed by GN model. Both theoretical and inference of η_{NL} show degradation of the rate of increase with respect to channel number, this is due to the fact that adding adjacent or close channels to the target channel causes much more nonlinear noise than distant channels. In this case, inference of η_{NL} saturates after adding 6 or more channels at a normalised value of 5.7. In contrast, inference of NF keeps constant while the loading state is changing, demonstrating an accurate and robust NF inference process.

5.6 Hybrid learning at network per-link level

In chapter 4 we have introduced GP as a regression method to cope with online learning task with restricted training data set. In this section, GP will be used as the H-step learning to predict any unestablished channel SNR to further estimate the hidden

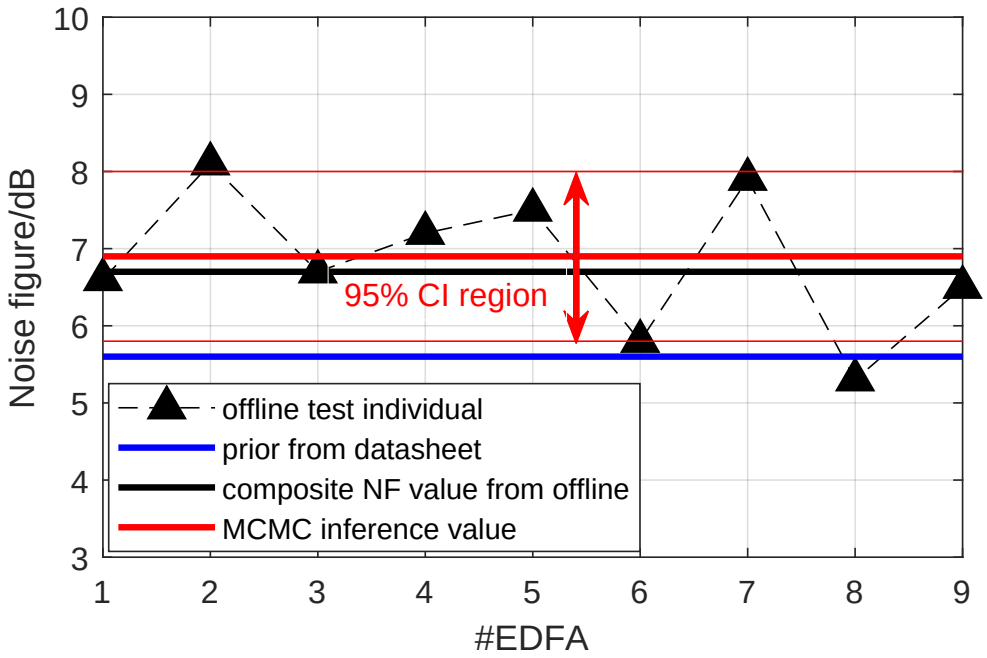

FIGURE 5.9. Offline measurement of noise figure of all the cascading EDFAs and their equivalent composite average as black line, inference of NF is shown as red line together with 95% confidence integral from posterior Gaussian distribution, data sheet indicated NF is shown in blue line.

parameters of the link.

Network level SNR estimation is often computed by summing up per-link level SNR performance, this also applies to situations where link-level SNR performance is unknown and has to be computed from the lightpaths passing through the link. The basic assumption is that both ASE and nonlinear noise are linearly accumulated along the lightpath as indicated in Fig. 5.11(a) with the following equation [68]

$$Q(\lambda)_{link\#j-1} = (Q(\lambda)_{path\#j} - Q(\lambda)_{path\#j-1})^{-1} \tag{5.16}$$

where $Q(\lambda)_{path\#j}$ and $Q(\lambda)_{path\#j-1}$ come from GP-based H-step inference for wavelength λ of link j using other wavelengths' OPM data of path j and j-1 respectively.

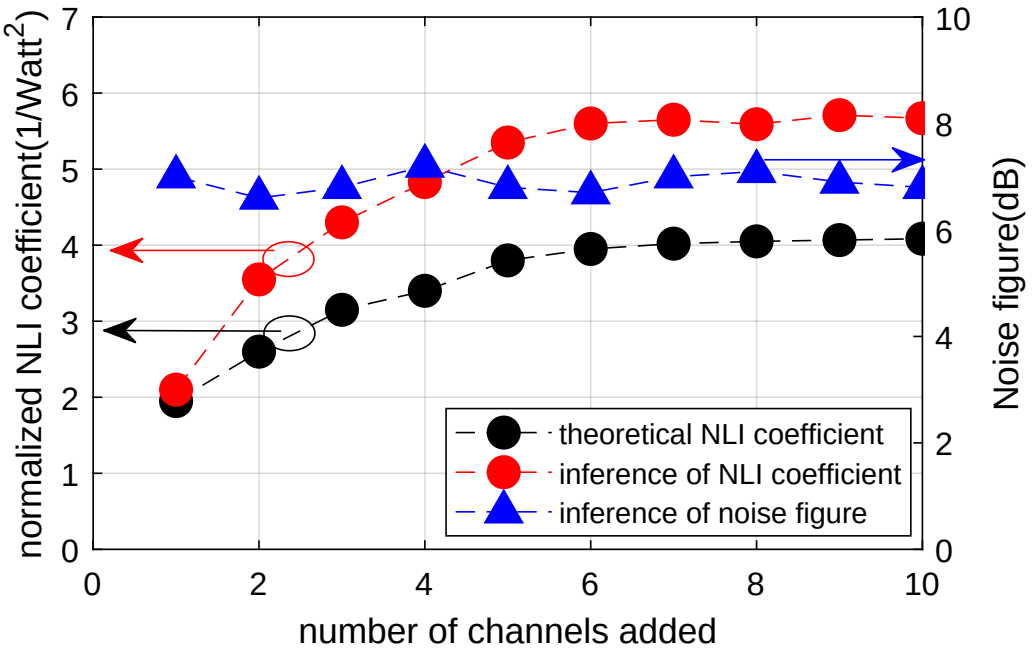

FIGURE 5.10. Inference of NLI coefficient and NF with change of channel loading, NLI for both learning and theoretical case reach saturation threshold when 6 or more channels are loaded.

To emulate such living network scenario, we transmit 16 equalised training channels at node A transmitter side, wavelength ranging from 1554nm to 1564nm. As shown in Fig. 5.11(b) which is a simplified view of Fig. 5.3, after the first NDFIS link, 8 of them are dropped and coherently received at the intermediate node B, the remaining channels are coherently received at node C, so path A-B ans A-C can be monitored. As previously explained, link A-B parameter set NF, η_{NL} can be inferred by applying MCMC to the OPM data collected at node B. However, to update the knowledge for link B-C parameter set we have to use equation (5.16) with the monitoring data generated at both node B and C.

As shown in Fig. 5.12, H-step GP regression is performed based on the OPM data collected at node B and C, representing path A-B and path A-C SNR performance respectively.

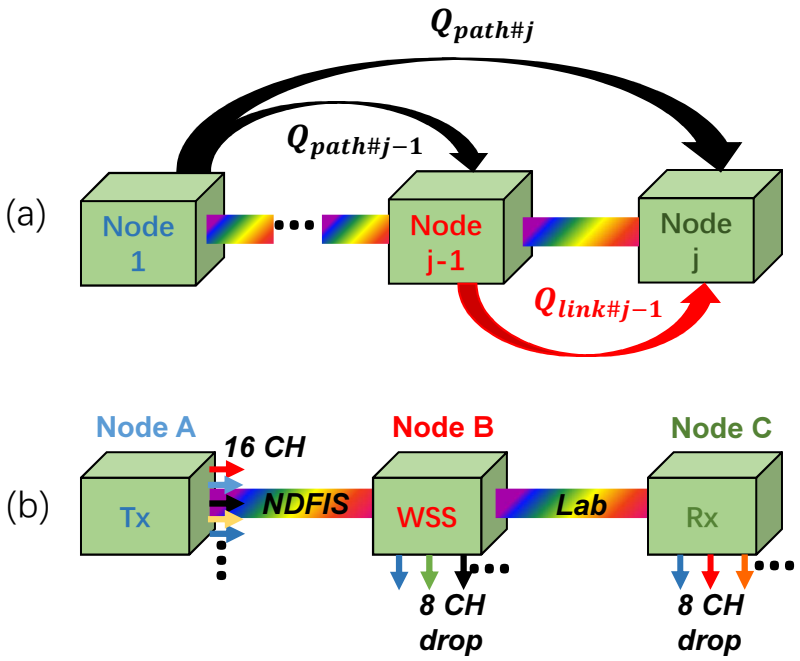

FIGURE 5.11. (a) Conceptual diagram of transmission performance Q over many links, the noise performance is assumed to be linearly accumulated so that a single link performance $Q(\lambda)_{link\#j-1}$ can be calculated from the path performance $Q(\lambda)_{path\#j}$ and the path performance ending at previous node j-1 with the same origin $Q(\lambda)_{path\#j-1}$. (b) Simplified network field trial scenario where 16 equalised 0dBm 50GHz-spaced 32Gbaud DP-QPSK signals are generated at node A and transmitted through A-B-C. 8 signals are dropped at the intermediate node B using a WSS. Link A-B is NDFIS-based transmission and link B-C is lab-based transmission. EDFAs compensate all the span loss.

Test set is generated by placing additional test channel to each of the empty slot and monitoring their SNR performances. GP returns SNR prediction error of 0.6dB RMSD, 0.9dB MAX for path A-C, and 0.3dB RMSD, 0.6dB MAX for path A-B. Link B-C SNR performance estimation (point R in the figure) is computed by selecting the channel of interest (wavelength #8 in the figure) and importing the SNR prediction data at GP intersection points P ($Q(\lambda)_{path\#j}$) and Q ($Q(\lambda)_{path\#j-1}$) into equation (5.16). It is worth noting that the estimated link B-C performance at λ = #8 excludes transceiver noise

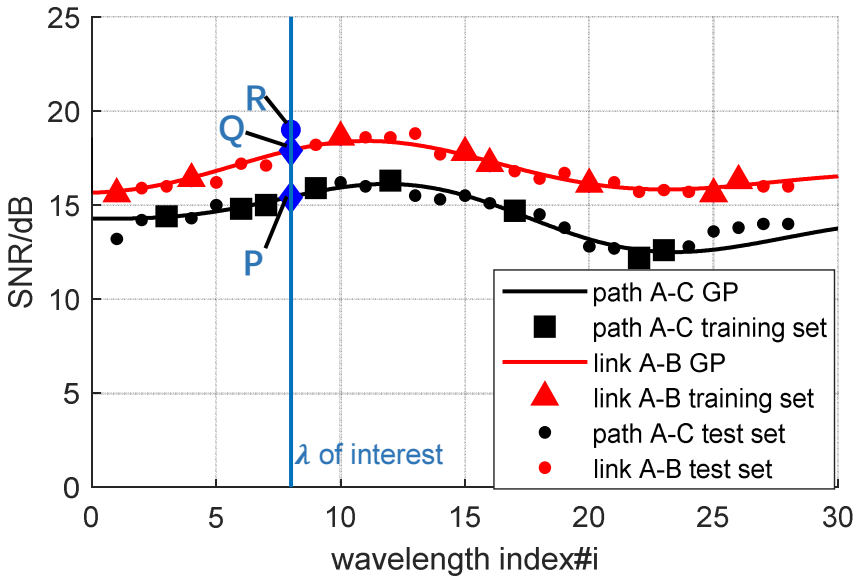

FIGURE 5.12. GP-based SNR learning using 8 training channels for path A-B and A-C, link B-C performance (point R) is further calculated at the corresponding wavelength of interest with GP intersection points P and Q using equation (5.16).

penalty SNR_{tx} as it is cancelled in the subtraction, hence this term is omitted in the GN model estimation. V-step inference for link B-C NF, η_{NL} is further performed using MCMC on top of prior knowledge and the GP returned data such as point R for $\lambda = \#8$.

In comparison, we also run Gradient Descent (GD) with respect to NF, η_{NL} which treats this inference process as an optimisation problem (fixed parameter and random data assumption in MLE), GD is seen as a frequentist iterative parameter tuning method which is commonly used in neural networks. As we are searching for the global minimum of the estimation error, GD is applicable. In cases where global maximum point is wanted, Gradient Ascent (GA) is used instead. The parameter set is updated based on the slope of descent [146]:

$$[NF, \eta_{NL}]_{new} = [NF, \eta_{NL}] - \alpha \nabla \sum \left\| Q_{monitored} - Q_{estimated} \right\|^2 \tag{5.17}$$

where α is the learning rate.

After refining knowledge of all the individual links by monitoring and learning, we substitute the parameters back into GN model equations. Parameter set $[NF, \eta_{NL}]$ is shared among the 7-slot window, i.e., the nearest existing parameter set within the window range is applicable to the target channel prediction. If multiple sets exist, the average value is used. In particular, the path level A-C SNR performance is computed by summing up all the concatenating links performance:

$$Q(\lambda)_{pathA-C} = (Q(\lambda)^{-1}_{linkA-B} + Q(\lambda)^{-1}_{linkB-C})^{-1} \tag{5.18}$$

Fig. 5.13 shows the SNR performance prediction error for each link A-B, B-C and A-C using the updated GN model. In comparison, model prediction error without parameter learning (using improper priors, black dots), only with NF parameter learning through MCMC (blue dots), and all-parameters learning through gradient descent (green dots) are also plotted. By keeping improper analytical η_{NL} prior and just using MCMC to update the NF, the model reduces the maximum prediction error over the wavelength set from 2.7dB to 1.4dB, resulting in 48% error reduction. Further error reduction is achieved by substituting updated η_{NL} which brings the prediction error further down to 0.8dB, resulting in 70% error reduction compared to the static case. Such further error reduction also verifies the accuracy and robustness of the MCMC inference process for η_{NL}.

In addition, parameter tuning using GD (red dots) results in the prediction error distribution having larger maximum error (1.3dB) and higher variance than MCMC, this is due to the its intrinsic over-confidence in parameter estimations that tends to overfit the training set. Depending on the initial point, gradient descent is likely to be stuck in local optima point which does not provide the parameter global distribution as MCMC. Fig. 5.14 shows a general case of local optima and global optima. In our inference case, as

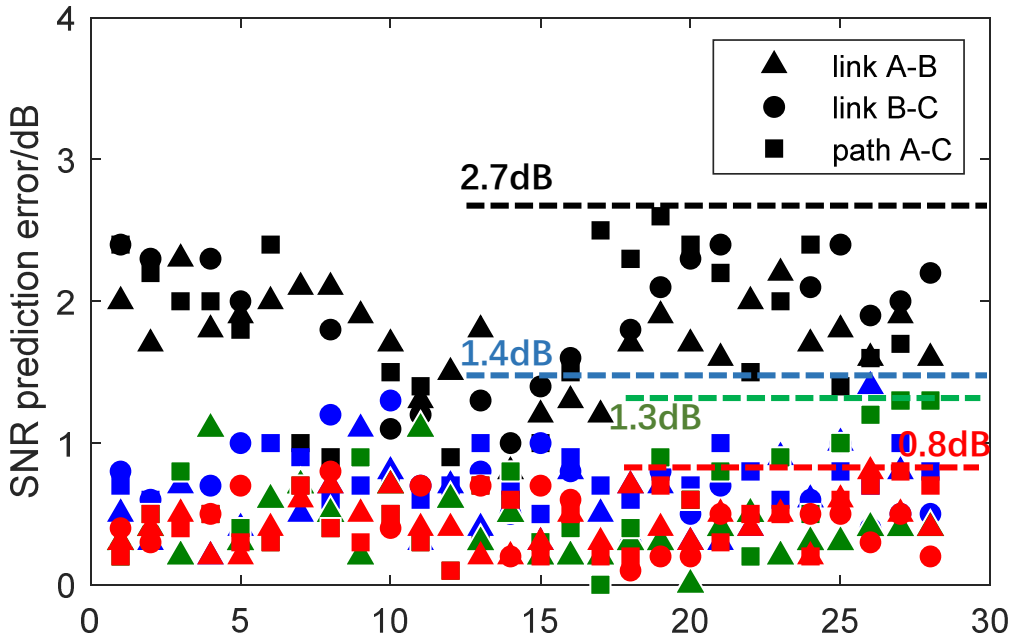

FIGURE 5.13. SNR prediction error plot for path A-B, B-C and A-C using static GN model with improper parameter knowledge (black dots), GN model with gradient descent learning for all parameters (green dots), GN model with MCMC self-learning NF ONLY (blue dots), and GN model with MCMC self-learning for all parameters (red dots) respectively. Specifically, with updated η_{NL} added in the model through MCMC inference, prediction error decreases from 1.4dB to 0.8dB, demonstrating an accurate nonlinear distortion parameter learning process. Gradient descent tends to overfit the training data as the error variance is relatively large shown by the green dots.

shown in Fig. 5.6 (c), η_{NL} PDF has several local maxima points which can give relative "good enough" solutions, but they are not the true value. GD is likely to be stuck in those local optima. The resulting prediction model is said to be not as generalisable as using MCMC.

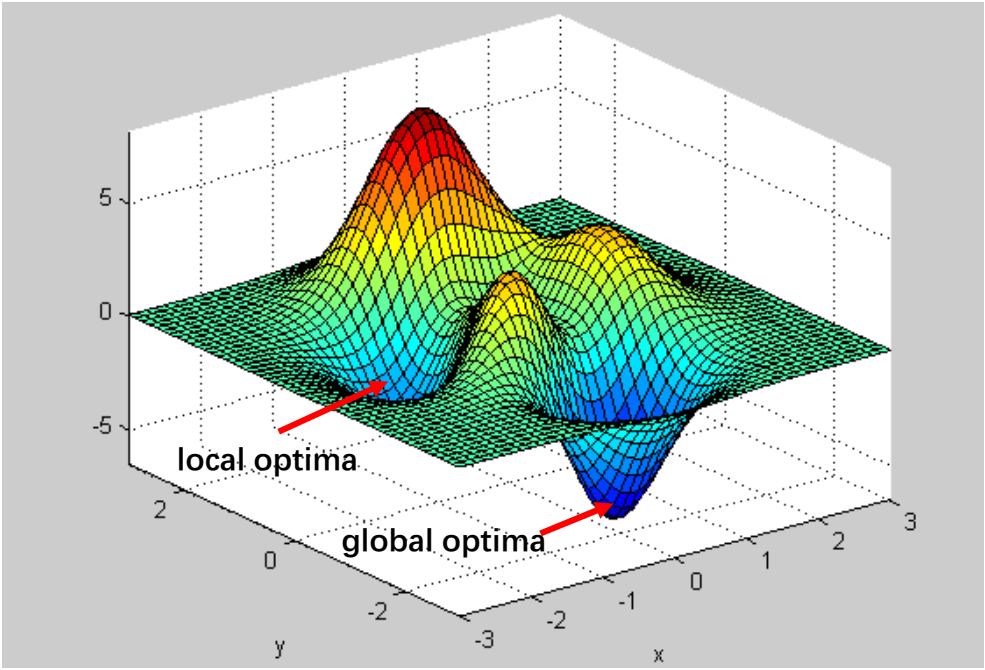

FIGURE 5.14. GD is likely to be stuck in the local minima or local optima position, it is hard for GD to jump out and find the global optima then.

5.7 Summary

We have shown that by applying hybrid supervised/unsupervised online learning, unobservable physical layer parameters such as EDFA noise figure and GN model nonlinear interference parameter η_{NL} can be extracted at network per-link level. These parameters represent critical lower level physical layer information that may not otherwise be traced in real time with direct monitoring. It is worth mentioning that the GN model does not need to be necessarily used for our method, any network models that can abstract physical layer and output certain observable features are applicable, inference can run on top of that model to draw posterior knowledge given the monitored features. To exemplify such learning capability, we configured a cognitive, field-trial testbed in which signals are transmitted through NDFIS network to emulate sufficient uncertainties. Under noise non-uniformity condition, we have shown that by applying H-step GP regression with

monitoring, we can make online predictions with high fidelity using monitoring data. GP model also allows to estimate SNR prediction uncertainties by computing confidence integrals. This quantified prediction uncertainty feature can be potentially leveraged as control plane algorithm constraint to further optimise global SNR uncertainty such as the monitoring-on-demand application [27]. Further details of how to leverage the confidence integrals will be demonstrated in Chapter 7.

By applying unsupervised V-step MCMC inference on top of GN model and path OPM data, we are able to refine the improper parameter priors placed on GN model and further enhance the prediction accuracy. In the case of EDFA NF parameter, our inference method achieves 0.1dB estimation error, which is 90.9% less compared to the static case (1.1dB) without learning. In common network scenarios where there is no end-to-end online monitoring data available for a specific path, simultaneous H/V inference can be applied given the monitoring data for other paths is available. It is worth noting that such probabilistic learning process does not find the exact value for each parameter to perfectly match the model prediction with the monitoring data as gradient descent does. Perfect matching normally results in model predictions not generalising well on future monitoring data sets, i.e., overfitting to the training set. By assuming Gaussian distribution of all the parameters, the adopted MAP value represents a good approximation of the true value with degrees of estimation uncertainties calculated from the closed-form expression of the distribution. Again the quantified parameter estimation uncertainty can be used for more applications as a byproduct. The accuracy of the parameter learning process is further examined by replacing the improper priors with the inference output. SNR prediction error is reduced from 2.7dB to 0.8dB, yielding 70% equivalent uncertainty reduction during dynamic network design and planning. Such parameter inference capability potentially provides a way to separate the ASE and nonlinear noise, hence delivering valuable real-time feedback information for control

plane optimisation algorithms.

In summary, we have proposed and demonstrated a comprehensive self-learning solution for optical networks which is enabled by centralised monitoring and hybrid online learning. By simultaneous supervised (H-step) and unsupervised (V-step) learning of the network system, physical layer impairment abstractions can be refined dynamically and autonomously with statistical scales of precision. Such quantified estimation probability can be potentially leveraged for control plane decision making. Knowledge uncertainties of the network is reduced significantly allowing the network to run close to its performance limit. Such probabilistic learning capability forms a powerful toolset towards ultimate optical network intelligence which is able to gain real-time physical layer insights autonomously.

CHAPTER 6

INTERMEDIATE NODE MONITORING

This chapter [1] contains relevant research work to integrate the intermediate node OSNR monitoring (in the linear regime) function into optical networks. Such monitoring capability is further leveraged to provide global network information for network diagnose and planning.

6.1 Introduction

Traditional optical networks establish rigid connections (lightpaths) at fixed bit rate, where the channels are modulated with a common (fixed) modulation format and fixed lightpaths. The planning and recovery decisions are made only by transmission distance and hardware assumptions which is unaware of the real-time conditions of the physical layer [5]. The emergence of heterogeneous QoS requirements from applications continues to drive the evolution of traditional optical networks. Advanced technologies such as flexible transponders [147], coherent transmission [31] and ROADMs [148] have con-

[1] This work is published in OFC conference proceeding [77]

siderably enhanced the network dynamicity and flexibility. Offline network planning methods are mainly developed under static optical transmission models, so they have difficulty in capturing such complex system behaviour [149]. As data rate grows from recent 100G to future 400G and above, the control plane has to dynamically adjust its resources (bandwidth, modulation format, lightpath, etc. according to each connection requirement. In this case, static planning can no longer support such a flexible network where impairments become more path dependent and unpredictable.

The advances of various OPM technologies have made the optical network fully cognitive, i.e., being able to perceive real-time optical performance and feed the information back to the control plane. In this case, OPM becomes indispensable to bridge the control plane and the underlying hardware. Previous research has shown that OPM plays an important role in network optimisation and re-planning. However, most of the information comes from the receivers and transmitters, hence the control plane holds limited information about each individual link [150].

The most critical feature that represents QoT in current flexible optical networks is OSNR [6]. In such case, OSNR monitoring is imperative and should be placed ubiquitously across the physical layer. In current coherent receivers, in-band OSNR can be easily computed by the statistical-moment based or the Error Vector Magnitude (EVM) based methods which represent lightpath-level metrics [6]. However, reliable and distributed in-band OSNR monitoring is also needed at intermediate nodes (e.g., ROADMs) to obtain OSNR performance at per-link level. Due to the lack of intermediate node monitoring, previous research proposes active monitoring [33] to measure unestablished lightpath performance. It works by indicating the minimum number of informative monitoring probes in order to maximise the network knowledge gain. Although this approach proves to be effective, the assumption that impairments are flat across the transmission spectrum may influence the prediction accuracy [75]. Such uncertainty exploration will

be addressed in Chapter 7. Moreover, the computational complexity of network kriging is high for large networks [76]. Therefore, an alternative method is proposed here, i.e., intermediate node monitoring, to solve the network uncertainty at link level. It is capable of providing straight-forward intermediate node OSNR information that can potentially enable low-complexity link-level network planning.

In this chapter, we propose and experimentally demonstrate in a field trial an "in-depth" optical network monitoring mechanism that applies both intermediate node and receiver side OSNR monitoring. We demonstrate that each link status can be monitored and used to update the network planning table, and the restoration decision is made based on the updated table. The closed-loop monitoring and control scheme runs throughout the life-cycle of each signal. The final results comparing with static planning shows the effect of the monitoring mechanism in guaranteeing QoT for the restored connections.

6.2 Intermediate node monitoring

In-band OSNR monitoring in principle should be Modulation Format (MF) independent and tolerant to spectrum narrowing effect. The latter is induced by cascaded WSS. We apply a reference optical spectrum based OSNR monitoring algorithm [16, 151, 152] using a high-resolution OSA. This method has been proven to be MF independent and WSS filtering effect insensitive. It is worth noting that in real applications this monitoring function can be implemented using lower cost coherent reception and Radio Frequency (RF) measurement device. The MF independence and spectrum narrowing tolerance capabilities were investigated in [16, 152]. We address the feasibility of integrating this monitoring function into ROADMs.

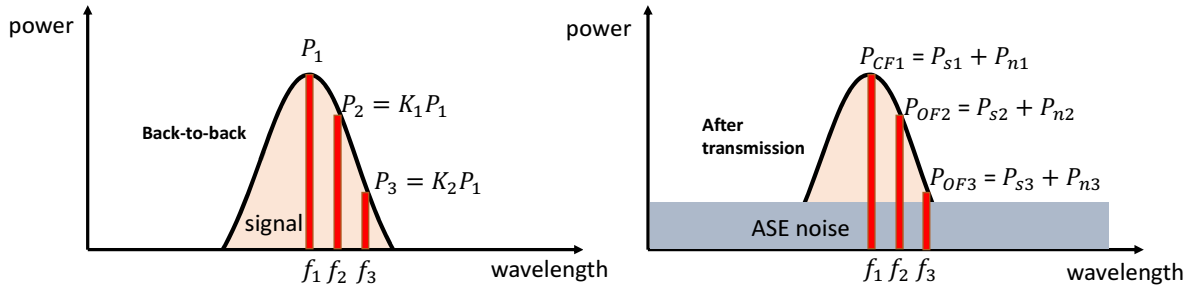

FIGURE 6.1. Offset frequency power monitoring method to compute in-band OSNR, the back-to-back spectrum is used to determine parameters K_1, K_2, ASE noise is assumed flat within the channel bandwidth.

6.2.1 In-band OSNR monitoring algorithm

Fig. 6.1 shows the working principle of the algorithm. The signal spectrum before transmission is monitored back-to-back as the reference. Three signal spectral powers P_1, P_2 and P_3 are measured at three frequencies f_1, f_2, f_3 within the signal band, f_1 is the center frequency and f_2, f_3 are two offset frequencies. The power ratios $K_1 = P_2/P_1$ and $K_2 = P_3/P_1$ are determined from the reference spectrum. After transmission, the signal OSNR will be degraded mainly due to the ASE noise which can be modelled as white Gaussian noise. Two parameters α and β are introduced to model WSS filtering penalty on the signal spectrum, by monitoring the spectral powers $P_{CF1}, P_{OF2}, P_{OF3}$ after transmission, we have

$$P_{CF1} = P_{s1} + P_{n1} \tag{6.1}$$

$$P_{OF2} = P_{s2} + P_{n2} = K_1 \alpha^N P_{s2} + P_{n1} \tag{6.2}$$

$$P_{OF3} = P_{s3} + P_{n3} = K_2 \beta^N P_{s3} + P_{n1} \tag{6.3}$$

N is the number of filters the signal traversed, P_{s1}, P_{s2}, P_{s3} are the signal power at f_1, f_2, f_3 respectively, and P_{n1} is the ASE noise power at f_1, f_2, f_3. Solving the above

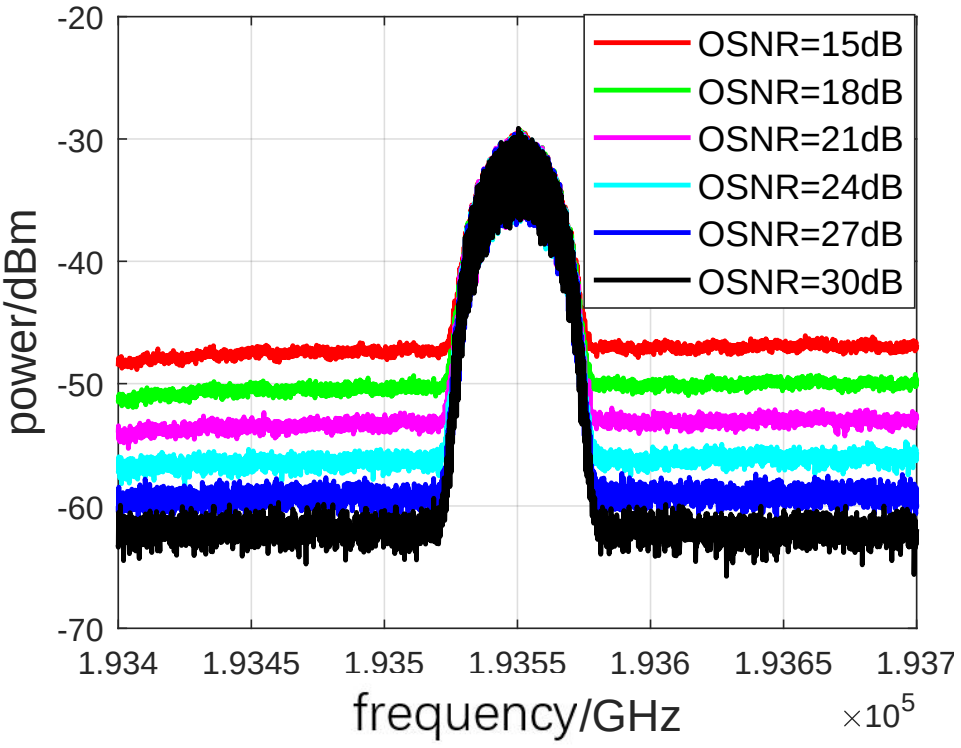

FIGURE 6.2. Coupling additional ASE noise into signal to emulate OSNR degradation and calibrate parameters for α, β, γ.

equations gives the value of P_{s1} and P_{n1} hence OSNR can be computed as

$$OSNR_{dB} = 10\log[\gamma \frac{P_{s1}}{P_{n1}}] \tag{6.4}$$

where $\gamma = 1.7$ is a calibration coefficient which depends on device power monitoring sensitivity and WSS filter setting [16, 152]. Such power-based OSNR monitoring technique only considers ASE noise induced by EDFAs, nonlinear noise is not considered.

6.2.2 Monitoring performance

By conducting back-to-back ASE noise loading for 32GBaud dual-polarization QPSK signals, the performance of the in-band OSNR algorithm using Finisar WaveAnalyzer 1500S [153] is evaluated. 50GHz fixed grid is used for each channel spacing. Different

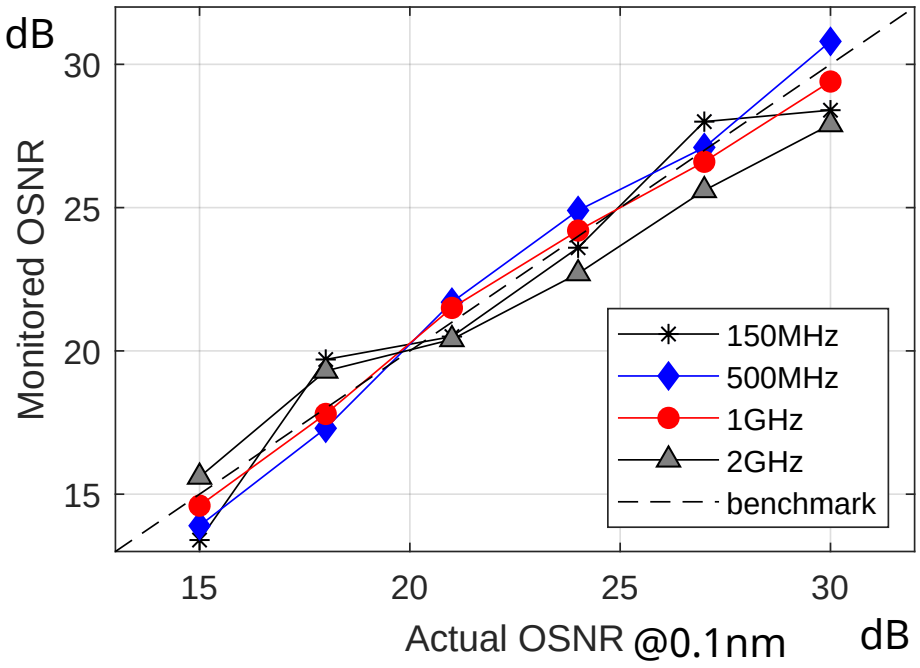

FIGURE 6.3. In-band OSNR (measured within 0.1nm noise bandwidth) monitoring accuracy with different WA frequency resolutions, 1GHz resolution gives the best accuracy with $\pm 0.6dB$ error.

OSNR levels after transmission are emulated by coupling additional ASE noise into the signal as shown in Fig. 6.2. The OSNR value ranges from 15dB to 30dB. As there is no intermediate filtering, N is set to 0, hence $\alpha^N = \beta^N = 1$. The choices of two spectral power measurement frequencies f_2, f_3 are set at $f_2 = f_1 + 20Hz, f_3 = f_1 + 23.5Hz$ according to [16]. The WaveAnalyser (WA) frequency resolution is set to 150MHz, 500MHz, 1GHz, 2GHz to explore the accuracy of the monitoring performance. Out-of-band OSNR computation is used to obtain the benchmark which is used to assess the monitoring performance [154]. As shown in Fig. 6.3, 1GHz resolution gives the best OSNR monitoring accuracy with a maximum error of 0.6dB while other resolution settings have worse accuracy. Theoretically, the finer resolution should give better accuracy [16], but due to the device monitoring sensitivity at finer frequency resolution ($\pm 1GHz$ error), the

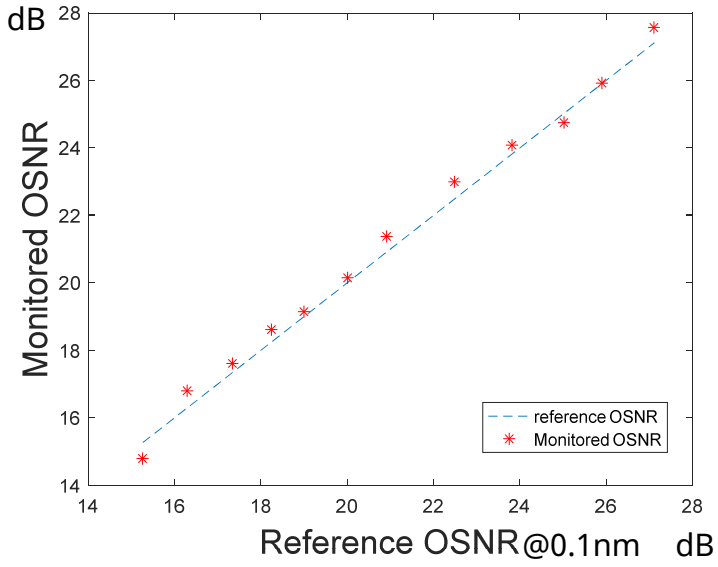

FIGURE 6.4. In-band OSNR (measured within 0.1nm noise bandwidth) monitoring accuracy for 26Gbaud DP-16QAM with $\pm 0.5dB$ error.

spectral power reading at the nominal frequency is not stable with 150MHz or 500MHz. So 1GHz resolution is used to relax the sensitivity issue. Similarly, this method is used to test 26Gbaud DP-16QAM signal and $\pm 0.5dB$ OSNR error is achieved with 1GHz frequency resolution as shown in Fig. 6.4.

6.2.3 Node architecture supporting monitoring

Fig. 6.5 shows the hardware implementation supporting the in-band OSNR monitoring function in the optical backplane switch [155]. The optical switch is an essential element in ROADMs. It is worth noting that the function can also be installed at any point of the network, for example, an inline EDFA output port. However, this will result in the device being only able to monitor a single route. The key components are tap coupler, WSS (or programmable optical filter) and WA. All the devices are pre-connected in the programmable optical switch. The signal power is tapped from the traffic port and then

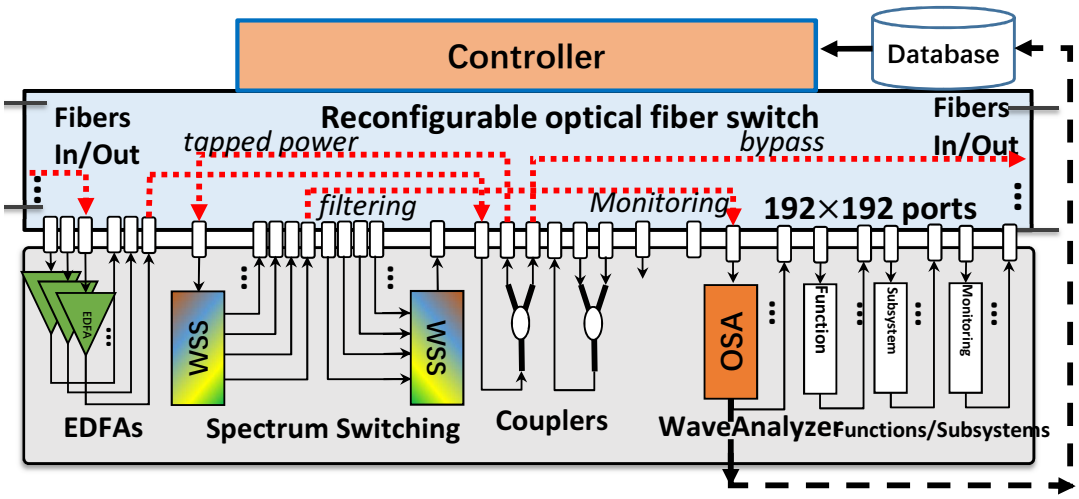

FIGURE 6.5. Physical node architecture to support flexible intermediate node monitoring.

fed into the WSS. The filter (bandpass with central frequency and bandwidth) is reconfigured dynamically to choose the channel of interest for monitoring. WA is connected to the output of the WSS for in-band OSNR computation. The signal spectrum data is stored in the database which is available for every intermediate node. The central and offset frequencies are autonomously located by searching for the spectrum peak power. Monitoring parameters $K_1, K_2, \alpha, \beta, \gamma$ are pre-calibrated and stored locally in the device controller.

6.3 Monitoring in the networking scenario

So far, we have introduced the intermediate node in-band OSNR monitoring function. This section will apply this integrated monitoring function in a field trial network testbed for centralised network planning.

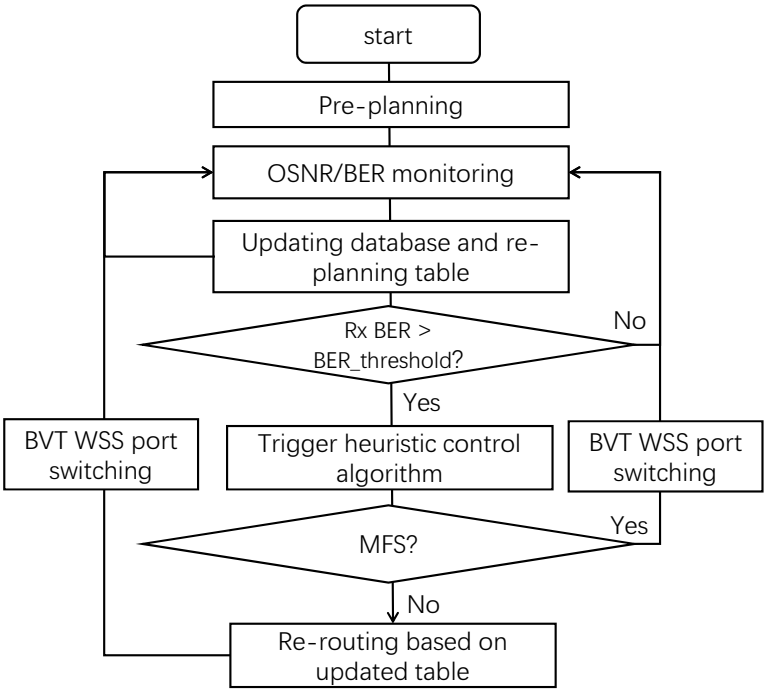

FIGURE 6.6. Flowchart of network service restoration using "in-depth" monitoring at intermediate nodes.

6.3.1 Field trial network

Fig. 6.6 shows the flowchart of the network restoration mechanism in the case of failure: (1) network pre-planning based on shortest path or physical layer impairment model [156]. (2) Link OSNR and receiver BER monitoring. In particular, in-band OSNR is monitored at per-link level using our proposed method, BER is monitored at the receiver side as a DSP by-product. (3) The control plane processes the monitoring information to update the planning table and trigger protection/restoration when failures happen. (4) Once failures are detected (receiver side BER exceeds a pre-FEC threshold), the control plane runs control plane heuristic algorithm to adopt either Modulation Format Switching (MFS) or LightPath Re-Routing (LPRR) for network service restoration [157]. (5) The control plane further switches the Bandwidth Variable Transmitter (BVT) WSS ports to perform the restoration process.

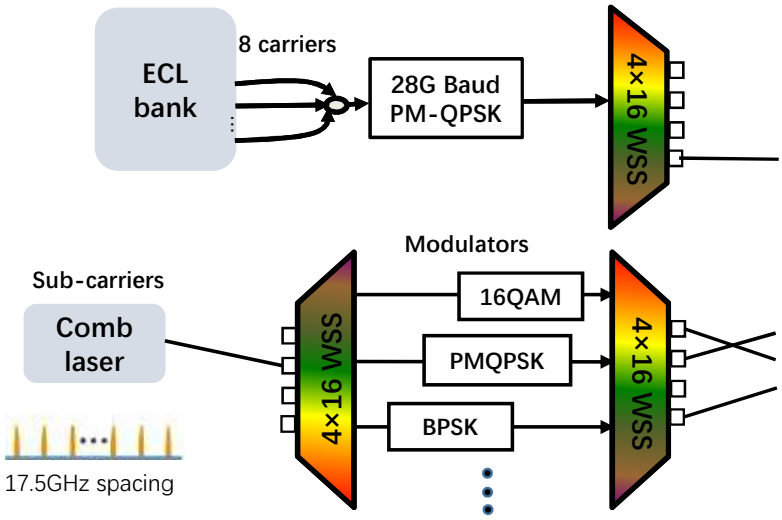

FIGURE 6.7. BVT setup at the transmitter side, MFS and LPRR are perfomed by programming the corresponding laser and WSS

The flexible BVT for on-demand signal MFS operation is shown in Fig. 6.7. Eight External Cavity Laser (ECL) sources ranging from 1551.721nm to 1555.747nm are combined and sent into a 32Gbaud DP-QPSK modulator which gives 50GHz-spaced transmission. The BVT contains a pool of optical subcarriers and modulators which are pre-connected to the input and outputs of the first WSS. The selection of subcarriers is performed by setting up the filter in the first WSS. The selection of modulations on a given subcarrier is achieved by directing this subcarrier to the output port of the WSS, where each of the output port is pre-connected with a modulator. Re-routing is realised by directing the modulated subcarrier to different output ports of the second WSS [158].

The NDFIS network is used to emulate a real networking scenario. Fig. 6.8 shows the network topology which uses four WSSs to emulate four intermediate nodes. Link 1, 3, 4, 5 are 50km and link 2 is 100km (all SSMF). NDFIS fibre system is used in link 1. It runs from the University of Bristol to Bradley Stoke and then loops back, forming 46km effective transmission length. Signals are transmitted through path A-B-D, A-B-C-D

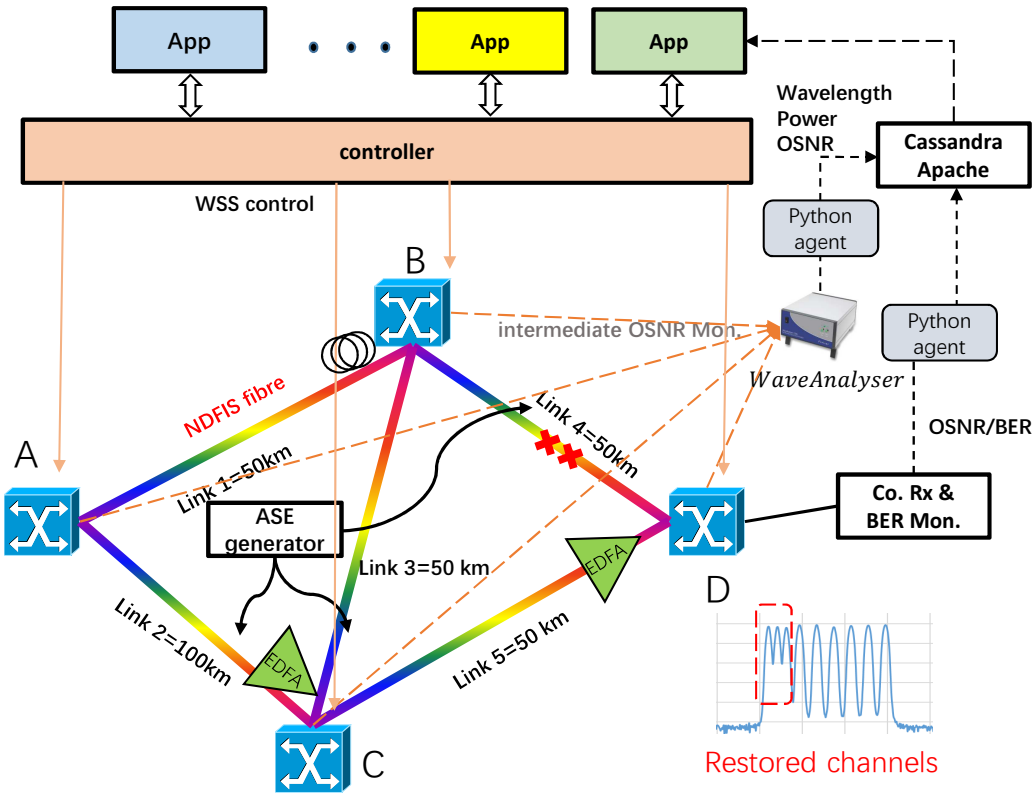

FIGURE 6.8. BVT setup at the transmitter side, MFS and LPRR are perfomed by programming the corresponding WSS ports

and A-C-D. Link launch power is set to +1dB. An ASE noise generator is switched and coupled into different links to emulate the link ASE noise. A high-resolution OSA Finisar WA is switched at any node for intermediate node monitoring by tapping the optical power. The proposed in-band OSNR monitoring technique is implemented in the WA for OSNR computation. The regression line (such as GP regression as proposed in Chapter 4) based on the monitoring OSNR data is used to predict unestablished channel OSNR performance for the link.

The monitored OSNR is stored in "Cassandra" database via a personal computer. The control plane north-bound application which is written in Python polls the database to gather monitored information and updates its planning table. The Python application

communicates with the control plane when restoration is required. The control plane further executes the command by talking to the WSS agents. Assuming M channels are monitored in each link, each link is indexed as j and connects node i and $i+1$, a new path has to pass J links. Then the cost function C for choosing the correct restoration in LPRR is

$$C = min \sum_{j=1}^{J} \frac{\sum_{m=1}^{M} [OSNR_i - OSNR_{i+1}]}{M} \tag{6.5}$$

6.3.2 Network re-planning performance

As shown in Fig. 6.9(a), (b) and (c), the in-band OSNR is monitored at each intermediate node using the proposed method. Three channels in each link are selected for monitoring. Before t0, all links perform as statically modelled, i.e., the noise performance correlates with distance. The path A-B-D is selected by default as it is the shortest path (Fig. 6.9(a)). From t0 to t3, the ASE noise is randomly coupled into link 2 (A-C), link 3 (B-C) and link 4 (B-D). For demonstration purpose, restoration is only performed for link 4 (B-D) where two 16QAM (channel 2, channel 3) and one QPSK (channel 1) signals are monitored. Link 4 is set as a permanently failed link.

As the OSNR monitored at node D (Path A-B-D) decreases as shown in Fig. 6.9(a), the control algorithm detects link 4 as a failed link. It deletes any candidate path that contains link 4 (B-D) and updates its planning table at t1 to select the newest best candidate path. The re-planning table shown in Fig. 6.9(d). At time t2, path A-B-C-D is selected as it is the current best route due to the monitoring data for both A-B-C-D and A-C-D. It also deletes 16QAM for path A-B-D from the planning table for protection purpose because the failed link can no longer support 16QAM QoT requirement.

The receiver side BER is also simultaneously monitored as shown in Fig. 6.9(e). At time t2, the BER of 16QAM signal reaches its pre-FEC (21%) threshold which is 2.4E-2 at

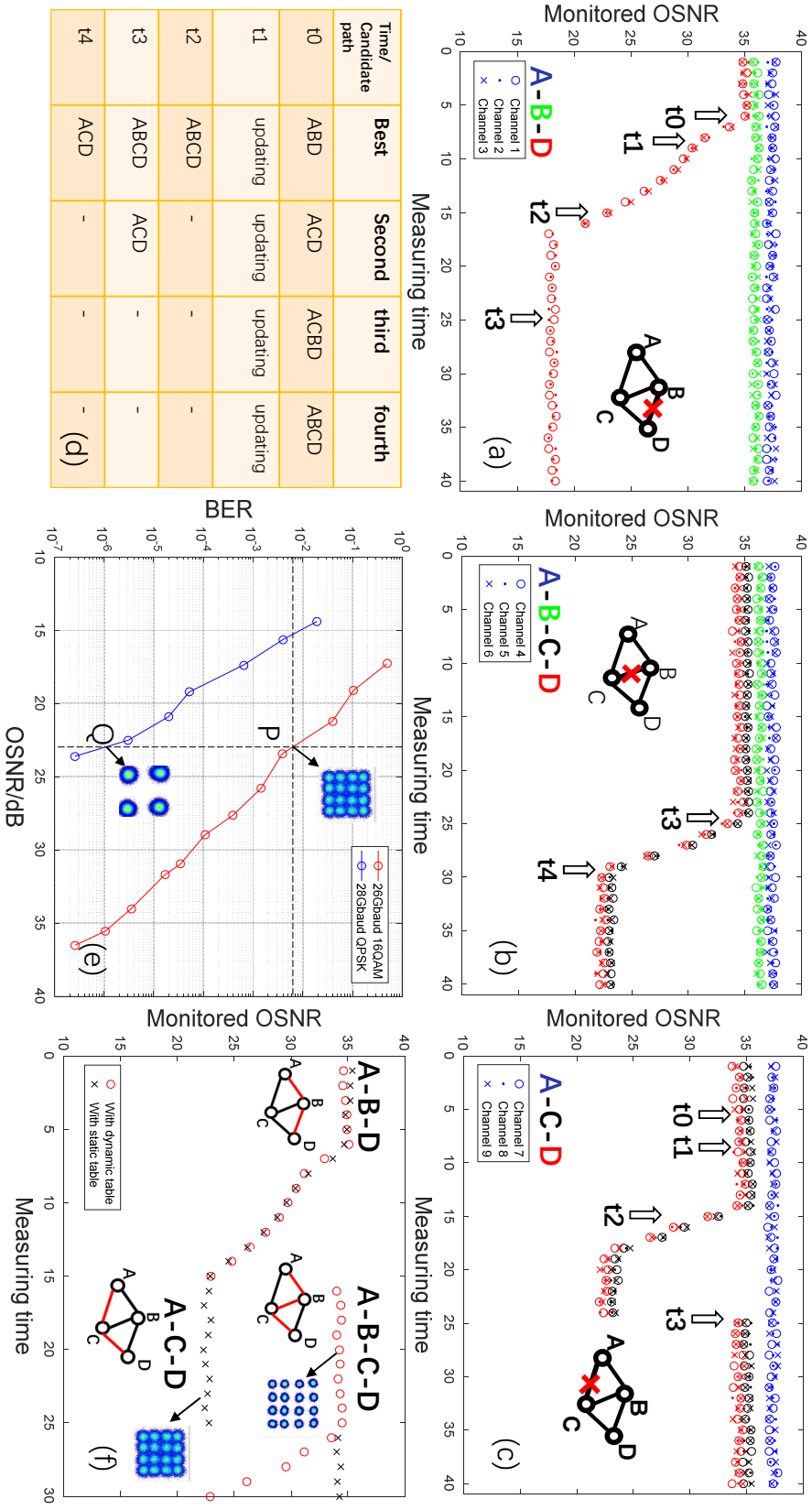

Time/ Candidate path	Best	Second	third	fourth
t0	ABD	ACD	ACBD	ABCD
t1	updating	updating	updating	updating
t2	ABCD	-	-	-
t3	ABCD	ACD	-	-
t4	ACD	-	-	-

(d)

FIGURE 6.9. Caption on the next page.

FIGURE 6.9. (a) Path A-B-D OSNR monitoring, at time t0 link B-D noise performance starts to degrade. (b) Path A-B-C-D OSNR monitoring, at time t3 link B-C noise performance starts to degrade. (c) Path A-C-D OSNR monitoring, at time t2 link A-C noise performance starts to degrade. (d) Dynamic network routing table, the planning table of candidate modulation format pool for each path is omitted. (e) 16QAM and QPSK BER performance vs OSNR is monitored at the receiver. (f) Receiver side OSNR monitoring with/without dynamic re-planning.

22.7dB OSNR. This indicates that 16QAM can no longer transmit along path A-B-D. For demonstration purpose, both MFS and LPRR are performed to restore the 16QAM signal with a lower-level modulation format (QPSK) and a new route (through monitoring) respectively. As shown in Fig. 6.9(e), the signal is switched from point P (16QAM) to Q (QPSK), the recovered QPSK constellation diagram shows less noise degradation. During the process of LPRR, the controller selects a new subcarrier wavelength from the BVT subcarrier pool. At time t2, link 2 (A-C) is degraded (Fig. 6.9(c)), the controller modifies the dynamic routing table as shown in Fig. 6.9(d), the new flexible path A-B-C-D is selected as the best candidate route.

The re-routed 16QAM constellation diagram shows better performance as shown in Fig. 6.9(f). From t3 to t4, ASE noise source is switched to link 3 (B-C), path A-C-D becomes available again and any path containing link3 (A-B-C-D) is deleted from the table (Fig. 6.9(d)). Fig. 6.9(f) shows the receiver side OSNR difference between the restored lightpath through LPRR with dynamic re-planning and static planning without intermediate node monitoring. In static planning, the restored channel is re-routed to path A-C-D (according to t0) where link 2 (A-C) is noisy. Since the receiver side monitoring data only provides path-level information, the controller cannot detect link 2 (A-C). The resulting received OSNR after LPRR to path A-C-D is much worse than path A-B-C-D selected by the intermediate node OSNR monitoring.

6.4 Conclusion

In this field trial, We have experimentally demonstrated a link-level cognitive optical network with dynamic re-planning capability. The dynamic re-planning and restoration are enabled by feeding the "in-depth" intermediate node OSNR information. The in-band OSNR monitoring technique is able to compute OSNR value for QPSK and 16QAM modulation formats within 0.6dB monitoring error. By feeding the monitoring data to a centralised database, the network control plane is able to gain a global view of the network status at per-link level and dynamically recover impaired signals. The final recovered lightpath OSNR using the proposed monitoring mechanism shows better performance compared to the static planning case. This "in-depth" monitoring capability can potentially provide a low-complexity, link-level optical network cognition without the need of network kriging.

CHAPTER 7

MONITORING ON DEMAND BY LEARNING

This chapter [1] contains relevant research work which demonstrates the optimum OSNR monitoring strategy at the intermediate nodes. The in-band OSNR monitoring technique and the experimental architecture used in this chapter are explained in Chapter 6, this chapter is an expanded work.

In current dynamic optical networks with cascaded filters and amplifiers, OSNR can vary significantly from channel to channel. Under such uncertainty, OSNR prediction for unestablished channels becomes indispensable but remains a big challenge. For protective network planning purposes such as margin threshold setting or wavelength assignment, it is desirable to evaluate the worst OSNR performance of each network link. Such exploration will unavoidably employ active monitoring probes which may cause interruptions to the network. An efficient active monitoring strategy that optimises the choice of probes or monitoring trials is needed. We propose a "self-learning" monitoring strategy integrated at intermediate nodes. Our method can intelligently select the

[1] This work is a top-scored OFC conference proceeding paper [27] and is accepted by the Journal of Optical Communications and Networking (JOCN) as an invited OFC special issue journal

channel to be monitored in order to search for the target global maxima of OSNR degradation for a specific link. Our monitoring scheme detects intermediate node OSNR in the linear regime. It is shown that our method can predict the target OSNR value with only 0.5dB error while reducing the required monitoring data by up to 91% compared with conventional methods.

7.1 Introduction

As shown in chapter 6, in-band OSNR monitoring function can be potentially integrated into ROADMs to obtain per-link OSNR information for each signal. However, For the purpose of designing a proactive network with efficient self-diagnose capability, it is not necessary to monitor the entire network. As the network expands, large amounts of data will be generated from the ubiquitous monitoring devices across the network. This may cause additional operational load of the network control plane due to finite flow entries [159, 160]. The aforementioned data is not only restricted to QoT estimation, but also to offline machine/deep learning training and cross-layer network optimisation. The latter may require data from the past or different network layers. On the other hand, probe signals are often utilised for active monitoring purposes [33, 161] which can cause additional interference and blocking with existing network services [162, 163]. Since sending probe signal is both operationally expensive and influential to network performance, it is desirable to minimise the number of probes or monitoring trials. The strategy used in this chapter assumes that no active probe is required if there is an established connection, otherwise probe channels may be used for unestablished connections.

Besides optimising active monitoring trials, network diagnosis also needs to be agile and real-time. In the case of end-to-end coherent service provisioning, the OSNR of

each channel can be monitored simultaneously by each corresponding receiver as a DSP by-product [6]. However, for intermediate nodes where a single OSNR monitoring device is deployed, the OSNR of each channel cannot be monitored simultaneously. As such, sharing the intermediate-node monitoring device among multiple channels remains an unsolved challenge.

For proactive network planning, the worst OSNR performance of the link is critical to be tracked. Failures can be proactively avoided once the worst OSNR degradation case is addressed. It can be used as a satisficing constraint (no more than the worst case threshold) when performing wavelength assignment and routing. As studied in Chapter 4, the state-of-the-art EDFA comes with intrinsic gain and NF spectrum non-uniformity characteristics. This further contributes to OSNR non-uniformity across the C-band [164, 165]. Even under static gain equalisation control, EDFA power excursion and offset filtering problems also lead to OSNR uncertainty [129]. Such uncertainty is difficult to formulaically analyse. Furthermore, the network status can change quickly due to dynamic add-drops, which makes the system a "black box". Instead of conducting complete examination of the black box, intelligent monitoring strategies are required to search for the worst OSNR performance of a link with as few monitoring trials as possible.

In Chapter 4 we propose and demonstrate a Gaussian Process (GP) based SNR learning method under noise uncertainty. In Chapter 6 we introduced a centralised intermediate node in-band OSNR monitoring. In this chapter, we propose and experimentally demonstrate a Monitoring on-Demand (MoD) strategy at intermediate nodes to eliminate redundant monitoring trials based on the work done in Chapter 4 and 6. The experiment is carried in a 100Gb-based 50 GHz-spaced 16-channel cross-city field trial network. Techniques in Chapter 4 and Chapter 6 serve as the principal methods supporting this chapter. We expand the work in the previous chapters by further demonstrating that

pure GP learning without BO requires much more monitoring data for our prediction purpose. It can be shown that through learning of the existing channel performance and on-demand hardware switching, MoD retrieves key OSNR information with up to 91% data saving and significant time saving than other strategies, which enables an intelligent and data-efficient monitoring process.

7.2 MoD node architecture

The flexible monitoring function at intermediate nodes is realised using the node architecture proposed in Chapter 6. Fig. 7.1 shows the architecture again. The key components are tap coupler, WSS (or programmable optical filter) and WaveAnalyser (WA). All these hardware devices are pre-connected in the programmable optical switch. The signal power is tapped from the traffic port and then fed into the WSS. The filter (bandpass with central frequency and bandwidth) is re-configured dynamically to choose the channel of interest for monitoring. WA is connected to the output of the WSS for the in-band OSNR computation. The signal spectrum data is stored in the database which is available for every intermediate node.

The controller computes the OSNR value of the current channel (see Chapter 6) and dynamically re-configures the filter to choose the next channel of interest. The process of making the re-configuration decision follows the Bayesian optimisation learning model. The decision is influenced by the OSNR performance it has monitored so far.

As mentioned in chapter 6, this monitoring function can be implemented using lower cost coherent reception and RF measurement device [16, 152]. In such case, to realise physical layer autonomous in-band OSNR monitoring, single channel filtering is important so that the algorithm can autonomously locate the central frequency by searching for the maximum power (as there is only one channel). Then accurate offset frequencies can

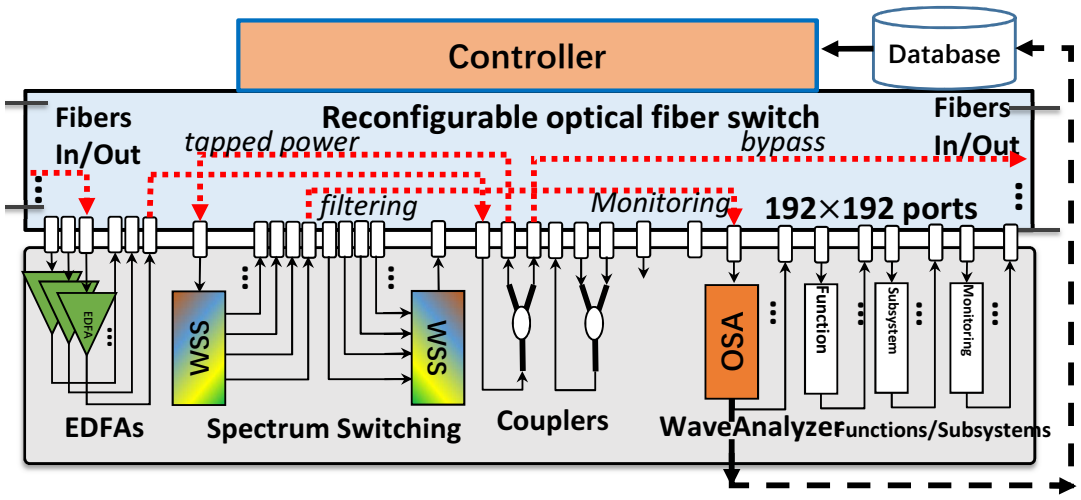

FIGURE 7.1. Monitoring on-demand physical architecture where all programmable devices are pre-connected in the optical switch integrated in ROADMs for dynamic on-demand switching, signal power is tapped and then filtered by a WSS to choose the channel of interest for OSNR monitoring.

be located accordingly. It is worth noting that there actually exist many methods in literature to monitor the in-band OSNR. For example, the Delay-Line Interferometer (DLI) based methods [166, 167] which are based on single channel filtering. Our proposed MoD algorithm is not restricted to monitoring with WA, it aims to be applicable to other in-band OSNR monitoring techniques as well. So single channel filtering is assumed.

7.3 Bayesian optimisation

As mentioned in Chapter 4, optical transmission systems come with intrinsic ASE noise spectrum non-uniformity due to EDFAs, filters, etc. This non-uniformity problem gets even worse after cascading many independent EDFAs in a transmission link. This causes distant channels to be less OSNR-representative than the neighbour ones. As it is analytically intractable to parameterise the ASE spectrum in dynamic optical networks, GP model can be used to "learn" from monitoring data. An important feature of GP is

that it computes the ECI that forms critical constraints for control decision making, ECI quantifies posterior prediction uncertainty which goes high where there is no monitoring data, and goes low where there is enough monitoring data. 95% pointwise ECI is a common choice.

Each time a single channel is monitored, the control strategy of the monitoring device based on the MoD architecture follows a "self-taught" monitoring process. Bayesian Optimisation (BO) determines the next monitoring point (λ_{next}) based on learning from the OSNR performances that have been monitored so far. Fig. 7.2 shows the flow chart of the overall learning model.

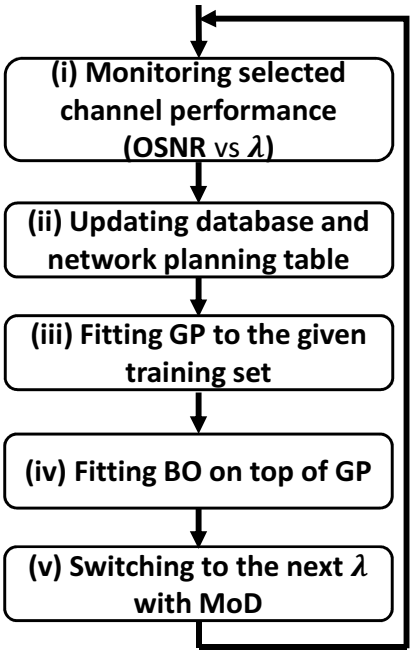

FIGURE 7.2. Monitoring on-demand switching strategy driven by Bayesian optimisation.

BO is intrinsically a decision trade-off algorithm on top of GP ECI. A large ECI area is an indicator of a high variance. The bounded region becomes more explorable because of the high estimation uncertainty. In the meantime, since we are only interested in the worst case OSNR performance, i.e., the global maximum point of OSNR degradation per

link, the region around the monitored high OSNR degradation values (high mean) is likely to contain a worse value. Therefore we should also exploit this high mean region. Here we define that for link i connecting node j and $j+1$, the OSNR degradation in dB is

$$OSNR^{i}_{deg} = OSNR^{j} - OSNR^{j+1} \tag{7.1}$$

To fit BO to GP, a utility (or acquisition) function "probability of improvement" (PI) [168] is applied to deal with this fundamental exploration and exploitation trade-off. PI computes the probability of establishing the next probe channel to be monitored (or filtered) as

$$\begin{aligned} U_{PI}(\lambda_{next}; D_n) &:= \Pr[OSNR(\lambda_{next}) > \mu^{+}_{OSNR}] \\ &= \Phi[(\mu_n(\lambda_{next}) - \mu^{+}_{OSNR})/\sigma_n(\lambda_{next})] \end{aligned} \tag{7.2}$$

where μ^{+}_{OSNR} is the best $OSNR_{deg}$ been monitored so far, $\mu_n(\lambda_{next})$ and $\sigma_n(\lambda_{next})$ represent the posterior GP returned $OSNR_{deg}$ mean (quantified degree of exploitation) and variance (quantified degree of exploration), Φ is the standard cumulative distribution function. PI returns the area under the posterior Gaussian distribution above μ^{+}_{OSNR}, the larger the area, the higher probability of improvement. The point with the highest probability of improvement (the maximal expected utility) is selected [169]. BO returns the next optimised monitoring or probing choice λ_{next} by maximising the utility function U_{PI}. The pseudocode of BO-driven MoD function is summarised in Algorithm 3.

7.4 Field trial testbed

Fig. 7.3 depicts the field trial network using part of the UK NDFIS system. The NDFIS allows experiments to be carried out in a real-world operating network, hence introducing sufficient operational uncertainties. 16 equalised 50GHz-spaced 32Gbaud DP-QPSK signals are available at the transmitter side and ready to be launched into the network.

Input:
$t = 1 : n$ - - total number of channels;
$\mathbf{D}[\lambda(wavelength), OSNR]$ - - GP regression of channel OSNR;
$\sigma_Q^2, \mathbf{K}$ - - GP kernel function and monitoring variance;
Target: λ_t - - next probing channel;
Algorithm:
for t = 1,2,...,n **do** {
find λ_t by combining attributes of the posterior distribution in the PI function U_{PI} and maximising
$\lambda_t = \text{argmax}_\lambda[U_{PI}(\lambda|\mathbf{D}_{1:t-1})]$
monitor the objective value OSNR(λ_t)
augment the data set
$\mathbf{D}_{1:t} = \{\mathbf{D}_{1:t-1}, [\lambda_t, OSNR(\lambda_t)]\}$
update GP
} **end for**
Return: λ_t, $\mathbf{D}_{1:t}$

Algorithm 3: BO-driven MoD function for channel selection

Channel power is set to 0 dBm/channel/span by each EDFA to avoid unwanted nonlinear distortion. Signals first enter the NDFIS link running from Bristol to Brandley Stoke and further to Froxfield which gives 236km effective loop-back transmission distance. Another 200km fibre link (lab-based) is connected after the loop-back (giving 436km in total) where signals are amplified every 50km. Launch OSNR is kept to 30dB by coupling additional noise to all the 16 channels to simplify the scenario. Channels with different wavelengths undergo different OSNR degradations after the link. We treat the transmitter as the first node, MoD is performed in the intermediate node where signals pass WSS (add-drop), coupler (tapping power), filter (selecting the channel of interest), and enter WA for in-band OSNR monitoring.

The WA monitoring device can be either shared among different fibre links by switching the optical switch ports, or among different channels in the same link by controlling the filter. In this work, we are focused on the latter case where the exploration and

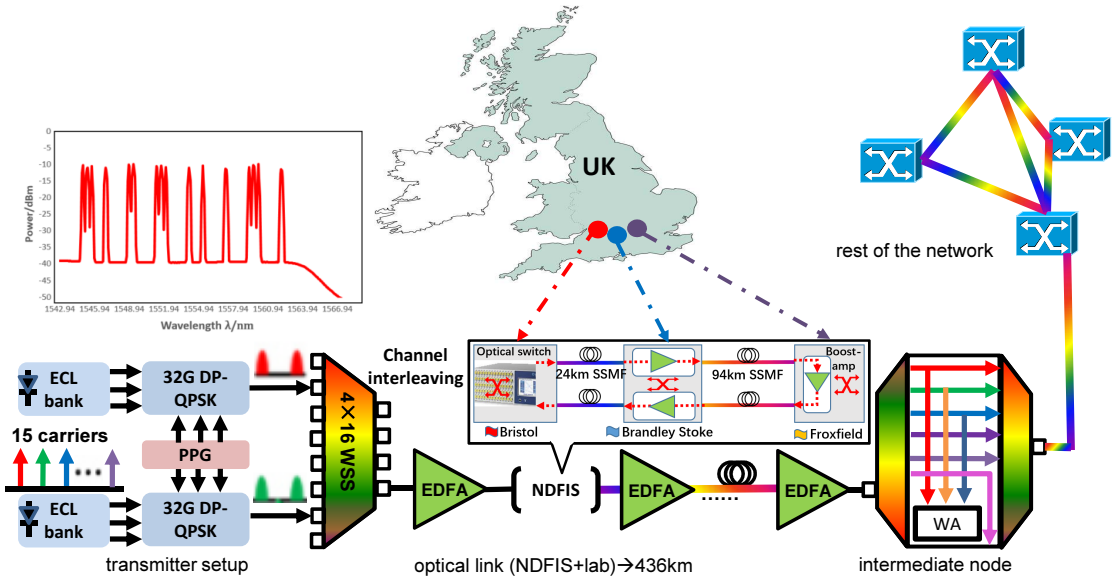

FIGURE 7.3. Field trial testbed using NDFIS, signals are transmitted from Bristol to Froxfield and looped back to Bristol, the detailed intermediate node architecture is shown in Fig. 7.2, ECL (external cavity laser), PPG (pulse pattern generator), DP-QPSK (dual polarisation quadrature phase shift keying), SSMF (standard single mode fibre).

exploitation trade-off is made to find the worst OSNR performance of a target link with as few monitoring trials as possible. Specifically our target is to find $max[OSNR^{i}_{deg}]$, in this experimental setup this is equal to finding $max[30dB - OSNR^{j+1}]$ according to equation 7.1 where $OSNR^{j+1}$ is the intermediate node to be monitored.

It is worth noting that our proposed method is also applicable to mesh networks, i.e., with different signal launch OSNR at the beginning of each link. As section II describes, we are able to monitor any intermediate node $OSNR^{j}$, hence this makes OSNR degradation possible for each individual link using equation 7.1. If we are interested in the lightpath metric, we can sum up the degradations of the traversed links. Or we can use the

following equation [68]

$$\frac{1}{OSNR_{path}} = \sum_{i=1}^{n} \frac{1}{OSNR_{link-i}} \tag{7.3}$$

where $OSNR_{link-i}$ is the end-to-end OSNR for link i.This assumes that ASE noise is linearly accumulated throughout the lightpath. If an unestablished signal OSNR is unknown for a specific link, we can use the proposed GP regression method to infer the OSNR for the wavelength in that link.

7.5 GP performance evaluation

BO computes PI according to GP ECI (selection of the next channel to be monitored). The global OSNR degradation maximum point is estimated by further GP regression with the newly monitored data. It is necessary to evaluate the performance of GP prediction for un-established channel OSNR with limited online monitoring data.

Fig. 7.4 show the GP predictions of unestablished channel OSNR under different link loading and monitoring conditions. Wavelength is indexed into 1 to 81 representing 1562.6nm to 1530.7nm at 0.4nm grid (50GHz ITU), i.e., covering the whole C band. Hyperparameters are optimised to be $\sigma_f^2 = 2.07$ and $l = 1.53$. The measurement uncertainty is set to $\sigma_Q = 0.1dB$. All the OSNR reference values are used as test data to evaluate the corresponding GP prediction accuracy. We define the true/reference OSNR of the link as the OSNR values that are monitored by our proposed in-band method. They are used as benchmark. The OSNR test data is measured by setting up a single test channel at each of the empty wavelength slot. It is torn down each time the reference value is recorded. Due to cascaded EDFA power amplification characteristics, the link OSNR performance varies with the loading status, by setting up only a single test channel, the impact of channel loading to EDFA is kept to minimum.

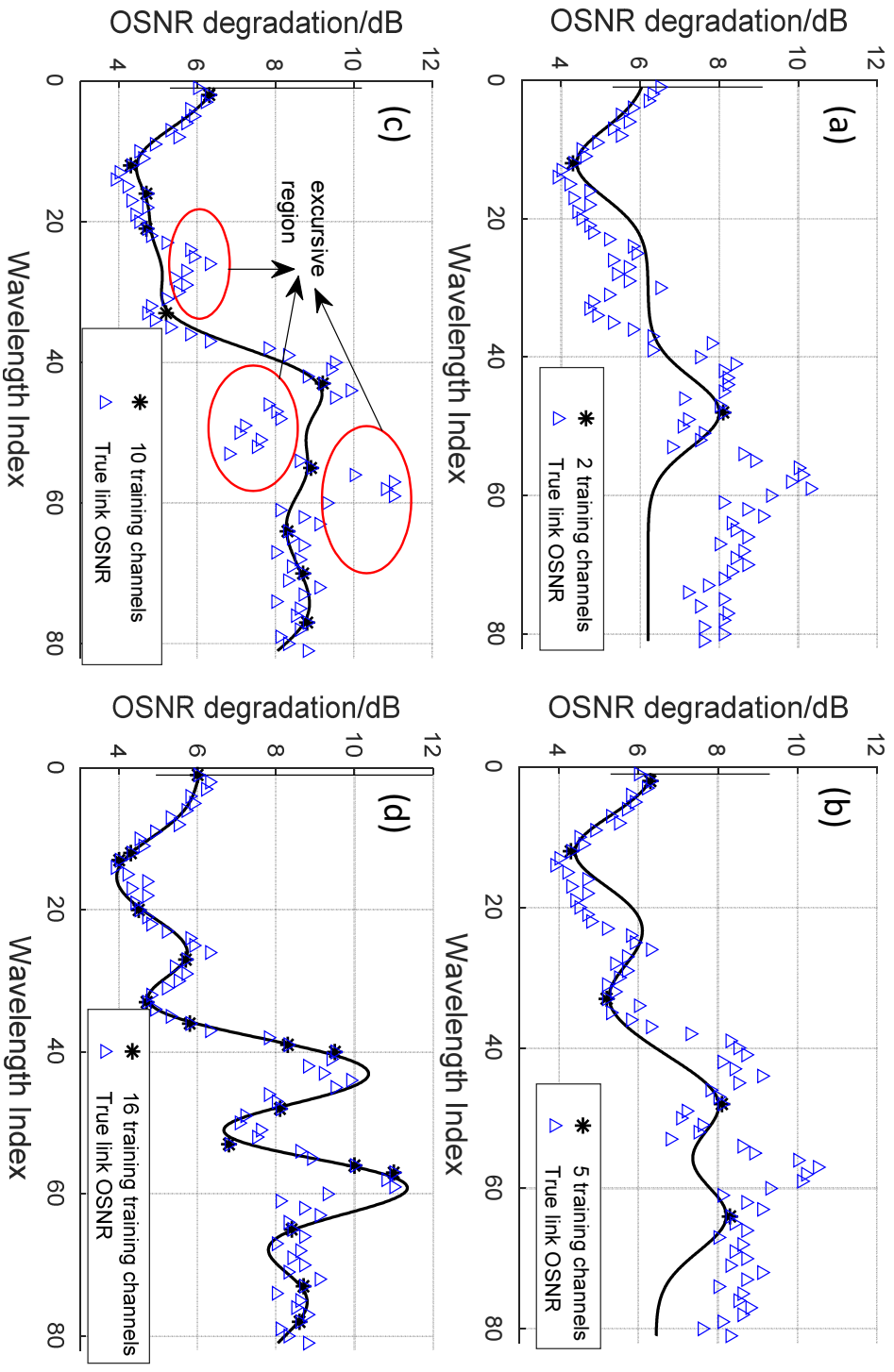

FIGURE 7.4. GP prediction of unestablished channel OSNR performance with (a) 2 training channels, (b) 5 training channels, (c) 10 training channels, (d) 16 training channels.

Fig. 7.4(a) has only two monitoring/training channels, it can be seen that the fitted GP curve can hardly capture the link OSNR performance due to too few training data points available. Fig. 7.4(b) and Fig. 7.4(c) increase the training data size to 5 and 10 respectively, each shows relative improvement in capturing the true link OSNR behaviour. However, the performance is still poor in some excursive regions including the global maximum point. Finally GP is able to predict the whole link OSNR with reasonable accuracy when the number of training channels reaches 16, as shown in Fig. 7.4(d). The prediction error for each training case is shown in Fig. 7.5. Training cases with 2 training channels, 5 training channels, 10 training channels and 16 training channels have root mean squared error (RMSE) of 1.5dB, 1.2dB, 0.8dB and 0.5dB respectively. This means that adequate online monitoring data (more than 16) is essential to capture accurate link OSNR performance.

It is worth noting that, without involving the self-taught MoD function, GP prediction with randomly generated training set does not guarantee that the current estimated global maximum point is the true target value, i.e., the worst OSNR degradation of the link. The only way to gain confidence about this estimation is to use as many monitoring data points as possible for training. Such amount of online monitoring data is hard to obtain without sending monitoring probes. In the case of active monitoring, the number of monitoring probes should be optimised to avoid interruption to existing services.

7.6 Self-learning on-demand monitoring

By applying BO on top of GP, the next monitoring channel of interest depends on the ECI computed by GP posterior mean and variance as well as the current global maxima monitoring points. Fig. 7.6 and Fig. 7.7 show the details of BO process. Different monitoring decisions are made depending on the normalised acquisition function (AF) u_{PI}

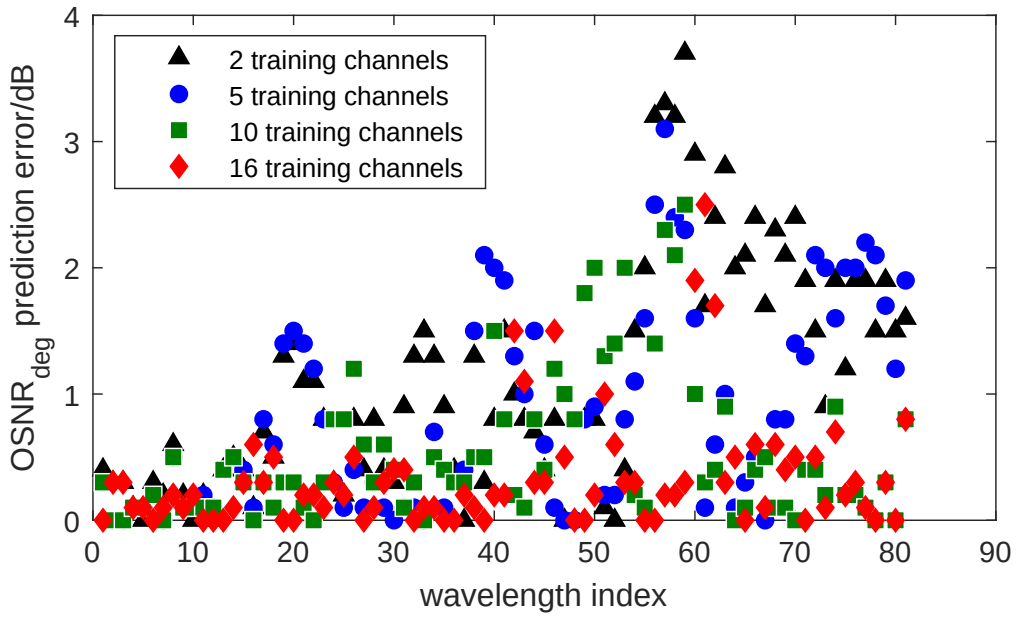

FIGURE 7.5. OSNR degradation prediction error with different GP training data sets. It can be shown that with more training channels, the corresponding mean and variance of the prediction error decrease.

computed by PI. The cyan region represents the estimation uncertainty (95% confidence integral) which goes high where there is no monitoring data, and goes low where there is monitoring data. The next channel of interest (next best guess) is marked by a star on the AF curve.

In Fig. 7.6 which contains 4 monitoring data points, the algorithm tends to prioritise exploration given the 4 points spread in large ranges across the wavelength band. So the indicated next best guess locates within high ECI region. After 5 steps, in Fig. 7.7, MoD starts to exploit the region with high posterior mean according to GP as the indicated next best guess no longer locates in high ECI region. As more channels are monitored and utilised to be the next step GP training data, the BO decision will be made around the global maximum. It is worth mentioning that due to the stochastic function sampling process of GP, each time BO re-runs, the posterior mean and variance may differ from the previous value. So the choice for the next channel of interest may vary.

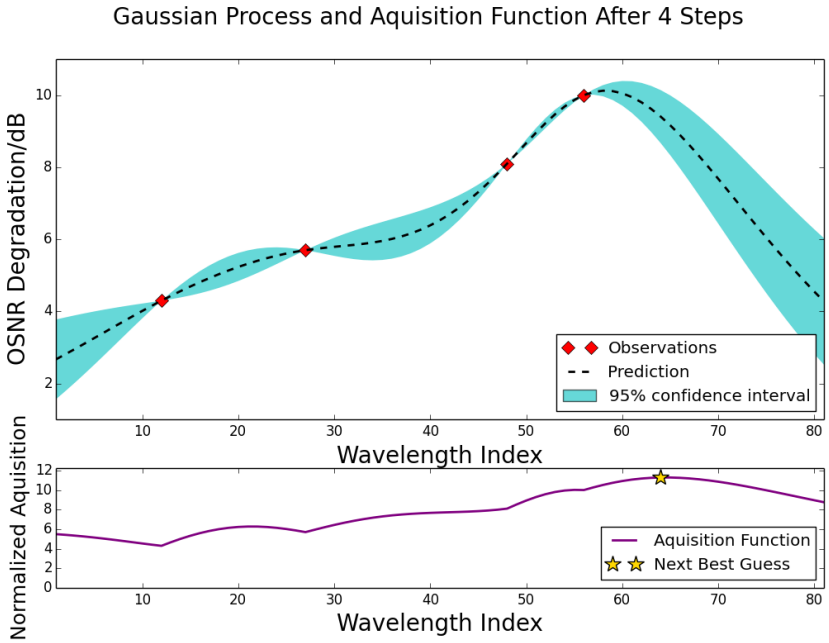

FIGURE 7.6. BO-driven MoD after GP fitting with 4 training set where the algorithm tends to explore high ECI region as indicated by the normalised acquisition function.

Fig. 7.8 evaluates the number of filter switching times required to find $OSNR_{deg}$ global maximum. As mentioned in Chapter 6, the in-band OSNR monitoring device can only compute a single channel OSNR, so selection of the next channel of interest is done by adjusting the filter (or WSS in our experiment) position in the MoD architecture. Two other switching strategies are used to assess the performance of MoD: 1. Sequential Monitoring (SM): sequentially switching to each channel in the link from left to right; 2. Random Monitoring (RM): the switching or monitoring order is stochastic. Note that by using SM and RM strategies, active probing method becomes clumsy since the required monitoring probe has to loop across the whole C band without optimisation. In the case of 16 channels monitoring (Fig. 7.4(d)), with a total number of 40 switching times, BO first finds the highest OSNR degradation located at λ = 194650GHz (wavelength index #59) with 8 switching times, 62.5% quicker than SM (13 times) and 400% quicker than RM (40 times). 75% of the BO data (after 8 switching times) is constant when searching for

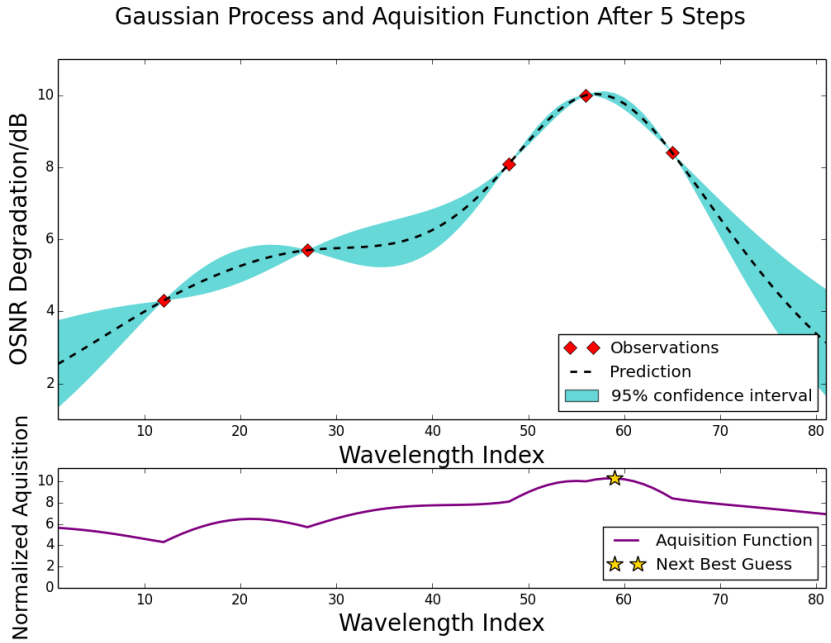

FIGURE 7.7. BO-driven MoD after GP fitting with 5 training set where the algorithm starts to exploit high posterior mean region as indicated by the normalised acquisition function.

the link worst OSNR degradation (11dB). This means the rest of the constant data can be omitted after the first detection, resulting in 50% saving (8 channels out of 16). This demonstrates that BO can take the monitoring process out of the loop by intelligently selecting the channels that provide the largest information gain.

Fig. 7.9 demonstrates the capability of BO in locating the target OSNR with "just enough" monitoring data. The complete link OSNR performance for each wavelength slot is tested and recorded as benchmark data, the fitted GP curve using BO has the posterior global maxima at exactly the same point as using all the 16 training channels that capture the whole link OSNR performance as already shown. BO achieves 0.5dB prediction error (relative to the reference value) for the target OSNR while the data needed is halved. This proves the capability of MoD in retrieving the most critical OSNR information with up to 91% data saving (8 out of 88 if C band is fully loaded), and in the mean time,

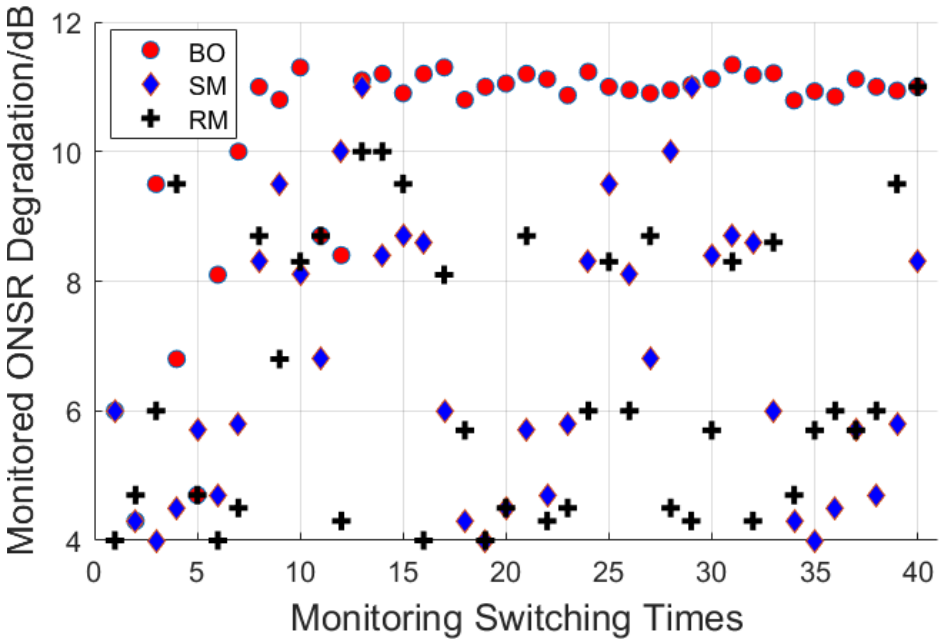

FIGURE 7.8. Monitoring performance in terms of switching times needed to find the global maxima.

retaining identical prediction accuracy compared to full exploration with 16 channels.

7.7 Summary

In this field trial we have demonstrated a self-taught monitoring-on-demand function driven by Bayesian optimisation on top of Gaussian process at intermediate nodes where a single in-band OSNR monitoring device has to be shared among different routes and channels. We apply the in-band OSNR monitoring algorithm described in Chapter 6 which is implemented in a high-resolution OSA and can be dynamically switched to monitor any channel on-demand. The algorithm takes back-to-back signal spectrum as reference spectrum together with real-time offset monitoring power to compute target in-band OSNR value. The algorithm achieves OSNR monitoring accuracy of 0.6dB with 1GHz device frequency resolution.

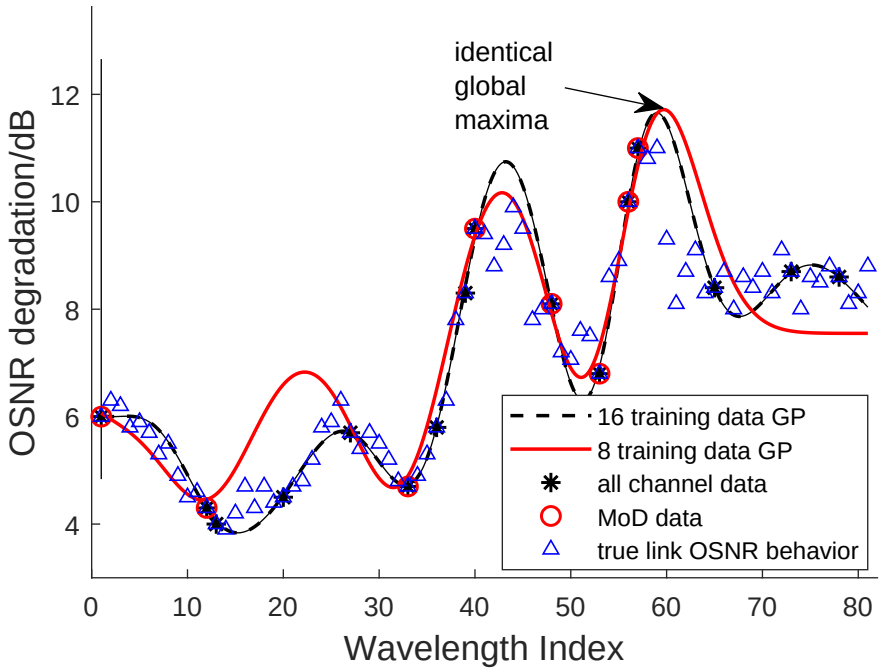

FIGURE 7.9. Prediction of $OSNR_{deg}$ global maxima with MoD (8 monitoring trials) and complete GP fitting (16 monitoring trials).

With such monitoring capability, Bayesian optimisation is then applied to learn from already established connections. It aims to minimise the number of monitoring trials needed for locating the worst OSNR degradation of the link. It has been shown that by using pure GP regression, at least 16 sparsely distributed monitoring channels are required to completely capture the whole link OSNR performance including the global maximum. BO significantly accelerates the process with only 8 monitoring trials to rapidly find the target OSNR value. In situations where active monitoring probe has to be used, BO is expected to save up to 91% of the monitoring trials (whole C band channels) while accurately predicting the global maximum with 0.5dB error. In practice, the global minima points are also of interest to operators, more channels can be allocated to the lower degradation regions to allow better transmission performance. Such intelligent self-taught learning strategy enables a data-efficient, out-of-the-loop monitoring process. It can be critical in accelerating the monitoring process and saving the number of probe

signals for active monitoring purposes.

CHAPTER 8

CONCLUSION AND FUTURE WORK

This thesis contains relevant research work that applies machine learning and data mining techniques to optical networks. Through using effective optical monitoring data, it is shown that much more valuable network knowledge can be generated. These knowledge offers robust solutions to optical network planning and management and cannot be obtained by any other means without learning.

8.1 Summary

This work began by introducing relevant cognitive architectures that support ML in optical networks. They rely on the ubiquitous monitoring capabilities across the network. For example, monitoring from the EDFA I/O ports, receiver DSP units, intermediate node, etc. Apart from the monitoring capability, device programmability realises network flexibility which makes intelligent network re-configuration possible. All these decisions are made in the network control plane.

Such network flexibility unavoidably brings uncertainties of network knowledge. The uncertainty in physical layer impairments such as ASE or nonlinear noise will ultimately result in unreliable network planning which leads to resource over-provisioning or network failure. Simple monitoring data can only provide observable straight-forward information. To obtain more insightful knowledge or accurate prediction performance, data mining or machine learning techniques are needed.

In the literature review chapter, relevant research work that applies ML and AI techniques to help optimise network performance is extensively reviewed. As AI in optical networking is a relatively new area of research, research work on other networks using AI such as network virtualisation is also introduced. In the physical layer domain, neural network is a common method that has been widely used in QoT estimations, EDFA control and optical performance monitoring. Unsupervised algorithms such as EM clustering or PCA are shown to be effective for nonlinear noise mitigation. A common point is that none of these proposed learning solutions can do without real-time monitoring. In the networking domain, AI can leverage the SDN architecture to function as the control plane management applications for global network optimisation. For example, genetic algorithm is especially helpful in physical topology design and resource allocation given a global view of the network. Bayesian inference is a powerful tool to detect and locate network failures or anomaly intrusions. AI methods are not only applied to optical networks, but also data centre networking and virtual networks.

Although there is lots of work addressing AI methods in optical networks, few of them mentions the fact that the optical networks are difficult to generate a huge amount of data (big data) like other machine learning applications. This causes an argument within the field as to whether it is a suitable time to employ deep learning. Another critical issue with a lot of existing literature is that they apply offline learning models to learn an online/running network performance. Such learning process does not guarantee to

Learning improvements over traditional methods				
methods	mean SNR prediction error	NF estimation error	Link-level SNR prediction error	MoD number of monitoring trial
traditional method	2.5dB	1.1dB	2.7dB	88
heuristic learning method	1.3dB	N/A	1.3dB	16
Probabilistic learning method	0.7dB	0.1dB	0.8dB	8

Table 8.1: Summary of learning performance improvements over traditional and heuristic methods.

capture the real-time network behaviour and is intrinsically an unreliable solution. This thesis addresses network online learning capability while the network is evolving. Such online learning capability depends on relatively small data set from a sliding window. How to efficiently leverage the small online monitoring dataset is one of the key points of this work.

As can be seen from Table 8.1, ML methods can significantly improve the performance of a network planning model compared to traditional methods with no learning or heuristically low-level learning. The low-level learning refers to simple ML methods such as averaging neighbouring points, MLE, etc. The KPI is the prediction error reduction for QoT metrics. Such prediction performance improvement can adapt each signal to its transmission performance limit, and hence increase the network throughput [2]. It has been shown in [170] that, compared to the worst case design, controlling the prediction error to 0.1dB results in a reduction of the maximum number of regenerators to 16% -

47% depending on the network load for a national network topology. Further reduction of the error from 0.1dB to 0 (perfect knowledge) results in another 4% regenerator saving. Therefore, the acceptable prediction error for a specific system depends on the budget for regenerator placement, or the expected throughput of the network.

Due to system uncertainties, Gaussian process is proposed to estimate online signal SNR without any prior system knowledge which takes real-time passive monitoring data of existing services as training data. It has been shown that 1.2dB MAX SNR prediction error and 0.7dB RMSD error are achieved across a large wavelength range which outperforms other learning methods. GP model also allows estimating SNR prediction uncertainties by computing confidence integrals. This quantified prediction uncertainty feature can be potentially leveraged as control plane algorithm constraint to further accelerate on-demand monitoring process, or even more probabilistic control actions.

GP forms the Horizontal-step (H-step) to explore network surface performance (SNR prediction) while Bayesian inference method MCMC can be used to further gain deeper network insights. By applying unsupervised Vertical-step (V-step) MCMC inference on top of the GN model, we are able to refine the improper parameter priors placed on the GN model and further enhance the prediction accuracy. These parameters can abstract the system ASE and nonlinear noise performance hence are critical to be traced in real-time. In the case of EDFA NF parameter, our inference method achieves 0.1dB estimation error, which is 90.9% less compared to the static case (1.1dB) without inference. Hybrid H/V learning is proposed and demonstrated in a field trial network to achieve per-link noise parameter abstraction. SNR prediction error is reduced from 2.7dB to 0.8dB by substituting the refined parameters into the GN model, yielding 70% equivalent uncertainty reduction during dynamic network design and planning.

Besides using the receiver DSP monitoring as the raw data fuelling learning models,

intermediate node in-band OSNR monitoring is also implemented using an on-demand node architecture. The in-band OSNR monitoring technique adopting offset optical power monitoring is shown to measure OSNR value for QPSK and 16QAM modulation formats within 0.6dB monitoring error. By feeding all the "in-depth" monitoring data to the SDN controller, it is demonstrated that efficient network protection and restoration can be performed with programmable bandwidth-adaptive transmitters.

As the intermediate node OSNR monitoring device has to be shared among many channels, an on-demand self-taught monitoring strategy is proposed to eliminate redundant monitoring data and accelerate the monitoring process. By utilising the confidence integrals computed by GP regression, Bayesian optimisation technique can be used to locate the next channel of interest in order to find the global maxima of the OSNR degradation for fibre links with as few monitoring trials as possible. It is demonstrated in a field trial that BO can save up to 91% of the monitoring data in the worst case when C-band is fully loaded. Such intelligent monitoring strategy enables a data-efficient, out-of-the-loop monitoring process and can be critical in saving monitoring trials when sending probing signals for monitoring purposes is operationally harmful and expensive, or when control decisions have to be made rapidly.

There are also drawbacks of the proposed methods. Bayesian methods are suitable for learning with small dataset since the given information is relatively incomplete. GP intrinsically is equivalent to a NN model with an infinite number of hidden layers. This property makes GP computationally expensive with large training set as the kernel matrix dimension will become excessively large. If the training phase has abundant monitoring data, for example, over thousands of training data points, frequentist methods such as NN should be used. The same complexity problem applies to MCMC inference because the Monte Carlo sampling process has to iterate over thousands of samples to converge. Gibbs' sampling is one potential solution to reduce the computational

complexity.

Introducing monitoring capability at network intermediate nodes has the potential to reduce the computational complexity of algorithms such as network kriging. It can also avoid sending active measurement probes when the passive monitoring signals are not enough. However, additional cost is needed to deploy the monitoring device ubiquitously at each intermediate node. There is a trade-off between the extra cost of intermediate-node monitoring and the computational complexity of active or kriging methods.

As can be seen from this work, AI and ML methods can be used in many aspects to optimise the network performance. For example, QoT prediction, parameter inference and on-demand monitoring strategy. In a nutshell, AI and ML can make accurate predictions and perform optimal control plane decision making based on the prediction. To avoid black-box issues, ML models should be complementary to existing planning models. It is believed that the state-of-the-art ML is able to help further with optical network planning to achieve ultimate network intelligence under uncertainty.

8.2 Future work

Deep learning (DL) has gained much attention in recent years, whether it is suitable for current optical networking to embrace DL or not becomes an interesting topic. As shown in Fig. 8.1, the performance of AI prediction capability grows with the increase of training data size. When the training data size is small, most traditional ML models perform better than DL. But after a critical point, the DL performance exceeds traditional models and becomes much better while traditional model performance reaches a bottleneck.

As to a specific network system, finding the critical point is non-trial for optimised

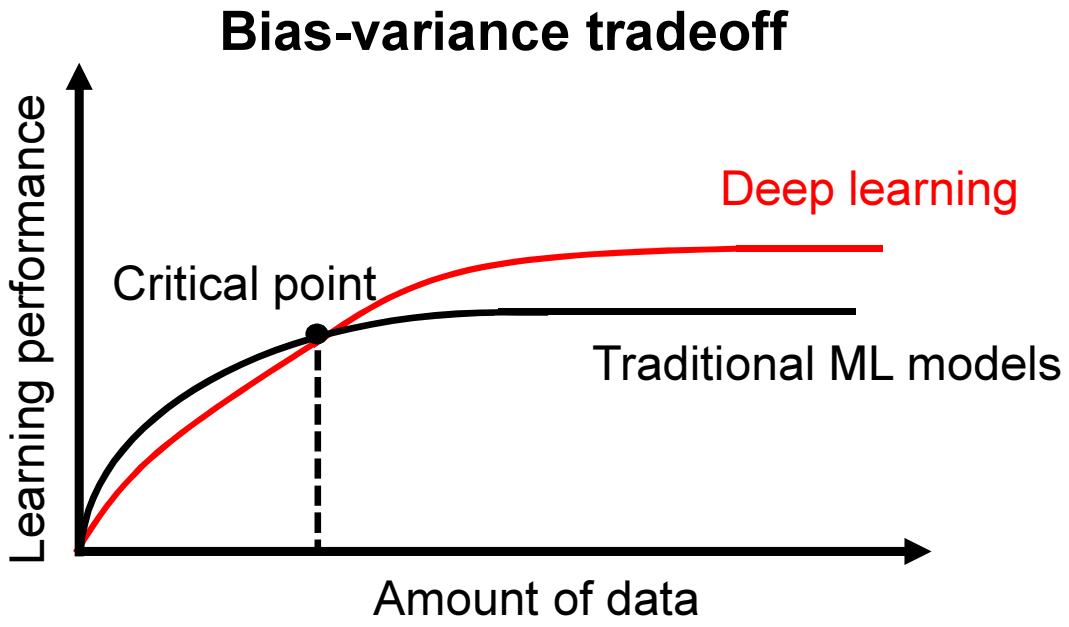

FIGURE 8.1. AI performance with increase of the amount of training data.

performance. To increase the training data size, more features should be considered, for example, different loading conditions, different launch power, different modulation formats, different data rates, etc. DL models normally have to rely on some form of big data analytic tools with data cleaning and pre-processing (such as pruning) capabilities. It is significant to have a monitoring platform that can collect all kinds of monitoring data ubiquitously in the network, such a platform forms the fundamental building block for DL research. It is worth mentioning that such monitoring platform can only generate large training data set over a long time period while the network is live for client services. It is very hard for such data collection to be carried out in research labs, therefore collaborations with commercial telecommunication companies are desired. Recent findings show that sophisticated DL models such as RNN and LSTM do not show better performance than traditional time series forcasting methods such as ARIMA [103]. This finding addresses the importance of setting the appropriate traditional methods as

the baseline.

The same extension work can also be applied to GP learning. given current optical network performance monitoring data size is far from enough, DL performance is much worse than traditional learning models. In this work, we have only considered identical modulation format (QPSK), power (0dBm) and bit rate (32Gbaud). Further work should consider more complex network states when applying GP prediction. In that case, the regression is no longer a 1-D model, but a multi-dimensional model. By increasing the dimensionality or the feature space, the final GP learning model will be more adaptive to more complex systems. Different kernels can be explored accordingly. Also, the experiment carried out in this work uses a metro-size NDFIS system. Further research can be carried out to study ultra long-haul transmission and short-distance access network. The former network has much longer transmission distance hence introduces large uncertainties to be addressed by ML. Suitable ML-assisted planning model should be adopted based on the network topology size, the level of programmability or flexibility of the network, and the technology used in the network (such as WDM, flex-grid, space division multiplexing, etc.).

Increasing the feature space or dimensionality is not always a good solution. It is different from increasing the training data size, which in most scenarios, can make ML models better. A large feature space can lead to overuse of ML computing resources. For example, in a Neural Network (NN), increasing the feature space means adding more neurons to the input layer. As the input layer size increases, the hidden layer size may also need to increase to support the enhanced algorithm flexibility. As such, a good trade-off between the ML model performance and the feature space is needed. This can be solved by applying unsupervised learning methods such as principal component analysis. Or domain expertise can be applied prior to ML models to analyse the importance of each feature.

The work undertaken in both Chapter 4 and Chapter 5 provides a probabilistic way of dealing with network planning and optimisation. The MCMC inference process is able to sample across the whole distribution of interested network parameters, hence giving quantified estimation uncertainty. This feature can be further used to form control plane constraints. For example, as GP generates Confidence Integrals (CI), during the wavelength assignment process, new channels are preferred to be assigned to large CI regions in order to explore more information about the wavelength region. As the network nonlinearity can be estimated by GN model parameters with Gaussian probability distribution, future control plane RMSA algorithms can take this Gaussian distribution as a range constraint for nonlinearity-aware optimisation. Moreover, different sampling techniques can be explored to find the minimum number of iterations needed for parameter distribution inference. This would accelerate the inference process, but may compromise with higher computation.

As shown in Chapter 5, ML models can be used together with theoretical models in a hybrid way to learn a network performance. In the control plane routing algorithms, monitoring data can also be used as a hybrid component with heuristic functions. For example, we can define a hybrid function as f(n) = h(n) + p(n) where h(n) is the heuristic model and p(n) is the monitoring data, or the function that can learn from the monitoring data. Hence the hybrid function becomes physical layer aware, and at the same time, analytically tractable. Such hybrid method balances the issues that pure ML models will transform the system into a black box, and that pure heuristic models are not cognitive.

As shown in Table 8.2, different flows of future research work are listed in a prioritised order on top of this work. Considering the long-run research directions, the benefit of this work is to evoke the importance of online machine learning to optical network management as a complementary tool. With the frameworks of network cognition, the power of real-time data resources can be fully utilised to generate much more valuable

Future work list	
1.	Exploring the proposed online learning methods with different network topology (linear, mesh), different network size (long-haul, metro, access), different modulation formats and baud rates.
2.	Exploring deep-learning methods to find the correct level of training data size to drive a deep learning model. Compare the performance gain of DL models with our proposed online learning.
3.	Developing an online data monitoring and preprocessing platform to drive different types of ML models.
4.	Reducing the computational cost of complex ML models so that the learning process is rapid and can be adapted to more advanced networks such as 5G network.
5.	Combining monitoring and ML predictions with optical network heuristic functions to develop a hybrid planning method for control plane decision making.

Table 8.2: A schematic summary of future work.

network knowledge. Unlike offline learning method, online learning is more suitable for networking case as it captures real-time system performance and is able to adapt rapidly while the system is evolving. Machine learning has great potential to revolutionise optical network planning and management under uncertainty.

BIBLIOGRAPHY

[1] Y. Lee and B. Mukherjee, "Traffic engineering in next-generation optical networks," *IEEE communications surveys & tutorials*, vol. 6, no. 3, 2004.

[2] Y. Pointurier, "Design of low-margin optical networks," *IEEE/OSA Journal of Optical Communications and Networking*, vol. 9, pp. A9–A17, Jan 2017.

[3] D. Medhi, "Network reliability and fault-tolerance," *Wiley Encyclopedia of Computer Science and Engineering*, 2007.

[4] H. F. H. Omar, K. B. Saadan, and K. B. Seman, "Determining the influence of the reliability of service quality on customer satisfaction: The case of libyan e-commerce customers," *International Journal of Learning and Development*, vol. 5, no. 1, pp. 86–89, 2015.

[5] I. Tomkos, S. Azodolmolky, J. Solé-Pareta, D. Careglio, and E. Palkopoulou, "A tutorial on the flexible optical networking paradigm: State of the art, trends, and research challenges," *Proceedings of the IEEE*, vol. 102, no. 9, pp. 1317–1337, 2014.

[6] Z. Dong, F. N. Khan, Q. Sui, K. Zhong, C. Lu, and A. P. T. Lau, "Optical performance monitoring: A review of current and future technologies," *Journal of Lightwave Technology*, vol. 34, pp. 525–543, Jan 2016.

[7] T. Panayiotou, S. P. Chatzis, and G. Ellinas, "Performance analysis of a data-driven quality-of-transmission decision approach on a dynamic multicast- capable metro optical network," *IEEE/OSA Journal of Optical Communications and Networking*, vol. 9, pp. 98–108, Jan 2017.

[8] P. Poggiolini, G. Bosco, A. Carena, V. Curri, Y. Jiang, and F. Forghieri, "The GN-model of fiber non-linear propagation and its applications," *Journal of Lightwave Technology*, vol. 32, pp. 694–721, Feb 2014.

[9] D. M. Baney, P. Gallion, and R. S. Tucker, "Theory and measurement techniques for the noise figure of optical amplifiers," *Optical Fiber Technology*, vol. 6, no. 2, pp. 122 – 154, 2000.

[10] G. S. Zervas and D. Simeonidou, "Cognitive optical networks: Need, requirements and architecture," in *Transparent Optical Networks (ICTON), 2010 12th International Conference on*, pp. 1–4, IEEE, 2010.

[11] W. Wei, C. Wang, and J. Yu, "Cognitive optical networks: Key drivers, enabling techniques, and adaptive bandwidth services," *IEEE Communications magazine*, vol. 50, no. 1, 2012.

[12] M. N. Dharmaweera, J. Zhao, L. Yan, M. Karlsson, and E. Agrell, "Traffic-grooming- and multipath-routing-enabled impairment-aware elastic optical networks," *IEEE/OSA Journal of Optical Communications and Networking*, vol. 8, pp. 58–70, Feb 2016.

[13] A. Jirattigalachote, Y. Yamada, C. Cavdar, P. Monti, L. Wosinska, H. Hasegawa, and K. Sato, "Impairment-aware routing and waveband assignment for efficient optical transport networks," in *OFC/NFOEC*, p. OW3A.2, March 2012.

[14] A. G. Rahbar, "Review of dynamic impairment-aware routing and wavelength assignment techniques in all-optical wavelength-routed networks," *IEEE Communications Surveys Tutorials*, vol. 14, pp. 1065–1089, Fourth 2012.

[15] I. Sartzetakis, K. Christodoulopoulos, C. Tsekrekos, D. Syvridis, and E. Varvarigos, "Quality of transmission estimation in WDM and elastic optical networks accounting for space–spectrum dependencies," *IEEE/OSA Journal of Optical Communications and Networking*, vol. 8, no. 9, pp. 676–688, 2016.

[16] Z. Dong, K. Zhong, X. Zhou, C. Lu, A. P. T. Lau, Y. Lu, and L. Li, "Modulation-format-independent OSNR monitoring insensitive to cascaded filtering effects by low-cost coherent receptions and RF power measurements," *Optics express*, vol. 23, no. 12, pp. 15971–15982, 2015.

[17] M. R. C. et al., "Demonstration of in-service wavelength division multiplexing optical-signal-to-noise ratio performance monitoring and operating guidelines for coherent data channels with different modulation formats and various baud rates," *Opt. Lett.*, vol. 39, pp. 1605–1608, Mar 2014.

[18] A. Nag, M. Tornatore, and B. Mukherjee, "Optical network design with mixed line rates and multiple modulation formats," *Journal of Lightwave Technology*, vol. 28, no. 4, pp. 466–475, 2010.

[19] D. L. Poole and A. K. Mackworth, *Artificial Intelligence: foundations of computational agents. Chapter 8: Reasoning with Uncertainty.*
Cambridge University Press, 2010.

[20] F. Forghieri, R. Tkach, and A. Chraplyvy, "Fiber nonlinearities and their impact on transmission systems," *Optical Fiber Telecommunications IIIA*, vol. 1, 1997.

[21] A. Krizhevsky, I. Sutskever, and G. E. Hinton, "Imagenet classification with deep convolutional neural networks," in *Advances in neural information processing systems*, pp. 1097–1105, 2012.

[22] W. D. Mulder, S. Bethard, and M.-F. Moens, "A survey on the application of recurrent neural networks to statistical language modeling," *Computer Speech and Language*, vol. 30, no. 1, pp. 61 – 98, 2015.

[23] B. Karanov, M. Chagnon, F. Thouin, T. A. Eriksson, H. Bülow, D. Lavery, P. Bayvel, and L. Schmalen, "End-to-end deep learning of optical fiber communications," *arXiv preprint arXiv:1804.04097*, 2018.

[24] S. Yan, F. N. Khan, A. Mavromatis, D. Gkounis, Q. Fan, F. Ntavou, K. Nikolovgenis, F. Meng, E. H. Salas, C. Guo, *et al.*, "Field trial of machine-learning-assisted and SDN-based optical network planning with network-scale monitoring database," in *43rd European Conference on Optical Communication (ECOC 2017)*, 2017.

[25] W. Mo, C. L. Gutterman, Y. Li, S. Zhu, G. Zussman, and D. C. Kilper, "Deep-neural-network-based wavelength selection and switching in ROADM systems," *Journal of Optical Communications and Networking*, vol. 10, no. 10, pp. D1–D11, 2018.

[26] G. E. Box and G. C. Tiao, *Bayesian inference in statistical analysis*, vol. 40. John Wiley & Sons, 2011.

[27] F. Meng, A. Mavromatis, Y. Bi, S. Yan, R. Wang, Y. Ou, K. Nikolovgenis, R. Nejabati, and D. Simeonidou, "Field trial of monitoring on-demand at intermediate-nodes through bayesian optimization," in *Optical Fiber Communication Conference*, p. M3A.2, Optical Society of America, 2018.

[28] I. de Miguel, R. J. Duran, T. Jimenez, N. Fernandez, J. C. Aguado, R. M. Lorenzo, A. Caballero, I. T. Monroy, Y. Ye, A. Tymecki, I. Tomkos, M. Angelou, D. Klonidis, A. Francescon, D. Siracusa, and E. Salvadori, "Cognitive dynamic optical networks [invited]," *IEEE OSA Journal of Optical Communications and Networking*, vol. 5, pp. A107–A118, Oct 2013.

[29] R. M. Morais, C. Pavan, A. N. Pinto, and C. Requejo, "Genetic algorithm for the topological design of survivable optical transport networks," *Journal of optical communications and networking*, vol. 3, no. 1, pp. 17–26, 2011.

[30] I. Tomkos, M. Angelou, R. J. D. Barroso, I. de Miguel, R. M. L. Toledo, D. Siracusa, E. Salvadori, A. Tymecki, Y. Ye, and I. T. Monroy, "Next generation flexible and cognitive heterogeneous optical networks," in *The Future Internet Assembly*, pp. 225–236, Springer, 2012.

[31] K. Kikuchi, "Fundamentals of coherent optical fiber communications," *Journal of Lightwave Technology*, vol. 34, pp. 157–179, Jan 2016.

[32] F. Meng, Y. Ou, S. Yan, K. Sideris, M. D. G. Pascual, R. Nejabati, and D. Simeonidou, "Field trial of a novel SDN enabled network restoration utilizing in-depth optical performance monitoring assisted network re-planning," in *2017 Optical Fiber Communications Conference and Exhibition (OFC)*, p. Th1J.8, March 2017.

[33] Y. Pointurier, M. Coates, and M. Rabbat, "Cross-layer monitoring in transparent optical networks," *Journal of Optical Communications and Networking*, vol. 3, no. 3, pp. 189–198, 2011.

[34] A. Mestres, A. Rodriguez-Natal, J. Carner, P. Barlet-Ros, E. Alarcón, M. Solé, V. Muntés-Mulero, D. Meyer, S. Barkai, M. J. Hibbett, *et al.*, "Knowledge-defined networking," *ACM SIGCOMM Computer Communication Review*, vol. 47, no. 3, pp. 2–10, 2017.

[35] X. Cao, N. Yoshikane, I. Popescu, T. Tsuritani, and I. Morita, "Software-defined optical networks and network abstraction with functional service design [invited]," *IEEE/OSA Journal of Optical Communications and Networking*, vol. 9, pp. C65–C75, April 2017.

[36] J.-L. Augé, "Can we use flexible transponders to reduce margins?," in *Optical Fiber Communication Conference*, pp. OTu2A–1, Optical Society of America, 2013.

[37] S. J. Savory, "Digital filters for coherent optical receivers," *Optics express*, vol. 16, no. 2, pp. 804–817, 2008.

[38] G. P. Agrawal, "Nonlinear fiber optics," in *Nonlinear Science at the Dawn of the 21st Century*, pp. 195–211, Springer, 2000.

[39] L. G. et al., "On the limits of digital back-propagation in the presence of transceiver noise," *Opt. Express*, vol. 25, pp. 4564–4578, Feb 2017.

[40] G. Saavedra, M. Tan, D. J. Elson, L. Galdino, D. Semrau, M. A. Iqbal, I. D. Phillips, P. Harper, A. Ellis, B. C. Thomsen, *et al.*, "Experimental analysis of nonlinear impairments in fibre optic transmission systems up to 7.3 THz," *Journal of Lightwave Technology*, vol. 35, no. 21, pp. 4809–4816, 2017.

[41] M. Pal, M. C. Paul, A. Dhar, A. Pal, R. Sen, K. Dasgupta, and S. K. Bhadra, "Investigation of the optical gain and noise figure for multi-channel amplification in EDFA under optimized pump condition," *Optics Communications*, vol. 273, no. 2, pp. 407–412, 2007.

[42] R. Anthony and S. Biswas, "Temperature dependent gain analysis of a cascaded C-band EDFA DWDM network," *Procedia Technology*, vol. 4, pp. 92–96, 2012.

[43] P. Poggiolini, "The GN model of non-linear propagation in uncompensated coherent optical systems," *Journal of Lightwave Technology*, vol. 30, no. 24, pp. 3857–3879, 2012.

[44] A. Carena, V. Curri, G. Bosco, P. Poggiolini, and F. Forghieri, "Modeling of the impact of nonlinear propagation effects in uncompensated optical coherent transmission links," *Journal of Lightwave technology*, vol. 30, no. 10, pp. 1524–1539, 2012.

[45] C. M. Bishop, *Pattern recognition and machine learning*.
Springer-Verlag New York, 2006.

[46] D. C. Montgomery, E. A. Peck, and G. G. Vining, *Introduction to linear regression analysis*, vol. 821.
John Wiley & Sons, 2012.

[47] M. T. Hagan, H. B. Demuth, M. H. Beale, *et al.*, *Neural network design*, vol. 20.
Pws Pub. Boston, 1996.

[48] I. Steinwart and A. Christmann, *Support vector machines*.
Springer Science & Business Media, 2008.

[49] A. K. Jain, M. N. Murty, and P. J. Flynn, "Data clustering: a review," *ACM computing surveys (CSUR)*, vol. 31, no. 3, pp. 264–323, 1999.

[50] S. Wold, K. Esbensen, and P. Geladi, "Principal component analysis," *Chemometrics and intelligent laboratory systems*, vol. 2, no. 1-3, pp. 37–52, 1987.

[51] N. G. Gonzalez, D. Zibar, and I. T. Monroy, "Cognitive digital receiver for burst mode phase modulated radio over fiber links," in *Optical Communication (ECOC), 2010 36th European Conference and Exhibition on*, p. Tu4A.3, IEEE, 2010.

[52] A. Ng, "Cs229 lecture notes," *CS229 Lecture notes*, vol. 1, no. 1, 2000.

[53] X. Wu, J. A. Jargon, R. A. Skoog, L. Paraschis, and A. E. Willner, "Applications of artificial neural networks in optical performance monitoring," *Journal of Lightwave Technology*, vol. 27, pp. 3580–3589, Aug 2009.

[54] J. Thrane, J. Wass, M. Piels, J. C. M. Diniz, R. Jones, and D. Zibar, "Machine learning techniques for optical performance monitoring from directly detected PDM-QAM signals," *Journal of Lightwave Technology*, vol. 35, pp. 868–875, Feb 2017.

[55] J. A. Jargon, X. Wu, H. Y. Choi, Y. C. Chung, and A. E. Willner, "Optical performance monitoring of QPSK data channels by use of neural networks trained with parameters derived from asynchronous constellation diagrams," *Optics Express*, vol. 18, no. 5, pp. 4931–4938, 2010.

[56] T. S. R. Shen, K. Meng, A. P. T. Lau, and Z. Y. Dong, "Optical performance monitoring using artificial neural network trained with asynchronous amplitude histograms," *IEEE Photonics Technology Letters*, vol. 22, no. 22, pp. 1665–1667, 2010.

[57] D. Zibar, "Machine learning techniques applied to system characterization and equalization," in *Optical Fiber Communication Conference*, pp. Tu3K–1, Optical Society of America, 2016.

[58] T. B. Anderson, A. Kowalczyk, K. Clarke, S. D. Dods, D. Hewitt, and J. C. Li, "Multi impairment monitoring for optical networks," *Journal of Lightwave Technology*, vol. 27, no. 16, pp. 3729–3736, 2009.

[59] T. Tanimura, T. Hoshida, J. C. Rasmussen, M. Suzuki, and H. Morikawa, "OSNR monitoring by deep neural networks trained with asynchronously sampled

data," in *OptoElectronics and Communications Conference (OECC) held jointly with 2016 International Conference on Photonics in Switching (PS), 2016 21st*, IEEE, 2016.

[60] B. Szafraniec, T. S. Marshall, and B. Nebendahl, "Performance monitoring and measurement techniques for coherent optical systems," *Journal of Lightwave Technology*, vol. 31, no. 4, pp. 648–663, 2013.

[61] D. Zibar, M. Piels, R. Jones, and C. G. Schäeffer, "Machine learning techniques in optical communication," *Journal of Lightwave Technology*, vol. 34, no. 6, pp. 1442–1452, 2016.

[62] M. C. Tan, F. N. Khan, W. H. Al-Arashi, Y. Zhou, and A. P. T. Lau, "Simultaneous optical performance monitoring and modulation format/bit-rate identification using principal component analysis," *IEEE/OSA Journal of Optical Communications and Networking*, vol. 6, pp. 441–448, May 2014.

[63] T. Jiménez, J. C. Aguado, I. de Miguel, R. J. Durán, M. Angelou, N. Merayo, P. Fernández, R. M. Lorenzo, I. Tomkos, and E. J. Abril, "A cognitive quality of transmission estimator for core optical networks," *Journal of Lightwave Technology*, vol. 31, no. 6, pp. 942–951, 2013.

[64] G. Guizzardi and G. Guizzardi, "Ontological foundations for structural conceptual models," 2005.

[65] M. Koohzadi and N. M. Charkari, "Survey on deep learning methods in human action recognition," *IET Computer Vision*, vol. 11, no. 8, pp. 623–632, 2017.

[66] T. Panayiotou, G. Ellinas, and S. P. Chatzis, "A data-driven QoT decision approach for multicast connections in metro optical networks," in *2016 International Conference on Optical Network Design and Modeling (ONDM)*, May 2016.

[67] F. Meng, S. Yan, K. Nikolovgenis, Y. Ou, R. Wang, Y. Bi, E. Hugues-Salas, R. Nejabati, and D. Simeonidou, "Field trial of gaussian process learning of function-agnostic channel performance under uncertainty," in *Optical Fiber Communication Conference*, p. W4F.5, Optical Society of America, 2018.

[68] S. Oda, M. Miyabe, S. Yoshida, T. Katagiri, Y. Aoki, T. Hoshida, J. C. Rasmussen, M. Birk, and K. Tse, "A learning living network with open ROADMs," *Journal of Lightwave Technology*, vol. 35, pp. 1350–1356, April 2017.

[69] L. Barletta, A. Giusti, C. Rottondi, and M. Tornatore, "QoT estimation for unestablished lighpaths using machine learning," in *Optical Fiber Communication Conference*, p. Th1J.1, Optical Society of America, 2017.

[70] D. B. Chua, E. D. Kolaczyk, and M. Crovella, "Network kriging," *IEEE Journal on Selected Areas in Communications*, vol. 24, no. 12, pp. 2263–2272, 2006.

[71] R. Castro, M. Coates, G. Liang, R. Nowak, and B. Yu, "Network tomography: Recent developments," *Statistical science*, pp. 499–517, 2004.

[72] Y. Pointurier, M. Coates, and M. Rabbat, "Cross-layer monitoring in transparent optical networks," *IEEE/OSA Journal of Optical Communications and Networking*, vol. 3, pp. 189–198, March 2011.

[73] N. Sambo, Y. Pointurier, F. Cugini, L. Valcarenghi, P. Castoldi, and I. Tomkos, "Lightpath establishment assisted by offline QoT estimation in transparent optical networks," *IEEE/OSA Journal of Optical Communications and Networking*, vol. 2, pp. 928–937, November 2010.

[74] M. Angelou, Y. Pointurier, D. Careglio, S. Spadaro, and I. Tomkos, "Optimized monitor placement for accurate QoT assessment in core optical networks,"

IEEE/OSA Journal of Optical Communications and Networking, vol. 4, no. 1, pp. 15–24, 2012.

[75] C. V. Saradhi and S. Subramaniam, "Physical layer impairment aware routing (PLIAR) in WDM optical networks: issues and challenges," *IEEE Communications Surveys & Tutorials*, vol. 11, no. 4, 2009.

[76] H. Braham, S. B. Jemaa, B. Sayrac, G. Fort, and E. Moulines, "Low complexity spatial interpolation for cellular coverage analysis," in *Modeling and Optimization in Mobile, Ad Hoc, and Wireless Networks (Wiopt), 2014 12Th International Symposium On*, pp. 188–195, IEEE, 2014.

[77] F. Meng, Y. Ou, S. Yan, K. Sideris, M. Pascual, R. Nejabati, and D. Simeonidou, "Field trial of a novel SDN enabled network restoration utilizing in-depth optical performance monitoring assisted network re-planning," in *Optical Fiber Communication Conference*, p. Th1J.8, Optical Society of America, 2017.

[78] Y. Huang, W. Samoud, C. L. Gutterman, C. Ware, M. Lourdiane, G. Zussman, P. Samadi, and K. Bergman, "A machine learning approach for dynamic optical channel add/drop strategies that minimize EDFA power excursions," in *ECOC 2016; 42nd European Conference on Optical Communication*, p. Tu4A.3, Sept 2016.

[79] Y. Huang, P. B. Cho, P. Samadi, and K. Bergman, "Dynamic power pre-adjustments with machine learning that mitigate EDFA excursions during defragmentation," in *2017 Optical Fiber Communications Conference and Exhibition (OFC)*, p. M1K.4, March 2017.

[80] E. d. A. Barboza, C. J. A. Bastos-Filho, J. F. Martins-Filho, U. C. de Moura, and J. R. F. de Oliveira, "Self-adaptive erbium-doped fiber amplifiers using machine

learning," in *2013 SBMO/IEEE MTT-S International Microwave Optoelectronics Conference (IMOC)*, Aug 2013.

[81] J. R. Oliveira, A. Caballero, E. Magalhães, U. Moura, R. Borkowski, G. Curiel, A. Hirata, L. Hecker, E. Porto, D. Zibar, *et al.*, "Demonstration of EDFA cognitive gain control via GMPLS for mixed modulation formats in heterogeneous optical networks," in *Optical Fiber Communication Conference*, pp. OW1H–2, Optical Society of America, 2013.

[82] C. J. Bastos-Filho, E. d. A. Barboza, J. F. Martins-Filho, U. C. de Moura, and J. R. de Oliveira, "Mapping EDFA noise figure and gain flatness over the power mask using neural networks," *Journal of Microwaves, Optoelectronics and Electromagnetic Applications (JMOe)*, vol. 12, pp. 128–139, 2013.

[83] U. Moura, M. Garrich, H. Carvalho, M. Svolenski, A. Andrade, A. C. Cesar, J. Oliveira, and E. Conforti, "Cognitive methodology for optical amplifier gain adjustment in dynamic DWDM networks," *Journal of Lightwave Technology*, vol. 34, pp. 1971–1979, April 2016.

[84] A. Napoli, Z. Maalej, V. A. Sleiffer, M. Kuschnerov, D. Rafique, E. Timmers, B. Spinnler, T. Rahman, L. D. Coelho, and N. Hanik, "Reduced complexity digital back-propagation methods for optical communication systems," *Journal of lightwave technology*, vol. 32, no. 7, pp. 1351–1362, 2014.

[85] N. V. Irukulapati, D. Marsella, P. Johannisson, E. Agrell, M. Secondini, and H. Wymeersch, "Stochastic digital backpropagation with residual memory compensation," *Journal of Lightwave Technology*, vol. 34, no. 2, pp. 566–572, 2016.

[86] D. Wang, M. Zhang, Z. Li, Y. Cui, J. Liu, Y. Yang, and H. Wang, "Nonlinear decision boundary created by a machine learning-based classifier to mitigate nonlinear

phase noise," in *Optical Communication (ECOC), 2015 European Conference on*, p. W3H.4, IEEE, 2015.

[87] D. Wang, M. Zhang, M. Fu, Z. Cai, Z. Li, Y. Cui, and B. Luo, "KNN-based detector for coherent optical systems in presence of nonlinear phase noise," in *Opto-Electronics and Communications Conference (OECC) held jointly with 2016 International Conference on Photonics in Switching (PS), 2016 21st*, IEEE, 2016.

[88] J. J. G. Torres, A. Chiuchiarelli, V. A. Thomas, S. E. Ralph, A. M. C. Soto, and N. G. González, "Adaptive nonsymmetrical demodulation based on machine learning to mitigate time-varying impairments," in *Avionics and Vehicle Fiber-Optics and Photonics Conference (AVFOP), 2016 IEEE*, pp. 289–290, IEEE, 2016.

[89] E. Giacoumidis, J. Wei, S. Mhatli, M. F. Stephens, N. J. Doran, A. D. Ellis, and B. J. Eggleton, "Nonlinear inter-subcarrier intermixing reduction in coherent optical OFDM using fast machine learning equalization," in *Optical Fiber Communications Conference and Exhibition (OFC), 2017*, p. Th3H.2, IEEE, 2017.

[90] M. A. Jarajreh, E. Giacoumidis, I. Aldaya, S. T. Le, A. Tsokanos, Z. Ghassemlooy, and N. J. Doran, "Artificial neural network nonlinear equalizer for coherent optical OFDM," *IEEE Photonics Technology Letters*, vol. 27, no. 4, pp. 387–390, 2015.

[91] T. S. R. Shen and A. P. T. Lau, "Fiber nonlinearity compensation using extreme learning machine for DSP-based coherent communication systems," in *Opto-Electronics and Communications Conference (OECC), 2011 16th*, pp. 816–817, IEEE, 2011.

[92] S. J. Savory and F. V. Caballero, "Machine learning based noise estimation in optical fiber communication networks," in *2018 IEEE Photonics Society Summer Topical Meeting Series (SUM)*, pp. 57–58, IEEE, 2018.

[93] D. J. Ives, P. Bayvel, and S. J. Savory, "Routing, modulation, spectrum and launch power assignment to maximize the traffic throughput of a nonlinear optical mesh network," *Photonic Network Communications*, vol. 29, no. 3, pp. 244–256, 2015.

[94] F. Musumeci, C. Rottondi, A. Nag, I. Macaluso, D. Zibar, M. Ruffini, and M. Tornatore, "A survey on application of machine learning techniques in optical networks," *arXiv preprint arXiv:1803.07976*, 2018.

[95] N. Fernández, R. J. Durán, I. de Miguel, N. Merayo, P. Fernandez, J. C. Aguado, R. M. Lorenzo, E. J. Abril, E. Palkopoulou, and I. Tomkos, "Virtual topology design and reconfiguration using cognition: Performance evaluation in case of failure," in *Ultra Modern Telecommunications and Control Systems and Workshops (ICUMT), 2013 5th International Congress on*, pp. 132–139, IEEE, 2013.

[96] N. Fernández, R. J. D. Barroso, D. Siracusa, A. Francescon, I. de Miguel, E. Salvadori, J. C. Aguado, and R. M. Lorenzo, "Virtual topology reconfiguration in optical networks by means of cognition: Evaluation and experimental validation," *Journal of Optical Communications and Networking*, vol. 7, no. 1, pp. A162–A173, 2015.

[97] F. Morales, M. Ruiz, and L. Velasco, "Virtual network topology reconfiguration based on big data analytics for traffic prediction," in *Optical Fiber Communication Conference*, pp. Th3I–5, Optical Society of America, 2016.

[98] F. Morales, M. Ruiz, L. Gifre, L. M. Contreras, V. López, and L. Velasco, "Virtual network topology adaptability based on data analytics for traffic prediction," *Journal of Optical Communications and Networking*, vol. 9, no. 1, pp. A35–A45, 2017.

[99] T. Ohba, S. Arakawa, and M. Murata, "A bayesian-based approach for virtual network reconfiguration in elastic optical path networks," in *Optical Fiber Communication Conference*, pp. Th1J–7, Optical Society of America, 2017.

[100] L. Gifre, F. Morales, L. Velasco, and M. Ruiz, "Big data analytics for the virtual network topology reconfiguration use case," in *Transparent Optical Networks (ICTON), 2016 18th International Conference on*, IEEE, 2016.

[101] N. Fernández, R. J. Durán, I. de Miguel, N. Merayo, D. Sánchez, M. Angelou, J. C. Aguado, P. Fernández, T. Jiménez, R. M. Lorenzo, *et al.*, "Cognition to design energetically efficient and impairment aware virtual topologies for optical networks," in *Optical Network Design and Modeling (ONDM), 2012 16th International Conference on*, IEEE, 2012.

[102] N. Fernández, R. J. Durán, I. de Miguel, N. Merayo, J. C. Aguado, P. Fernández, T. Jiménez, I. Rodríguez, D. Sánchez, R. M. Lorenzo, *et al.*, "Survivable and impairment-aware virtual topologies for reconfigurable optical networks: A cognitive approach," in *Ultra Modern Telecommunications and Control Systems and Workshops (ICUMT), 2012 4th International Congress on*, pp. 793–799, IEEE, 2012.

[103] S. Makridakis, E. Spiliotis, and V. Assimakopoulos, "Statistical and machine learning forecasting methods: Concerns and ways forward," *PloS one*, vol. 13, no. 3, p. e0194889, 2018.

[104] K. Christodoulopoulos, N. Sambo, and E. M. Varvarigos, "Exploiting network kriging for fault localization," in *Optical Fiber Communication Conference*, pp. W1B–5, Optical Society of America, 2016.

[105] M. Ruiz, F. Fresi, A. P. Vela, G. Meloni, N. Sambo, F. Cugini, L. Poti, L. Velasco, and P. Castoldi, "Service-triggered failure identification/localization through monitoring of multiple parameters," in *ECOC 2016; 42nd European Conference on Optical Communication; Proceedings of*, p. W1G.3, 2016.

[106] S. R. Tembo, S. Vaton, J.-L. Courant, and S. Gosselin, "A tutorial on the em algorithm for bayesian networks: application to self-diagnosis of GPON-FTTH networks," in *Wireless Communications and Mobile Computing Conference (IWCMC), 2016 International*, pp. 369–376, IEEE, 2016.

[107] S. R. Tembo, J.-L. Courant, and S. Vaton, "A 3-layered self-reconfigurable generic model for self-diagnosis of telecommunication networks," in *SAI Intelligent Systems Conference (IntelliSys), 2015*, pp. 25–34, IEEE, 2015.

[108] S. Gosselin, J.-L. Courant, S. R. Tembo, and S. Vaton, "Application of probabilistic modeling and machine learning to the diagnosis of FTTH GPON networks," in *Optical Network Design and Modeling (ONDM), 2017 International Conference on*, IEEE, 2017.

[109] A. P. Vela, M. Ruiz, F. Fresi, N. Sambo, F. Cugini, G. Meloni, L. Potì, L. Velasco, and P. Castoldi, "BER degradation detection and failure identification in elastic optical networks," *Journal of Lightwave Technology*, vol. 35, no. 21, pp. 4595–4604, 2017.

[110] A. Vela, B. Shariati, M. Ruiz, F. Cugini, A. Castro, H. Lu, R. Proietti, J. Comellas, P. Castoldi, S.-J. B. Yoo, *et al.*, "Soft failure localization during commissioning

testing and lightpath operation," *Journal of Optical Communications and Networking*, vol. 10, no. 1, pp. A27–A36, 2018.

[111] S. B. Yoo, Y. Yin, and K. Wen, "Intra and inter datacenter networking: The role of optical packet switching and flexible bandwidth optical networking," in *Optical Network Design and Modeling (ONDM), 2012 16th International Conference on*, IEEE, 2012.

[112] H. Rastegarfar, M. Glick, N. Viljoen, M. Yang, J. Wissinger, L. LaComb, and N. Peyghambarian, "TCP flow classification and bandwidth aggregation in optically interconnected data center networks," *Journal of Optical Communications and Networking*, vol. 8, no. 10, pp. 777–786, 2016.

[113] M. Glick and H. Rastegarfar, "Scheduling and control in hybrid data centers," in *Photonics Society Summer Topical Meeting Series (SUM), 2017 IEEE*, pp. 115–116, IEEE, 2017.

[114] C.-H. Wang and T. Javidi, "Adaptive policies for scheduling with reconfiguration delay: An end-to-end solution for all-optical data centers," *IEEE/ACM Transactions on Networking (TON)*, vol. 25, no. 3, pp. 1555–1568, 2017.

[115] T. V. y Villalba, S. M. Rossi, M. P. Mokarzel, M. R. Salvador, H. M. A. Neto, A. C. Cesar, M. A. Romero, and M. d. L. Rocha, "Design of passive optical networks using genetic algorithm," in *Microwave and Optoelectronics Conference (IMOC), 2009 SBMO/IEEE MTT-S International*, pp. 682–686, IEEE, 2009.

[116] A. Kokangul and A. Ari, "Optimization of passive optical network planning," *Applied Mathematical Modelling*, vol. 35, no. 7, pp. 3345–3354, 2011.

[117] U. R. Bhatt, N. Chouhan, R. Upadhyay, and C. Agrawal, "ONU placement in fiber-wireless (FiWi) access networks using teacher phase of teaching learning

based optimization (TLBO) algorithm," in *Computational Intelligence & Communication Technology (CICT), 2017 3rd International Conference on*, IEEE, 2017.

[118] P. Sarigiannidis, A. Sarigiannidis, I. Moscholios, and P. Zwierzykowski, "Diana: A machine learning mechanism for adjusting the TDD uplink-downlink configuration in XG-PON-LTE systems," *Mobile Information Systems*, vol. 2017, 2017.

[119] C. T. Huang, "The study of balance traffic load with genetic algorithm for PON," in *2008 International Conference on Intelligent Information Hiding and Multimedia Signal Processing*, pp. 39–42, Aug 2008.

[120] N. Moradpoor, G. Parr, S. McClean, and B. Scotney, "A mathematical model for a GA-based dynamic excess bandwidth allocation algorithm for hybrid PON and wireless technology integrations for next generation broadband access networks," in *Computer Science and Electronic Engineering Conference (CEEC), 2013 5th*, pp. 23–28, IEEE, 2013.

[121] I.-S. Hwang, J.-Y. Lee, and A.-T. Liem, "Genetic expression programming: A new approach for QoS traffic prediction in EPONs," in *Ubiquitous and Future Networks (ICUFN), 2012 Fourth International Conference on*, pp. 249–254, IEEE, 2012.

[122] T. Jiménez, N. Merayo, A. Andrés, R. J. Durán, J. C. Aguado, I. de Miguel, P. Fernández, R. M. Lorenzo, and E. J. Abril, "An auto-tuning PID control system based on genetic algorithms to provide delay guarantees in passive optical networks," *Expert Systems with Applications*, vol. 42, no. 23, pp. 9211–9220, 2015.

[123] N. Merayo, D. Juárez, J. C. Aguado, I. De Miguel, R. Durán, P. Fernández, R. Lorenzo, and E. Abril, "PID controller based on a self-adaptive neural network to ensure QoS bandwidth requirements in passive optical networks," *Journal of Optical Communications and Networking*, vol. 9, no. 5, pp. 433–445, 2017.

[124] P. Samadi, D. Amar, C. Lepers, M. Lourdiane, and K. Bergman, "Quality of transmission prediction with machine learning for dynamic operation of optical WDM networks," in *Optical Communication (ECOC), 2017 European Conference on*, IEEE, 2017.

[125] A. Willner and S.-M. Hwang, "Passive equalization of nonuniform EDFA gain by optical filtering for megameter transmission of 20 WDM channels through a cascade of EDFA's," *IEEE Photonics technology letters*, vol. 5, no. 9, pp. 1023–1026, 1993.

[126] M. Li, W. Jiao, Y. Song, X. Zhang, S. Dong, and Y. Poo, "Investigation of the EDFA effect on the BER performance in space uplink optical communication under the atmospheric turbulence," *Optics Express*, vol. 22, no. 21, pp. 25354–25361, 2014.

[127] C. Merkle, "Degradation model for erbium-doped fiber amplifiers to reduce network downtime," in *Meeting of the European Network of Universities and Companies in Information and Communication Engineering*, pp. 198–208, Springer, 2010.

[128] C. E. Rasmussen, "Gaussian processes in machine learning," in *Advanced lectures on machine learning*, pp. 63–71, Springer, 2004.

[129] Y. Huang, C. L. Gutterman, P. Samadi, P. B. Cho, W. Samoud, C. Ware, M. Lourdiane, G. Zussman, and K. Bergman, "Dynamic mitigation of EDFA power

excursions with machine learning," *Optics express*, vol. 25, no. 3, pp. 2245–2258, 2017.

[130] C. E. Rasmussen and H. Nickisch, "Gaussian processes for machine learning (GPML) toolbox," *Journal of Machine Learning Research*, vol. 11, no. Nov, pp. 3011–3015, 2010.

[131] M. G. Genton, "Classes of kernels for machine learning: a statistics perspective," *Journal of machine learning research*, vol. 2, no. Dec, pp. 299–312, 2001.

[132] M. Ebden, "Gaussian processes for regression: a quick introduction.," *University of Oxford*, 2008.

[133] A. Krishnamoorthy and D. Menon, "Matrix inversion using cholesky decomposition," in *Signal Processing: Algorithms, Architectures, Arrangements, and Applications (SPA), 2013*, pp. 70–72, IEEE, 2013.

[134] F. Meng, S. Yan, R. Wang, Y. Ou, Y. Bi, R. Nejabati, and D. Simeonidou, "Robust self-learning physical layer abstraction utilizing optical performance monitoring and markov chain monte carlo," in *2017 European Conference on Optical Communication (ECOC)*, Sept 2017.

[135] A. J. Stark, Y.-T. Hsueh, T. F. Detwiler, M. M. Filer, S. Tibuleac, and S. E. Ralph, "System performance prediction with the gaussian noise model in 100g PDM-QPSK coherent optical networks," *Journal of Lightwave Technology*, vol. 31, no. 21, pp. 3352–3360, 2013.

[136] B. G. Bathula, A. L. Chiu, R. K. Sinha, and S. L. Woodward, "Routing and regenerator planning in a carrier's core ROADM network," in *Optical Fiber Communication Conference*, pp. Th4F–4, Optical Society of America, 2017.

[137] M. Cantono, R. Gaudino, and V. Curri, "Data-rate figure of merit for physical layer in fixed-grid reconfigurable optical networks," in *Optical Fiber Communication Conference*, pp. Tu3F–3, Optical Society of America, 2016.

[138] J. Pesic, T. Zami, P. Ramantanis, and S. Bigo, "Faster return of investment in WDM networks when elastic transponders dynamically fit ageing of link margins," in *Optical Fiber Communications Conference and Exhibition (OFC), 2016*, p. W4J.3, IEEE, 2016.

[139] T. O'Shea and J. Hoydis, "An introduction to deep learning for the physical layer," *IEEE Transactions on Cognitive Communications and Networking*, vol. 3, no. 4, pp. 563–575, 2017.

[140] R. A. Jacobs and J. K. Kruschke, "Bayesian learning theory applied to human cognition," *Wiley Interdisciplinary Reviews: Cognitive Science*, vol. 2, no. 1, pp. 8–21, 2011.

[141] A. S. Thyagaturu, A. Mercian, M. P. McGarry, M. Reisslein, and W. Kellerer, "Software defined optical networks (SDONs): A comprehensive survey," *IEEE Communications Surveys & Tutorials*, vol. 18, no. 4, pp. 2738–2786, 2016.

[142] P. Diaconis and D. Ylvisaker, "Conjugate priors for exponential families," *The Annals of statistics*, pp. 269–281, 1979.

[143] G. O. Roberts and J. S. Rosenthal, "Examples of adaptive MCMC," *Journal of Computational and Graphical Statistics*, vol. 18, no. 2, pp. 349–367, 2009.

[144] H. T. Friis, "Noise figures of radio receivers," *Proceedings of the IRE*, vol. 32, no. 7, pp. 419–422, 1944.

[145] D. M. Baney, P. Gallion, and R. S. Tucker, "Theory and measurement techniques for the noise figure of optical amplifiers," *Optical fiber technology*, vol. 6, no. 2, pp. 122–154, 2000.

[146] L. Bottou, "Large-scale machine learning with stochastic gradient descent," in *Proceedings of COMPSTAT'2010*, pp. 177–186, Springer, 2010.

[147] M. Cantono, R. Gaudino, and V. Curri, "Potentialities and criticalities of flexible-rate transponders in DWDM networks: A statistical approach," *IEEE/OSA Journal of Optical Communications and Networking*, vol. 8, pp. A76–A85, July 2016.

[148] Y. Li, L. Gao, G. Shen, and L. Peng, "Impact of ROADM colorless, directionless, and contentionless (CDC) features on optical network performance [invited]," *IEEE/OSA Journal of Optical Communications and Networking*, vol. 4, pp. B58–B67, Nov 2012.

[149] T. Panayiotou, S. P. Chatzis, and G. Ellinas, "Performance analysis of a data-driven quality-of-transmission decision approach on a dynamic multicast-capable metro optical network," *Journal of Optical Communications and Networking*, vol. 9, no. 1, pp. 98–108, 2017.

[150] S. Yan, A. Aguado, Y. Ou, R. Nejabati, and D. Simeonidou, "Demonstration of an SDN based monitoring framework for converged packet and optical networks analytic," in *Optical Fiber Communication Conference*, pp. W3F–4, Optical Society of America, 2016.

[151] S. Oda, J. Y. Yang, Y. Akasaka, K. Sone, Y. Aoki, M. Sekiya, and J. C. Rasmussen, "In-band OSNR monitor using an optical bandpass filter and optical power measurements for superchannel signals," in *39th European Conference and Exhibition on Optical Communication (ECOC 2013)*, Sept 2013.

[152] G. Yin, S. Cui, C. Ke, and D. Liu, "Reference optical spectrum based in-band OSNR monitoring method for EDFA amplified multispan optical fiber transmission system with cascaded filtering effect," *IEEE Photonics Journal*, vol. 10, pp. 1–10, June 2018.

[153] Finisar, *WaveAnalyzer 1500S*. `https://www.finisar.com/optical-instrumentation/waveanalyzer-1500s-high-resolution-optical-spectrum-analyzer`.

[154] W. Moench, J. Larikova, and P. Winterling, "In-service measurement of the OSNR in ROADM-based networks," in *Photonic Networks, 2008 ITG Symposium on*, VDE, 2008.

[155] N. Amaya, G. S. Zervas, and D. Simeonidou, "Architecture on demand for transparent optical networks," in *2011 13th International Conference on Transparent Optical Networks*, June 2011.

[156] S. Azodolmolky, J. Perelló, M. Angelou, F. Agraz, L. Velasco, S. Spadaro, Y. Pointurier, A. Francescon, C. V. Saradhi, P. Kokkinos, *et al.*, "Experimental demonstration of an impairment aware network planning and operation tool for transparent/translucent optical networks," *Journal of Lightwave Technology*, vol. 29, no. 4, pp. 439–448, 2011.

[157] X. Cai, K. Wen, R. Proietti, Y. Yin, D. J. Geisler, R. P. Scott, C. Qin, L. Paraschis, O. Gerstel, and S. Yoo, "Experimental demonstration of adaptive combinational QoT degradation restoration in elastic optical networks," *Journal of Lightwave Technology*, vol. 31, no. 4, pp. 664–671, 2013.

[158] Y. Ou, S. Yan, A. Hammad, B. Guo, S. Peng, R. Nejabati, and D. Simeonidou, "Demonstration of virtualizeable and software-defined optical transceiver," *Journal of Lightwave Technology*, vol. 34, no. 8, pp. 1916–1924, 2016.

[159] L. Cui, F. R. Yu, and Q. Yan, "When big data meets software-defined networking: SDN for big data and big data for SDN," *IEEE Network*, vol. 30, pp. 58–65, January 2016.

[160] O. Grytsenko and V. Sayenko, "A method of network monitoring with reduced measured data," in *Scientific-Practical Conference Problems of Infocommunications. Science and Technology (PIC S&T), 2017 4th International*, pp. 477–482, IEEE, 2017.

[161] R. Borkowski, R. J. Durán, C. Kachris, D. Siracusa, A. Caballero, N. Fernández, D. Klonidis, A. Francescon, T. Jiménez, J. C. Aguado, *et al.*, "Cognitive optical network testbed: EU project CHRON," *Journal of Optical Communications and Networking*, vol. 7, no. 2, pp. A344–A355, 2015.

[162] W. Xiaolin, Q. Xiaogang, and L. Lifang, "Probe selection algorithm for faulty links localization in all-optical networks," in *Smart Grid and Electrical Automation (ICSGEA), 2017 International Conference on*, pp. 269–272, IEEE, 2017.

[163] H.-T. Luk and L.-K. Chen, "Active probing assisted monitoring for software defined networks," in *Optical Fiber Communications Conference and Exhibition (OFC), 2015*, IEEE, 2015.

[164] A. E. Willner and S.-M. Hwan, "Transmission of many WDM channels through a cascade of EDFA's in long-distance links and ring networks," *Journal of Lightwave Technology*, vol. 13, pp. 802–816, May 1995.

[165] R. Giridhar Kumar, I. Sadhu, and N. Sangeetha, "Gain and noise figure analysis of erbium doped fiber amplifier by four stage enhancement and analysis," *International Journal of Scientific and Research Publications*, vol. 4, no. 4, 2014.

[166] M. R. Chitgarha, S. Khaleghi, W. Daab, M. Ziyadi, A. Mohajerin-Ariaei, D. Rogawski, M. Tur, J. Touch, V. Vusirikala, W. Zhao, *et al.*, "Demonstration of WDM OSNR performance monitoring and operating guidelines for pol-muxed 200-gbit/s 16-QAM and 100-gbit/s QPSK data channels," in *Optical Fiber Communication Conference and Exposition and the National Fiber Optic Engineers Conference (OFC/NFOEC), 2013*, pp. 1–3, IEEE, 2013.

[167] A. Almaiman, M. R. Chitgarha, W. Daab, M. Ziyadi, A. Mohajerin-Ariaei, S. Khaleghi, M. Willner, V. Vusirikala, X. Zhao, D. Kilper, *et al.*, "Experimental demonstration of robustness and accuracy of a DLI-based OSNR monitor under changes in the transmitter and link for different modulation formats and baud rates," *Optics letters*, vol. 40, no. 9, pp. 2012–2015, 2015.

[168] B. Shahriari, K. Swersky, Z. Wang, R. P. Adams, and N. De Freitas, "Taking the human out of the loop: A review of bayesian optimization," *Proceedings of the IEEE*, vol. 104, no. 1, pp. 148–175, 2016.

[169] J. Snoek, H. Larochelle, and R. P. Adams, "Practical bayesian optimization of machine learning algorithms," in *Advances in neural information processing systems*, pp. 2951–2959, 2012.

[170] I. Sartzetakis, K. Christodoulopoulos, C. Tsekrekos, D. Syvridis, and E. Varvarigos, "Estimating QoT of unestablished lightpaths," in *2016 Optical Fiber Communications Conference and Exhibition (OFC)*, IEEE, 2016.